UNDERSTANDING AND IMPROVING THE SOIL MOISTURE RETRIEVAL ALGORITHM UNDER SPACE, TIME AND HETEROGENEITY

A Dissertation

by

MAHESHWARI NEELAM

Submitted to the Office of Graduate and Professional Studies of
Texas A&M University
in partial fulfillment of the requirements for the degree of

DOCTOR OF PHILOSOPHY

Chair of Committee,	Binayak P. Mohanty
Committee Members,	Yann Kerr
	Mark Everett
	Bruce McCarl
	Patricia K. Smith
Head of Department,	Stephen W. Searcy

August 2018

Major Subject: Biological and Agricultural Engineering

ABSTRACT

The spatial and temporal monitoring of soil moisture from remote sensing platforms plays a pivotal role in predicting the future food and water security. That is, improving soil moisture estimation at remote sensing platforms has remarkable impacts in the fields of meteorology, hydrology, agriculture, and global climate change. However, remote sensing of soil moisture for long is hindered by spatial heterogeneity in land surface variables (soil, biomass, topography, and temperature) which cause systematic and random errors in soil moisture retrievals.

Most soil moisture improvement methods to date focused on the downscaling of either coarse resolution soil moisture or brightness temperature based on fine scale ancillary information of land surface variables. Comparatively little work has been done on improving the parameterization of most sensitive variables to radiative transfer model that impact soil moisture retrieval accuracy. In addition, the classic radiative transfer model assumes the vegetation and surface roughness parameters, as constant with space and time which undermines the retrieval accuracy. Also, it is largely elusive so far the discussion on the non-linearity of microwave radiative transfer model and its relationship with energy and water fluxes.

In order to address the above mentioned limitations, this dissertation aims to develop and validate a soil moisture modeling framework with associated improved parameterizations for surface roughness and vegetation optical depth (VOD) in the homogeneous and heterogeneous environments. To this end, the following research work is specifically conducted: (a) conduct comprehensive sensitivity analysis on radiative transfer model with space, time and hydro-climates; (b) develop multi-scale surface roughness model which incorporates small (soil) and large (topography) surface undulations to improve soil moisture retrievals; (c) improve the parameterization of vegetation topical depth (VOD) using within-pixel biomass heterogeneity to

improved soil moisture accuracy; (d) investigate the non-linearity in microwave radiative transfer model, and its association with thermal energy fluxes.

The results of this study showed that: (a) the total (linear + non-linear) sensitivity of soil, temperature and biomass variables varied with spatial scale (support), time, and hydro climates, with higher non-linearity observed for dense biomass regions. This non-linearity is also governed by soil moisture availability and temperature. Among these variables, surface roughness and vegetation optical depth are most sensitive variables to radiative transfer model (RTM); (b) considering the spatial and temporal variability in parameterization of surface roughness and VOD has improved soil moisture retrieval accuracy, importantly in cropland and forest environments; and (c) the soil moisture estimated through evaporative fraction (EF) correlates higher with VOD corrected soil moisture.

DEDICATION

This dissertation is dedicated to my dear family.

ACKNOWLEDGEMENTS

I am grateful to my family, advisor, mentors, colleagues and friends for their constant encouragement and support during my Ph.D. study at Biological and Agricultural Engineering Department, Texas A&M University.

CONTRIBUTORS AND FUNDING SOURCES

This work was supervised by a dissertation committee consisting of Professor Binayak P. Mohanty [advisor] and Professor Patricia K. Smith of the Department of Biological and Agricultural Engineering, Professor Mark Everett of the Department of Geology, Professor Bruce McCarl of the Department of Agricultural Engineering, and Yann Kerr Director at CESBIO, France.

The Chapter 3 and Chapter 4 were conducted under collaborations with Andreas Colliander, and Dara Entekhabi respectively.

I'm grateful to the Schlumberger's Faculty for Future fellowship and funding agency NASA– SUSMAP (NNX16AQ58G) and THP (NNX09AK73G) for their financial support during the course of my Ph.D.

Its contents are solely the responsibility of the authors and do not necessarily represent the official views of any funding sources.

TABLE OF CONTENTS

Page

LIST OF FIGURES

Page

LIST OF TABLES

Page

1 GENERAL INTRODUCTION

1.1 Problem Statement

The remote sensing sensors collect data using different parts of the electromagnetic spectrum. These measurements are often linked to geophysical variables (soil moisture, evapotranspiration, biomass, etc.,) using retrieval algorithms. The large difference between the dielectric constant of liquid water and dry forms the basis for remote sensing of the soil moisture at microwave frequencies (Schmugge et al., 1986). This difference will be reduced with addition of water to the dry soil, i.e., with increase in soil moisture. The passive microwave which allows for all day/night, and all weather proof observational capability unlike active radars, is an attractive option for large scale soil moisture monitoring. Nevertheless, the poor spatial resolution of passive microwave remote sensing, incorporates uncertainties caused due to spatial heterogeneity in observed geophysical variables.

The importance of soil moisture is widely recognized in various hydrological and meteorological processes, e.g., evapotranspiration pattern and rate, run off, the weather prediction, flood forecasting, drought monitoring, crop yield, irrigation scheduling and many more. Therefore, it is critical to improve soil moisture estimates to reliably assess and make a decision support system which have direct relation to socio-economic impact.

Research has shown, L-band (1.4 GHz-21cm) is considerably sensitive to shallow soil moisture (~ 3-5 cm) than other higher frequencies due to moderate atmospheric and vegetation attenuation. At L-band, the brightness temperature of a given land surface importantly depends on soil moisture, surface roughness, soil type, effective soil temperature, and vegetation optical depth. The structural features such as soil roughness and vegetation geometry are assumed spatio-temporally constant. In addition, they are represented at satellite scale by plot/field scale estimates

which introduce large uncertainties (cite). Unfortunately, physical/semi-empirical models which account for spatial and temporal heterogeneity in geophysical variables is not common yet and even less common at satellite scales. Importantly, as environmental system is largely non-linear, it is unclear if the non-linearity observed at microwave frequencies relate to fluxes observed at thermal frequencies.

1.2 Motivation

The improvement in remote sensing of soil moisture is essentially a heterogeneity-scaling issue. Addressing this issue appropriately can better facilitate the research upon the land and atmosphere interactions. Motivated by the limitations discussed in section 1.1, this dissertation aims to address these limitations by (1) proposing better parameterizations for surface roughness and vegetation optical depth under heterogeneity; and (2) investigating the non-linearity in microwave radiative model, and its relationship with thermal fluxes.

1.3 Research Objectives

The overarching objective of the dissertation is to develop and validate a predictive soil moisture modeling framework with associated land surface interactions and improved parameterizations for dominant geophysical variables. To this end, the following objectives will be specifically pursued:

1. Examine the first order, the second order, and the total sensitivity measures of the radiative transfer model parameters. This objective is explored under spatio-temporally varying conditions with different wetness conditions and vegetation type.

2. Propose a framework for understanding the efficacy of a radiative transfer model (RTM) for soil moisture retrieval with different support scales, seasonality (time) and under land surface heterogeneity.

3. Develop and evaluate a new comprehensive surface roughness model by incorporating geophysical variables from different spatial and temporal scales.

4. Incorporate and evaluate the impact of biomass heterogeneity on soil moisture retrieval accuracy.

5. Quantify land surface interactions, and their variability with heterogeneity, hydro-climates, temporal scales and its relationship with thermal fluxes.

In Section 2, the variability in first order, the second order, and the total sensitivity measures of the radiative transfer model parameters is explored under spatio-temporally conditions using two different field campaign data.

In Section 3, the non-linearity in radiative transfer model is explored with varying support scales using four field campaign data from different hydro climates which provides theoretical framework for work in section 5.

Section 4 proposes a spatio-temporally varying semi-empirical model for surface roughness which can be adopted at any spatial resolution.

In Section 5, correction for biomass heterogeneity is presented, and its validation is conducted through LSM, insitu and EF estimated SM. In addition, an association between non-linearity in microwave radiative transfer model and thermal fluxes is discussed under hydro-climates, seasons, and land cover.

2 GLOBAL SENSITIVITY ANALYSIS OF THE RADIATIVE TRANSFER MODEL*

2.1 Synopsis

With the to-be launch of Soil Moisture Active Passive (SMAP) mission, it is very important to have a complete understanding of the radiative transfer model for better soil moisture retrievals and to direct future research and field campaigns in areas of necessity. Because natural systems show great variability and complexity with respect to soil, land cover, topography, precipitation, there exist large uncertainties and heterogeneities in model input factors. In this paper, we explore the possibility of using global sensitivity analysis (GSA) technique to study the influence of heterogeneity and uncertainties in model inputs on zero order radiative transfer (ZRT) model and also to quantify interactions between parameters. GSA technique is based on decomposition of variance and can handle non-linear and non-monotonic functions. We direct our analyses towards growing agricultural fields of corn and soybean in two different regions, Iowa, U.S.A (SMEX02) and Winnipeg, Canada (SMAPVEX12). We noticed that, there exists a spatio-temporal variation in parameter interactions under different soil moisture and vegetation conditions. Parameter interactions on average 14 % are observed in SMEX02 fields whereas 5% interactions are noticed in SMAPVEX12 fields. Also parameter interactions increased with vegetation water content (VWC) and roughness conditions. Interestingly, soil moisture shows an exponentially decreasing sensitivity function whereas parameters such as root mean square height (RMS height) and vegetation water content show increasing sensitivity with increasing moisture conditions. Overall, considering the SMAPVEX12 fields to be water rich environment (due to higher observed SM) and SMEX02 fields to be energy rich environment (due to lower SM and wide ranges of TSURF),

*This section is reprinted with permission from "Global sensitivity analysis of the radiative transfer model" by Neelam, M., and B. P. Mohanty (2015), Water Resour. Res., 51, 2428-2443, doi:10.1002/2014WR016534,

our results indicate that first order as well as interactions between the parameters change with water and energy rich environments.

2.2 Introduction

Soil moisture (SM) plays a fundamental role in governing the hydrological and the terrestrial carbon cycle, and demands a global and consistent monitoring for the future food and water security. Several missions in the past (SSM/I, AMSR-E, and SMOS) have made available satellite-derived soil moisture using both the active and the passive remote sensing. The most commonly used system for modeling the complex soil-vegetation-atmosphere interactions for soil moisture retrieval is described by ‘‘Radiative Transfer Equation’’ (RTE) [Ulaby et al., 1986; Kerr and Njoku, 1990]. Modeling of RTE however requires characterizing the complex land-atmosphere interactions in geophysical parameters which is a difficult task, since land surface parameters show a large heterogeneity, and not all of them are significant in describing the system at all scales. Thus, considering all parameters as significant and incorporating them into the model will result in either an over or an underdetermined system. Therefore, implementing RTE theory into practical soil moisture retrieval algorithm requires reducing the dimensionality by simplifying assumptions without compromising on the system information. This requires us to understand the model behavior and also the parameters which efficiently encapsulate all the processes. A sensitivity analysis (SA) is an effective methodology to attain this objective. SA can result in achieving factor fixing (FF) for non-influential parameters, or factor prioritization (FP) for important parameters, thereby reducing the output uncertainty. This also reduces number of parameters required for optimization hereby increasing computational efficiency without undermining the results [Saltelli et al., 2004]. Past studies [Davenport et al., 2005; Crosson et al., 2005; Calvet et al., 2011] have performed sensitivity analysis on brightness temperature to

determine the influential parameters using the One-Factor-at-a-Time (OAT) algorithm. This algorithm also called as the Local Sensitivity Analysis (LSA), computes local response of the model by varying a parameter locally while the other input parameters are fixed at their nominal values. LSA only provides a rough estimation of parameter ranking using limited number of model evaluations. These results are, however, qualitative and not quantitative. Soil moisture (SM) plays a fundamental role in governing the hydrological and the terrestrial carbon cycle, and demands a global and consistent monitoring for the future food and water security. Several missions in the past (SSM/I, AMSR-E, and SMOS) have made available satellite-derived soil moisture using both the active and the passive remote sensing. The most commonly used system for modeling the complex soil-vegetation-atmosphere interactions for soil moisture retrieval is described by ‘‘Radiative Transfer Equation’’ (RTE) [Ulaby et al., 1986; Kerr and Njoku, 1990]. Modeling of RTE however requires characterizing the complex land-atmosphere interactions in geophysical parameters which is a difficult task, since land surface parameters show a large heterogeneity, and not all of them are significant in describing the system at all scales. Thus, considering all parameters as significant and incorporating them into the model will result in either an over or an underdetermined system. Therefore, implementing RTE theory into practical soil moisture retrieval algorithm requires reducing the dimensionality by simplifying assumptions without compromising on the system information. This requires us to understand the model behavior and also the parameters which efficiently encapsulate all the processes. A sensitivity analysis (SA) is an effective methodology to attain this objective. SA can result in achieving factor fixing (FF) for non-influential parameters, or factor prioritization (FP) for important parameters, thereby reducing the output uncertainty. This also reduces number of parameters required for optimization, hereby increasing computational efficiency without undermining the results [Saltelli et al., 2004]. Past

studies [Davenport et al., 2005; Crosson et al., 2005; Calvet et al., 2011] have performed sensitivity analysis on brightness temperature to determine the influential parameters using the One-Factor-at-a-Time (OAT) algorithm. This algorithm also called as the Local Sensitivity Analysis (LSA), computes local response of the model by varying a parameter locally while the other input parameters are fixed at their nominal values. LSA only provides a rough estimation of parameter ranking using limited number of model evaluations. These results are, however, qualitative and not quantitative, and understanding about the underlying model assumptions and processes are restricted in the LSA methods. Also, OAT method is suitable for factor fixing but not for factor prioritization [Saltelli et al., 2008]. In contrast, global sensitivity analysis (GSA) method, comprehensively evaluates model response to variations in inputs in the entire allowable parameter ranges. In this paper, for the first time we explore the GSA technique in remote sensing arena to evaluate the Zero Order Radiative Transfer (ZRT) model behavior and along with the parameter interactions. We use a variance-based Sobol method which is a widely used GSA technique [Saltelli et al., 2004]. This method quantifies the amount of variance each parameter contributes to the total unconditional variance. Despite its computational demand, it provides a comprehensive sensitivity analysis, and a nonlinear relationship between the parameters. It is important to realize the individual and interaction effects of soil moisture (SM), soil texture (Clay fraction (CF)), surface roughness (RMS height 'S' and correlation length 'L'), vegetation parameters (vegetation water content 'VWC,' vegetation structure 'B' and scattering albedo 'ω') on brightness temperature (TB) to improve model and process understanding. For example, consider the similar scattering and screening effects of surface roughness and vegetation (increase TB and reduce soil moisture sensitivity) [Njoku and Chan, 2006] which makes it difficult to separate their individual impacts. We hypothesize that, there exists nonlinear interactions between these parameters which

need to be accounted for in modeling. We also hypothesize that, these interactions change with the local climate/climate zones since different parameters come into play under different conditions [Gaur and Mohanty, 2013; Joshi and Mohanty, 2010; Jana and Mohanty, 2012]. An understanding of these spatio-temporal interactions between parameters will result in improved modeling of radiative transfer processes. The objective of this paper is to examine the first order, the second order, and the total sensitivity measures of the ZRT model parameters. We explore this objective under spatio-temporally varying conditions with different wetness conditions and vegetation types. Our study focused on using two field campaigns, Soil Moisture Experiment 2002 (SMEX02) in Iowa and Soil Moisture Active Passive Validation Experiment 2012 (SMAPVEX12) in Winnipeg. Corn and soybean crops are selected for our analysis, since they are the major agricultural crops of the study regions in particular and North America in general. This analysis is carried out in climatologically similar (but locally different) regions such as Iowa, USA, and Winnipeg, Canada. We believe quantification of these interactions of geophysical parameters will help us direct our future soil moisture cal/val campaigns in areas which need more expertise to make accurate retrieval or predictions.

2.3 Materials and Methods

2.3.1 Climatology of Iowa and Winnipeg

According to the Koppen climate classification, Iowa and Winnipeg fall under humid continental climate zone [Peel et al., 2007]. Such a climatic region is classified with large seasonal temperature differences, with hot and humid summers and cold severe winters with significant precipitation in all the seasons. Iowa and Winnipeg are categorized as Dfa (high 30s and low 40s latitudes) and Dfb (high 40s and low 50s in latitude) climate zones respectively. Iowa is mainly characterized by hot summers with an average temperature greater than 22°C in the warmest

months and an average temperature above 10°C over a span of four months. Winnipeg is characterized by warm summers with warmest month temperature below 22°C and with at least four months average temperature above 10°C.

2.3.2 Soil Moisture Experiment 2002 (SMEX02)

SMEX02 (Soil Moisture Experiments in 2002) was conducted in central Iowa from June 24th- July 12th, 2002 to validate soil moisture retrieval algorithms for a range of soil and vegetation conditions from aircraft and satellite microwave instruments [Jacobs et al., 2004; Bindlish et al., 2006; Narayan et al., 2004; McCabe et al., 2005; Famiglietti et al., 2008]. Central Iowa is mainly an agricultural region with two major crops, corn and soybean. This experimental site is being used to test retrieval algorithms since agricultural fields are uniform in vegetation type but differ largely in landscape patterns such as soil texture, vegetation conditions and topography. The 19-day campaign collects wide range of soil and vegetation conditions for soybean and corn fields, thus forms an excellent database to perform spatio-temporal soil moisture sensitivity analysis.

2.3.2.1 Field Measurements

In this study, we selected four sampling days (DOY: 178, 182, 186 and 188) which best represent the soil moisture wetting and drying cycles under growing vegetation. For our analysis, we used ground measurements of volumetric soil moisture (VSM), soil temperature and vegetation water content from the same sampling days (except for 186, when VWC of 187 is used). Two rainfall events were observed in watershed with light showers on DOY_185/186, and more significant showers on DOY_187 elevating SM further. Ground sampling of VWC for corn and soybean noticed a significant increase from DOY_178 to188, with corn mean VWC increasing from 2.9 kg/m^2 to 4.5 kg/m^2, and soybean mean VWC increasing from 0.3 kg/m^2 to 0.77 kg/m^2. Grid board measurements of surface roughness, shows a wide range of RMS height (S) and

correlation length (L) for corn [S: 0.19-2.55cm; L: 0.55-26.9cm] and soybean [S: 0.21- 3.05 cm; L: 0-20.8cm]. These ranges represent the roughness conditions from rolled fields to ploughed surfaces [Álvarez-Mozos et al., 2006; Zhixiong et al., 2005].

2.3.3 Soil Moisture Active Passive Validation Experiment 2012 (SMAPVEX12)

SMAPVEX12 (Soil Moisture Active Passive Validation Experiment in 2012) was conducted in agricultural region south of Winnipeg, Manitoba (Canada) from June 6th to July 17th 2012. This site is about 15 km × 70 km within the large Red River Watershed. The climate of Winnipeg is classified as extreme humid continental with great difference in summer and winter temperatures. The annual average precipitation is about 52cm, with most of the precipitation occurring between May to September. Because of the extremely flat topography and substantial snowfall this region is prone to flooding. The watershed is mainly characterized by agricultural land use with a wide range of crop and soil conditions. Soils of this region vary within a distance of few kilometers with heavy clays in the east to loamy sands in the west. The major agricultural crops of the region include cereals, canola, corn and soybean [Heather et al., 2012 SMAPVEX experimental report]. A total of fifty-five agricultural sites have been chosen for SMAPVEX12 experiment of which soybean (15), canola (6), corn (10), spring wheat (14), winter-wheat (2), forage (1), bean (1) and pasture (6). Because of the favorable economic and environmental conditions early in season, more of the soybean fields were planted. Apart from field soil moisture measurements, SMAPVEX12 site is largely monitored with *insitu* soil moisture stations by United States Department of Agriculture (USDA), Agriculture and Agri-Food Canada (AAFC), Manitoba Agriculture, and Food and Rural Initiatives (MAFRI). Gravimetric and volumetric soil moisture data are collected almost every alternate day except for rainy days. With the wide range of soil

moisture, vegetation and texture conditions observed, SMAPVEX12 site provide an extensive data sets for development and validation of SMAP passive and active soil moisture retrieval algorithms.

2.3.3.1 Field Measurements

In this study, we use in-situ measurements of soil moisture, soil temperature, surface roughness and vegetation water content collected for soybean and corn fields. Soybean and corn fields show sharp variations in soil texture. Soybean fields show soil texture with sandy loam soils (Field ID: 14, 12, 11, 63, 82, 64, 52) to heavy clay soils (Field ID: 51, 114, 64, 51, 111, 123, 113, 101, 103, 109, 112, 34). Whereas corn fields are mainly sandy (Field ID: 24, 72, 71) and sandy loam (Field ID: 54, 83, 94, 54, 83, 53, 93). For our study we carefully selected seven (DOY: 159, 164, 169, 174, 181, 190 and 199) different wetness days from entire duration of SMAPVEX12 campaign. As mentioned earlier, these wetness days were selected such that they fully represent the wetting and drying cycles of soil moisture under temporally varying vegetation conditions.

2.4 Soil Moisture Retrieval Algorithm

The theory behind microwave radiative transfer model for remote sensing of soil moisture is the large contrast between the dielectric properties of soil (~4) and water (~ 80). As the amount of water content increases in soil, the dielectric constant increases, while emissivity reduces. The brightness temperature (T_B) of the soil surface is related to its physical effective temperature and emissivity such that:

$$T_{B(\theta,p)} = (1\text{-}R_{(\theta,p)}) \times T_{eff} = e_{(\theta,p)} \times T_{eff} \qquad (2.1)$$

where subscript p is the vertical (V) or horizontal (H) polarization and θ denotes incidence angle of the measurement. $R_{(\theta,p)}$ is the p polarized reflectivity from the surface, T_{eff} is the effective soil temperature, $e_{(\theta,p)} = 1\text{-}R_{(\theta,p)}$ is the emissivity of the surface which depends on the dielectric constant (ε) of the medium. The dielectric constant (ε) of soil is determined by several quantities such as

moisture content, bulk density, soil texture composition, soil temperature and salinity. Of these quantities, ε is majorly influenced by soil moisture. The penetration depth δ_p of microwave radiation varies with soil moisture content, such that $\delta_p \sim \lambda$ for volumetric moisture SM~0.04 gcm^{-3} and $\delta_p \sim 0.1\ \lambda$ for very wet soils [Ulaby et al., 1986]. Several studies [Newton et al., 1982; Schmugge, 1983] relating to sensing depth, have led to the conclusion that soil moisture sensing depth δ_m is on the order of $0.1\ \lambda$ or shallower. Thus, the brightness temperature shows sensitivity to the near surface soil moisture variations and reduced sensitivity to deeper soil moisture layers [Njoku et al., 1980]. Therefor any non-uniformity in temperature and dielectric constant profiles is significant only for the layer between the surface and the depth of δ_p, because beyond this depth contribution to the brightness temperature (T_B) is very small.

The most widely used radiative transfer model [Mo et al., 1982] under vegetation conditions is known as τ-ω model described in equation (2.2).

$$T_{B(p,f,\theta)} = e_{p,\theta}.T_{eff}.\exp\left(-\frac{\tau_{p,f}}{\cos\theta}\right) + T_c.\left(1-\omega_{p,f,\theta}\right).\left(1-\exp\left(-\frac{\tau_{p,f}}{cos\theta}\right)\right) +$$

$$T_c.\exp\left(-\frac{\tau_{p,f}}{cos\theta}\right).\left(1-\omega_{p,f,\theta}\right).\left(1-\exp\left(-\frac{\tau_{p,f}}{cos\theta}\right)\right).r_{p,f,\theta} \qquad (2.2)$$

where τ_p is the nadir optical depth, ω_p is the single scattering albedo, r_p is the rough surface reflectivity and T_{eff} and T_c are the effective physical temperatures of soil layers and vegetation, respectively. The subscripts, p, θ and f denote the polarization, angle of incidence, and frequency of measurement. Thus the total upward microwave emission is a summation of: 1) upward soil emission attenuated by the vegetation, 2) upward emission from vegetation, 3) vegetation emission reflected by soil and attenuated through canopy (Fig. 2.1). Several models [Njoku and Kong, 1977; Wilheit, 1978; Burke et al., 1979] are proposed to calculate brightness temperature for non-uniform dielectric and temperature medium. And a comparison between these different models [Schmugge and Choudhury, 1981] led to the conclusion that at longer wavelengths internal

reflections between the layered media can be ignored to calculate effective temperature. Thus for passive remote sensing at L-band, it is reasonable to assume the effective soil temperature to be equal to surface temperature (T_{eff} ~*TSURF*). The tau-omega is considered to be Zero-Order Radiative Transfer (ZRT) model, since it ignores multiple scattering within the vegetation layer. These assumptions are considered reasonable during early hours (6 am local time) when soil temperature profile is more uniform and vegetation is in thermal equilibrium with soil (T_{eff} ~*TSURF*~ T_c). Different models [Wang et al., 1983; Choudhury et al., 1979; Wigneron et al., 2011, Lawrence at al., 2013] formulated the smooth and rough surface reflectivity's. The effective rough surface reflectivity in horizontal (*H*) or vertical (*V*) polarization is given by

$$R_{rs}^{H,f}(\theta) = \left[\left(1 - Q_f\right) R_s^{H,f}(\theta) + Q_f \, R_s^{V,f}(\theta)\right] e^{-G(\theta) h_f} \qquad (2.3\text{ a})$$

$$R_{rs}^{V,f}(\theta) = \left[\left(1 - Q_f\right) R_s^{V,f}(\theta) + Q_f \, R_s^{H,f}(\theta)\right] e^{-G(\theta) h_f} \qquad (2.3\text{ b})$$

where f and θ are frequency and angle of incidence of the measurement. $R_s^{p,f}(\theta)$ are smooth Fresnel reflectivity, Q_f is a polarization mixing factor, h_f is equivalent roughness parameter related to surface RMS height, and horizontal correlation length, $G(\theta) = \cos^{n_p}(\theta)$ and n is an angular exponent. For model proposed in [Wang et al., 1983] assumes $G(\theta)=1$ for Eq. 2.3 (a,b), whereas model in [Choudhury et al., 1979] assume $G(\theta) = \cos^2(\theta)$ and $Q_f=0$. Other empirical models [Wigneron et al., 2011] developed later consider correlation length to calculate equivalent roughness parameter. Model developed in [Lawerence et al., 2013] allows Q_f and n_p to be calculated from RMS height 'S' and correlation length 'L'. This avoids the assumption of constant values for these parameters and is polarization dependent. In this study we use, roughness model proposed by Lawrence et al. (2013).

As mentioned earlier, canopy affects top of the atmosphere brightness temperature (ignoring atmospheric attenuation at L-band) by either radiating its own microwave radiation or

absorbing/scattering radiation emanated by the soil. These attenuation effects of vegetation are described by vegetation optical depth $\tau\ (\lambda, p)$ and single scattering albedo $\omega\ (\lambda, p, \theta)$ in (2). These factors are dependent on frequency, polarization, incidence angle, vegetation water content and canopy structure [Mo et al., 1982; Ulaby et al., 1983; Jackson et al., 1990, 1991; Van de Griend et al., 2004; Wigneron et al., 2011]. The knowledge about the variability of ω_p for *H* and *V* polarization are limited [Brunfeldt and Ulaby, 1986]. The difference between ω_H and $\omega_{V,}$ is essentially shown by vegetation exhibiting preferential orientation [Van De Griend et al., 1994]. The difference however is considered to be small, thus ω_p is polarization independent.

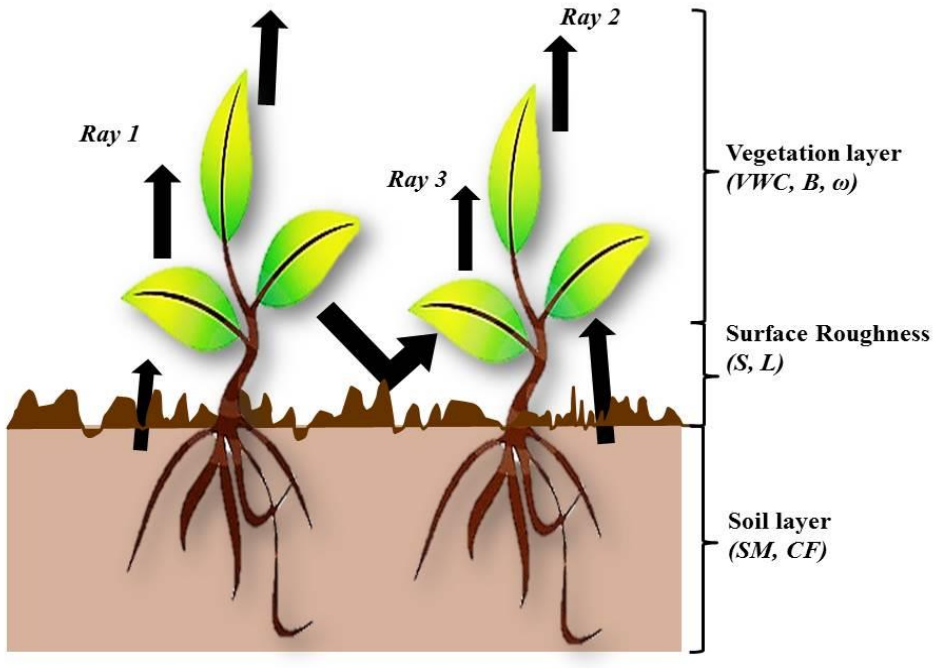

Figure 2.1 Three layer Zero Order Radiative Transfer (ZRT) Model, where *Ray 1*: Soil Emissions Intercepted-Scattered by Vegetation; *Ray 2*: Vegetation Emission; *Ray 3*: Soil-Vegetation Reflection/Attenuation

Table 2.1 Parameter ranges of corn and soybean SMAPVEX12 fields for selected sampling days

Parameters SMAPVEX12	Crop Type	DOY 159	DOY 164	DOY 169	DOY 174	DOY 181	DOY 190	DOY 199
Soil moisture *(SM)* (V/V)	Corn	0.02-0.34	0.07-0.46	0.1-0.45	0.05-0.37	0.012-0.3	0.03-0.43	0.03-0.38
	Soy bean	0.04-0.47	0.12-0.57	0.06-0.52	0.08-0.59	0.04-0.41	0.04-0.45	0.05-0.40
Clay fraction *(CF)* (%)	Corn	5 % - 38 %						
	Soy bean	4.5 % - 66 %						
RMS height *(S)* cm	Corn	0.3 - 1.7						
	Soy bean	0.2 – 2.0						
Correlation length *(L)* cm	Corn	4.5 - 23						
	Soy bean	5 - 23						
Surface Temp *(TSURF)*	Corn	293-300	281-294	288-293	287-295	292-298	291-300	291-296
Kelvin, K	Soy bean	292-302	281-292	287-293	286-292	290-298	292-299	292-299
Vegetation Water Content *(VWC)* Kg/m2	Corn	no veg	0.01-0.1	0.1-0.39	0.15-0.45	0.5-1.5	1.7-2.4	2.2-4.22
	Soy bean	no veg	0.03-0.13	0.04-0.25	0.05-0.29	0.05-0.52	0.08-0.7	0.17-2.7
Vegetation Structure *(B)*	Corn	0.1-0.15						
	Soy bean	0.05-0.1						
Scattering Albedo *(ω)*	Corn	0-0.05						
	Soy bean							

Table 2.2 Parameter ranges of corn and soybean SMEX02 fields for selected sampling days

Parameters SMEX02	Crop Type	DOY 178	DOY 182	DOY 186	DOY 188
Soil moisture (*SM*) (V/V)	Corn	0.07-0.16	0.05-0.15	0.06-0.27	0.11-0.37
	Soybean	0.07-0.16	0.04-0.14	0.05-0.23	0.1-0.29
Clay fraction (*CF*) (%)	Corn	10 % - 40 %			
	Soybean	10 % - 40 %			
RMS height (*S*) cm	Corn	0.19-2.5			
	Soybean	0.21-3.05			
Correlation length (*L*) cm	Corn	0.56-26.9			
	Soybean	0.43-20.80			
Surface Temperature (*TSURF*) Kelvin, K	Corn	296.15-318.5	299-310	296.15-304.5	295.85-299
	Soybean	296.15-320.65	300.15-312.55	297.4-310.75	294.65-309.65
Vegetation Water Content (*VWC*) Kg/m2	Corn	1.97-4.27	2.25-5.23	3-6	3.5-6.05
	Soybean	0.2-0.47	0.27-0.66	0.32-0.69	0.4-1.43
Vegetation Structure *(B)*	Corn	0.1-0.15			
	Soybean	0.05-0.1			
Scattering Albedo (ω)	Corn Soy bean	0-0.05			

The single scattering albedo ω accounts for the canopy single volume scattering (Ray 2 and 3, multiple scattering is considered zero, Fig. 2.1) and total extinction properties exhibited by the canopy. It is defined as the ratio of canopy scattering efficiency to the total extinction efficiency (sum of scattering and absorption within canopy) [Mo et al., 1982; Ulaby et al., 1983a]. By fitting model to experimental observations for vegetated fields, several studies [Brunfeldt and Ulaby, 1986; Pampaloni and Paloscia, 1986; Jackson, 1993] have estimated the value of single scattering albedo. The general consensus among these studies indicates that at 1.4GHz, ω is small and varies from 0.05 and 0.13.

The vegetation optical depth τ_p is related to the vegetation thickness and extinction efficiency of the canopy. The amount of radiation that is not scattered or absorbed by the vegetation is represented by optical depth τ_p, which describes the amount of radiation propagated through vegetation. Since canopy in essence acts as water cloud, τ_p is empirically related [Schmugge et al., 1986, Saleh et al., 2007] to the integrated canopy water content VWC as total mass of water contained in the vertical column of the canopy per unit ground surface area. The canopy architecture, orientation, thickness and density of vegetation characterize the extinction efficiency of the vegetation. The vegetation optical depth commonly used in soil moisture retrieval algorithms is given by $\tau_p = VWC \times B$, [Jackson et al., 1991] where B is vegetation parameter that depends on factors such as frequency, polarization, angle and vegetation type. Thus, the vegetation attenuation parameters $\tau_{p,f}$ and $\omega_{f,\theta}$ used in vegetation model are based on the assumption that 1) at L band, scattering albedo is small and multiple scattering may be ignored 2) the canopy reflectivity is zero, thus reflection losses at the boundary are not accounted, 3) due to small refractive index of vegetation layer, soil reflectivity is used in (2) instead of vegetation-soil reflectivity. Several soil moisture retrieval algorithms are developed and validated [Jackson, 1993; Owe et al., 2001;

De Jeu and Owe, 2003; Njoku and Chan, 2006; Jones et al., 2011; Santi et al., 2012] based on the above assumptions for soil and vegetation models.

2.5 Global Sensitivity Analysis: Sobol Method

Sensitivity analysis is generally used to identify and quantify the critical inputs (parameters and initial conditions) to a model. Several sensitivity techniques have been developed over time depending on the objective of the study and computational demand. When the input factors are known with little uncertainty, then sensitivity measure is computed by partial derivative of output function with respect to the input factors. This method as mentioned earlier is called local sensitivity analysis (LSA). LSA techniques are best suited for linear systems, since the impact on model output is studied by varying input factors one at a time and very close to the nominal values. On the other hand, land surface models (LSM) or in general any environmental model are rarely additive, since land surface processes are highly nonlinear and non-monotonic in nature, exhibiting higher order interactions between the parameters. In such cases using local SA methods are not suitable for quantitative analysis, since they fail to capture the heterogeneity in input factors. Therefore, techniques such as global sensitivity analysis (GSA) are used, which incorporate variability in the input factors through probability distribution functions using Monte Carlo simulations. Since, Sobol method is capable to handle non-linear and non-monotonic functions we use it to analyze our radiative transfer model. We briefly introduce the main concepts of Sobol method here for completeness.

The concept behind variance based technique is to quantify the amount of variance due to each input factor X_i contributed towards the unconditional variance of the output $V(Y)$. Suppose $Y=f(X)$ is a model function, then Y is the output, $X=(X_1,X_2,X_3....X_K)$ are K independent input parameters, each one varying over a probability distribution. Applying this configuration to our

analysis results in, Y as the output brightness temperature, f as the ZRT model, and $\boldsymbol{X_K}$ as the input parameter vector with K=8, and [X_1, X_2, X_3, X_4, X_5, X_6, X_7, X_8] as [Soil Moisture (SM), Clay Fraction (CF), Surface Roughness- RMS height (S), Surface Roughness- Correlation length (L), Surface Temperature (TSURF), Vegetation Water Content (VWC), Vegetation Structure (B), Scattering Albedo (ω)].

Sobol suggested that the function f can be decomposed into summands of increasing dimensionality;

$$f(X_1, X_2, \ldots . X_7) = f_0 + \sum_7 f_i\,(X_i) + \sum_{i<j} f_{ij}(X_i, X_j) + \cdots + f_{1\ldots 7}(X_1, \ldots .7) \qquad (2.4)$$

If each term in the above equation is square integrable with average zero and input parameters are not dependent, then f_0 is a constant and is equal to the expectation value of the output and summands are mutually orthogonal. And this decomposition is unique [Sobol, 1993]. With the assumption that the parameters are mutually orthogonal, the total unconditional variance is;

$$V_T = \sum_7 V_i + \sum_{i<j} V_{ij} + \cdots + \sum V_{1,2,3,\ldots 7}\,; \qquad (2.5)$$

$$V_i = V[E(Y|X_i)]; \quad V_{ij} = V[E(Y|X_i, X_j)] - V_i - V_j \qquad (2.6)$$

where $V[E(Y|X_i)]$ is the expected amount of variance that would be removed if the true value of X_i is learnt, $V_{ij} = V[E(Y|X_i, X_j)]$ describes the joint effect of pair (X_i, X_j) and is called second order effect, similarly higher order effects can be computed.

GSA ranks the input parameters based on the amount of variance that would disappear on learning the true value of x*. For a nonlinear model, the total output variance is decomposed into variances caused due to first (fractional variance of X_i to output) and higher order (variance caused due to interactions between the factors, X_{ij}, $i \neq j$).

Using first and other order variances, sensitivities indices S_i are calculated by diving $V[E(Y|X_i)]$ with total variance V_T.

First Order Sensitivity Measure: $S_i = \frac{V_i}{V}$; (2.7)

Second Order Sensitivity Measure: $S_{ij} = \frac{V_{ij}}{V}$; (2.8)

Total $S_{Ti} = S_i + \sum_{j \neq i} S_{ij} + \ldots$. (2.9)

where S_i is the first order sensitivity index for factor X_i, which measures variance contribution of parameter X_i on total model variance, S_{ij} measures variance of interactions between parameters i and j, and S_{Ti} is sum of main effects and all their interactions with the other parameters (up to k^{th} order). The calculation of S_{Ti} can be based on $E[V(Y|X_{-i})]$, variation of all parameters except Xi;

$S_{Ti} = \frac{E[V(Y|X_{-i})]}{V(Y)}$. (2.10)

For additive models, S_i and S_{Ti} are equal and sum of S_i(and thus S_{Ti}) is 1. For nonlinear models (or non-additive models) S_{Ti} is greater than S_i and $\sum S_i < 1$ ($\sum S_{Ti} > 1$). The difference between S_{Ti} and S_i is used to analyze the interactions between parameter X_i and the other parameters.

2.6 Evaluation of the Parameters using Sensitivity Analysis

A high value of S_i implies X_i as significant parameter and should be given priority in estimation, whereas a low value of S_{Ti} indicates that the parameter is not important either singularly or via interactions, and can be frozen to its optimal value (parameter fixing). We analyzed a time series Global Sensitivity Analysis (GSA) of Zero-Order Radiative Transfer (ZRT) Model to input parameters. The analysis was conducted for each of the four days in SMEX02 fields and for seven days in SMAPVEX12 fields. The field observations of SMEX02 and SMAPVEX12 are significantly different w.r.t soil moisture, soil texture, soil temperature, surface roughness and vegetation water content. It is assumed that the field observations are true representative of variability observed. In this study, we assume uniform distribution for all parameters to reproduce the heterogeneity observed in the fields. Field observations are used to represent maximum (max)

and minimum (min) values. Tables 2.1 and 2.2 show parameter ranges of corn and soybean for SMAPVEX12 and SMEX02. All fields of corn (or soybean) did not show a similar growth trend, which may be due to irregular planting periods. In addition, not all fields were sampled on all sampling days, and this has resulted in irregular ranges for VWC. Since we want to study the sensitivity analysis for growing vegetation, we used higher VWC values than previous sampling day. It is assumed that parameters such as Clay Fraction (CF), Surface Roughness RMS height (S), Surface Roughness Correlation Length (L), Vegetation structure (B) and scattering albedo (ω) are static during our analysis period, and same range is considered for all sampling days. Since, there were no major agricultural practices during the growing cycle, our assumption on similar surface roughness on all days holds valid.

To estimate first order and total sensitivity indices S_i, and S_{Ti} for k parameters with N sample size requires $N\ (k+2)$ model evaluations, i.e., for K=8 parameters and N=30,000 sample size, we performed 3,00,000 model evaluations. While computing Sobol indices, we employ Sobol quasi random sampling instead of standard Monte Carlo sampling schemes. To avoid lumped sampling or clustering, quasi random sampling adds samples to the sequence away from the earlier sampled points and fills the unit hypercube uniformly. Also quasi random sampling results in faster convergence rate of $1/n$ as compared to $1/\sqrt{n}$, which is necessary to reduce computational demands.

2.6.1 Bootstrapping

In order to build confidence intervals for the first order and total Sobol sensitivity indices, we use bootstrap technique with resampling (Efron et al., 1993), since it is computationally very demanding to repeat $N.(k+2)$ model runs several times. The N samples used for the model evaluations were sampled 1000 times with replacement, and sensitivity indices were calculated

each time. The 95 % confidence intervals were then constructed on the distributions obtained for S_i's and S_{Ti}'s using percentile method.

2.7 Results and Discussions

We analyzed our results at N=30,000, where the sensitivity indices were found to be stabilized (Fig. 2.2). In the following sections, we present and discuss the Sobol sensitivity indices for each parameter for SMAPVEX12 and SMEX02. For each parameter, a spatio-temporal variation in first order sensitivity index along with parameter interactions is presented. We also discuss the influence of soil moisture range on sensitivity measures. Tables 2.3 and 2.4 present first order and total sensitivity indices along with their 95% confidence intervals which are obtained through bootstrapping. We calculated the sensitivity indices of all parameters for 0.05 V/V increment in SM for selected days, and observed how parameter sensitivity changes for narrow range of SM; Fig 2.7(A-E). Though SMAPVEX12 and SMEX02 are climatically similar regions, they exhibited varied field conditions. SMAPVEX12 fields showed large variation in soil moisture (0.02-0.59) and clay fraction (0.045-0.66), whereas SMEX02 fields showed large variation in vegetation water content (1.9 - 6.05) and surface roughness.

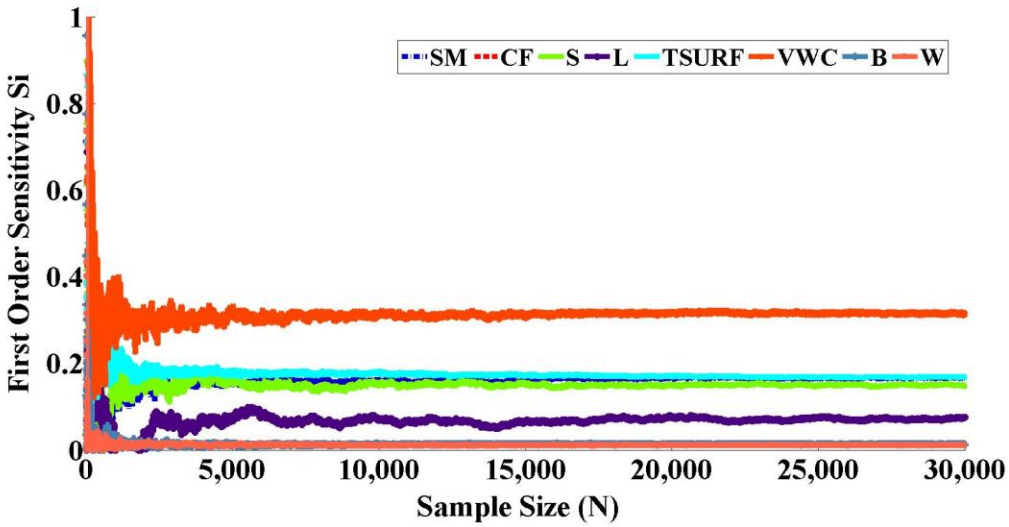

Figure 2.2 Evolution of first order sensitivity index for Soil Moisture *(SM)*, Clay fraction *(CF)*, RMS height*(S)*, Correlation length *(L)*, Surface Temperature *(TSURF)*, Vegetation Water Content *(VWC)*, Vegetation structure parameter *(B)*, Scattering Albedo *(ω)*.

2.7.1 First Order Sensitivity Measures

2.7.1.1 Soil Moisture (SM)

In general, brightness temperature showed higher sensitivity to SM in SMAPVEX12 than in SMEX02 due to wider SM ranges in case of SMAPVEX12 fields. A clear temporal variability in SM sensitivity due to wetting and drying cycle can be seen in both the fields. As expected, there is a decrease in SM sensitivity with increase in VWC, Figs. 2.3 and 2.5 (SMEX02: DOY_186, 188; SMAPVEX12: DOY_199). We also noticed that SM sensitivity to brightness temperature does not increase linearly with increase in SM. For example, DOY_164 and, 169 show high SM (max: 0.45 v/v) observed in corn fields for SMAPVEX12, however this increase in SM is not reflected in increased SM sensitivity to brightness temperature. Similar features are observed for DOY_188 during SMEX02. To analyze this behavior further, we calculated sensitivity indices for 0.05 V/V range in SM for selected days (Fig 2.7(A-E)). Soil moisture shows a decreasing exponential function (R^2~0.99) with very low sensitivity from 0.2 V/V onwards. Soil water in the range of 0.01-0.1V/V are tightly bound by adhesion forces to soil particles, thereby exhibiting emissitivities which are close to dry soil 0.95, but with increase in SM the unbound water also called as 'free water' increases thus reducing emissivities steeply to 0.6 for SM 0.2 V/V, beyond which there are no significant changes. This is because after a certain SM value ('transition soil moisture') any further increase does not influence emissivity significantly [Schmugge et al., 1974]. However, the transition soil moisture changes with soil texture, being higher for more clayey soils. SM shows higher sensitivity in lower clay soils with steep decrease in SM sensitivity with increase in SM ranges, whereas in higher clay soils the SM sensitivities are small and decreases less steeply (Fig 2.7 (C, D)). The increased dominance of texture in higher clay soils and higher sensitivity to roughness effects with increasing SM is also a reason for low SM sensitivity Fig. 2.7 (A-F).

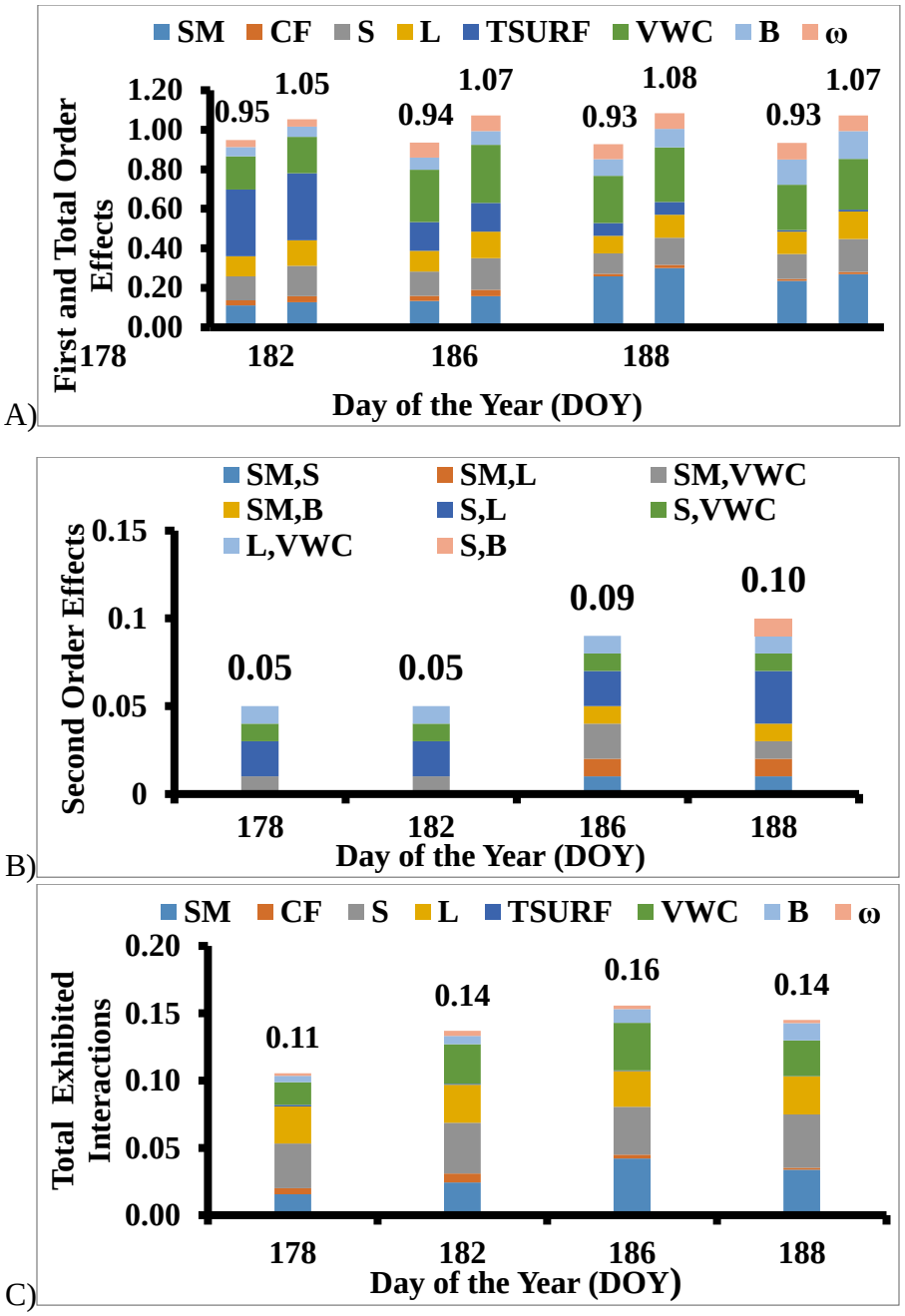

Figure 2.3 SMEX02 Corn Fields A) First Order S_i (left) and Total Sensitivity S_{Ti} (right), B) Second Order Sensitivity Measures S_{ij}, C) Total Parameter Interactions for DOY_178/182/186/188. Sum of sensitivity indices are mentioned on top of bars.

2.7.1.2 Clay Fraction (CF)

Compared to other parameters, brightness temperature shows consistently small sensitivity to CF in field condition for both SMAPVEX12 and SMEX02 when compared to other parameters. Higher CF sensitivities are realized in soybean fields in SMAPVEX12 due to higher CF % observed. As expected, CF signature is more visible in bare and dry conditions. Analyzing the CF sensitivity for increasing SM ranges, it is noticed that CF shows a concave sensitivity function with highest sensitivity noticed around 0.15-0.2 V/V for higher clay soils (soybean field in Winnipeg) and around 0.1-0.15 V/V for lower clay soils (corn fields in Winnipeg and SMEX02 fields). Soil texture is important, since it determines particle surface area, size and shape which influence the amount of bound and free soil water. Thus, sensitivity of CF increases till transition SM since it determines surface area for bound water. Beyond the transition SM, influence of CF through adhesion forces reduces, thereby reducing the sensitivity of CF with increase in SM. As this transition SM is higher in higher clay soils (SMAPVEX12) we notice a peak around SM range 0.15-0.2 V/V

2.7.1.3 Surface Roughness (S and L)

In general, significant surface roughness effects are noticed in SMEX02 fields than SMAPVEX12. Interestingly, for a similar surface roughness, brightness temperature shows higher sensitivity to roughness parameters (S and L) on wet days (SMAPVEX12: DOY_164, 169 and SMEX02: DOY_188) than on dry days. Analyzing the sensitivity of both RMS height 'S' and correlation length 'L' w.r.t. SM ranges, resulted in an increasing sensitivity function for S and L with increasing SM. As expected sensitivity indices of RMS height S is higher than L. But, surface roughness parameters (S and L) show different sensitivity functions w.r.t SM and soil texture (Fig 2.7 (A-F)). We notice, a linear sensitivity function in case of higher clay soils, (R^2~0.97: CF 0.05-

0.66, soybean in Winnipeg) and a logarithmic function in case of lower clay (R^2~0.94; CF 0.05-0.38, corn in Winnipeg) best fit the analysis. In case of soybean fields (Winnipeg, higher clay soils), S overrides SM and CF sensitivity curves around 0.05-0.1 V/V and 0.25-0.3V/V, respectively, whereas in case of corn fields (Winnipeg, low clay soils) S overrides SM and CF sensitivity around 0.1-0.15 V/V Fig. 2.7(C-D). Thus, the roughness observed before S overriding CF sensitivity could be accounted due to dielectric volume scattering in soils, whereas after which roughness effects are contributed mainly due to surface contributions (S and L). With further increase in SM, spatial variability of SM in horizontal direction due to lateral conductivity starts to dominate. This is clearly noticed with correlation length (L) overriding SM and CF sensitivity at 0.2-0.25 V/V and 0.35-0.4 V/V, respectively in soybean (Winnipeg, higher clay soils), whereas in case of corn (Winnipeg, lower clay soils) L overrides SM and CF sensitivity around 0.2-0.25V/V, Fig. 2.7(C-D). However, in Iowa, due to higher roughness conditions and lower CF range, S and L overrides SM at all moisture conditions (Fig 2.7. (A-B)). Chauhan et al. (2002) also found that surface roughness gain more impact in wetter conditions. Our results are also supported by, Wigneron et al. (2001), who proposed surface roughness may be a contribution of dielectric roughness and physical roughness. And, according to Panciera et al. (2009) higher roughness conditions are observed in clayey soils than sandy soils due to higher moisture heterogeneity exhibited by clayey soils.

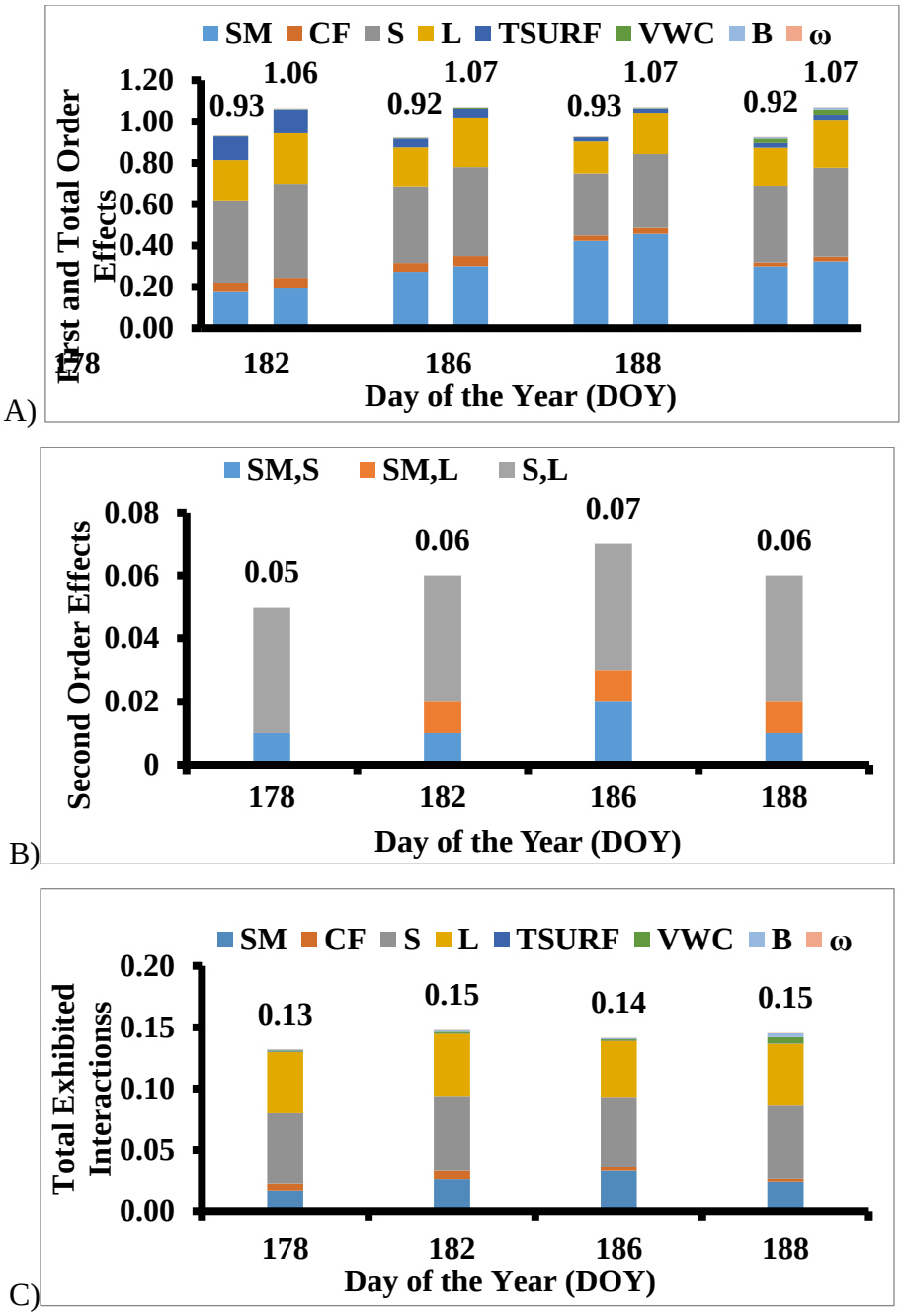

Figure 2.4 SMEX02 Soybean Fields A) First Order S_i (left) and Total Sensitivity S_{Ti} (right), B) Second Order Sensitivity Measures S_{ij}, C) Total Parameter Interactions for DOY_178/182/186/188. Sum of sensitivity indices are mentioned on top of bars.

2.7.1.4 Surface Temperature (TSURF)

Surface temperature effects are much less realized in SMAPVEX12 fields but shows significance on dry days of SMEX02 fields (DOY_178, 182) (Fig. 2.3(A), 2.4(A)). This is due to wide and higher ranges of TSURF observed in SMEX02. Also, TSURF shows a decreasing sensitivity function with increasing SM as expected. TSURF does not participate in any second order interactions. For any TSURF range, it shows higher sensitivity at lower SM ranges and gradually decreasing with increasing SM.

2.7.1.5 Vegetation Water Content (VWC)

Sensitivities of VWC exhibits clear spatio-temporal variation, with higher interactions observed on higher VWC and wet days. Due to wider and higher VWC ranges observed in SMEX02 fields, high first order sensitivities are observed in SMEX02 than in SMAPVEX12 (Figs. 2.3, 2.4, 2.5, and 2.6). We notice a consistency w.r.t VWC range and sensitivity between SMEX02 (DOY_178) and SMAPVEX12 (DOY_199), indicating the first order sensitivity of VWC remains similar with observed VWC ranges irrespective of other field conditions, however with different higher order interactions. A significant contribution from VWC is realized in case of corn plants all days of SMEX02 and SMAPVEX12 (DOY_181-199). Also, an increasing sensitivity function for VWC at higher SM ranges is observed Fig.2.7 (A, E, F). Vegetation shows an exponential growth in the SMAPVEX12 fields where significant VWC is noticed on last three sampling days of SMAPVEX12. The increased sensitivity to VWC for soybean on DOY_199, when mean (VWC) > 1kg/m^2 is observed, which otherwise is not noticed on other sampling days of SMAPVEX12.

2.7.1.6 Vegetation Structure (B)

Corn fields show more sensitivity to B parameter than soybean fields, due to the definite vertical structure of corn plants (Fig. 2.3), which is otherwise hardly noticed in soybean plants. The B parameter shows a gradual increase in its sensitivity with growing vegetation (VWC) and SM. With growing vegetation, there is a progressive change in canopy structure i.e., length, thickness and size of leaves, stalks, etc. This changing canopy structure modifies soil radiation through scattering and adds its own emissions, this result in soil and vegetation interactions as observed. The first order effects are realized for corn on all sampling days (SMEX02) and DOY_190,199 (SMAPVEX12). We clearly notice the interception/scattering of soil radiations by B through (SM, B) is for grown corn plants which otherwise not seen in soybean. Also, an increasing sensitivity function of B with SM is observed Fig. 2.7 (A, E, F).

2.7.1.7 Single Scattering Albedo (ω)

Similar to B parameter, brightness temperature shows primarily no sensitivity to albedo in soybean plants but its influence is realized in corn plants. Like VWC and B, albedo also shows increasing sensitivity with growing vegetation. Also, we noticed albedo did not participate in any higher order interactions. Nevertheless, this might not be the case at higher albedo values which are common in bushy and structured plants. However, unlike VWC and B, albedo shows a decreasing sensitivity with increasing SM. Therefore, assuming a constant look-up table for albedo and B, under all SM conditions, VWC and vegetation types will compromise SM retrieval accuracy. Because, B and albedo show increasing sensitivity with growing vegetation, a combined parameter dependent on VWC can be developed.

2.7.2 Second Order Interactions

SMEX02 fields show more of higher order interactions than SMAPVEX12 fields, due to higher VWC and roughness conditions observed in SMEX02 fields. In the following discussion, an overview of total interactions and second order interactions are presented. In past environmental studies using GSA, interactions are sufficiently captured by second order interactions, however in this soil moisture study we notice interactions greater than second order are also significant.

2.7.2.1 Interactions of Soil Moisture (SM, VWC), (SM, B), (SM, S) and (SM, L):

The upward soil emission contributing to the brightness temperature is interrupted by vegetation, thus determining the amount of soil radiation passing through canopy. This interception of soil emissions by vegetation water content (VWC) and vegetation structure (B) is reflected through interactions between (SM, VWC) and (SM, B). As such, a consistent (SM, VWC) interactions are seen on all sampling days in corn (SMEX02) and on DOY_181-199 (SMAPVEX12), clearly displaying the shielding effect of grown canopy which are otherwise not observed in early stages of field campaign of SMAPVEX12. Apart from VWC, vegetation structure (geometry, orientation and thickness etc.) also play a significant role in screening soil emissions and interception of rainwater, displaying an interaction of (SM, B) on DOY_186,188 (SMEX02) and DOY_199 (SMAPVEX12). Also, the influence of B parameter increases with growing canopy. Interestingly, an increase in SM on DOY_188 did not result in increased (SM, VWC) interactions, but produced interactions between surface-roughness with vegetation, discussed below. The scattering of soil emission by surface roughness (RMS (S) and (L)) are realized through interactions of (SM, S) and (SM, L). The scattering of soil radiations by RMS height (S) is realized on all sampling days, whereas (SM, L) is realized only on higher SM conditions and smaller L values (SMEX02 fields (DOY_182-188). This is because, the

connectivity of soil water flow in horizontal direction starts to influence at higher SM conditions. The correlation lengths (L) which is the periodicity of surface will then define soil water flow, thereby displaying (SM, L) interactions. Whereas, the (SM, S) are expected in all conditions due to the scattering influence of random roughness (S) on soil emissions. This can also be realized through Fig. 2.7 (A-F) where increase in SM, sensitivity of surface S and L parameters increases.

A)

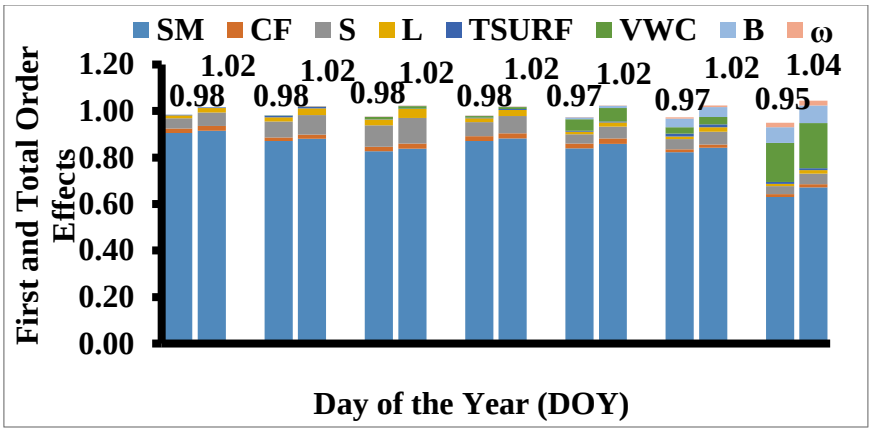

B)

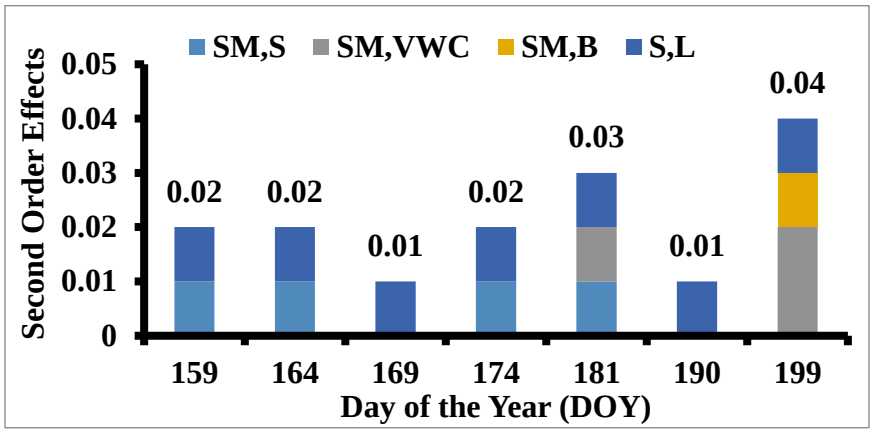

C)

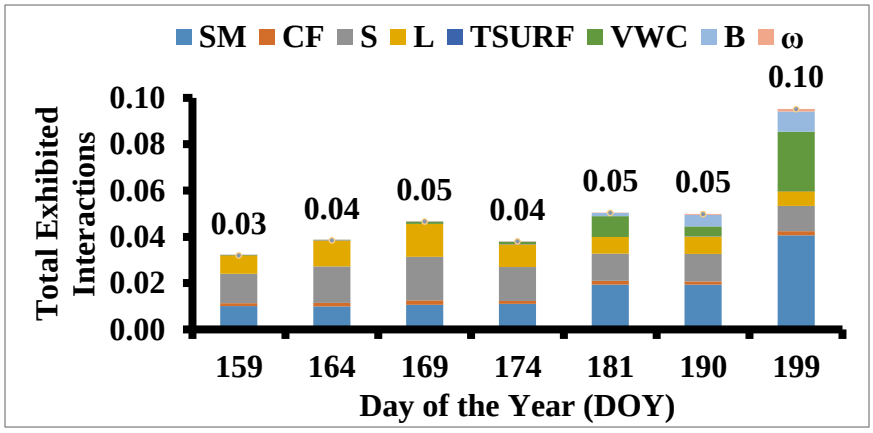

Figure 2.5 SMAPVEX12 Corn fields a) First Order S_i (left) and Total Sensitivity S_{Ti} (right), b) Below: Parameter interactions, c) Second Order Sensitivity Measures S_{ij} for DOY_178/182/186/188. Sum of sensitivity indices are mentioned on top of bars.

A)

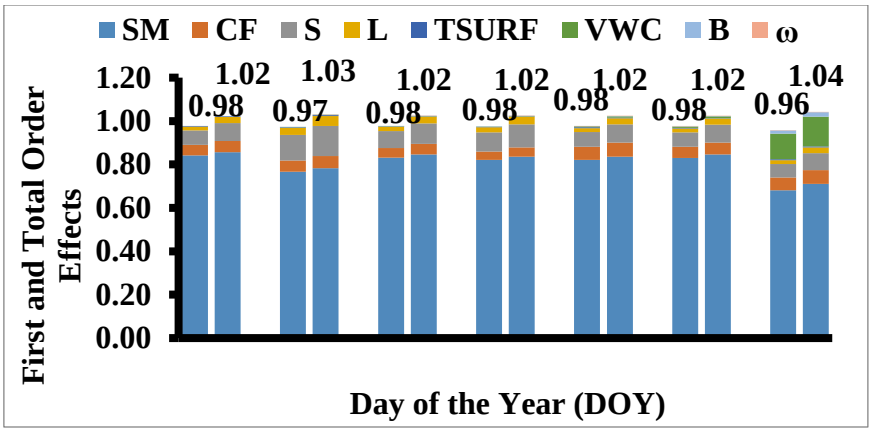

B)

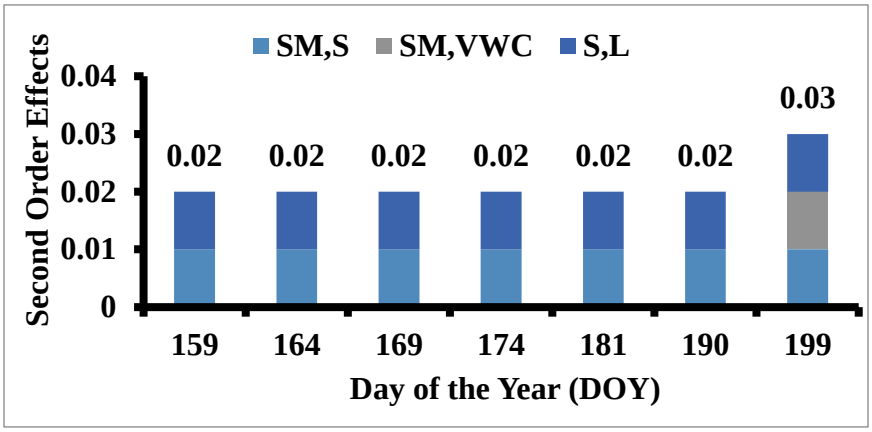

C)

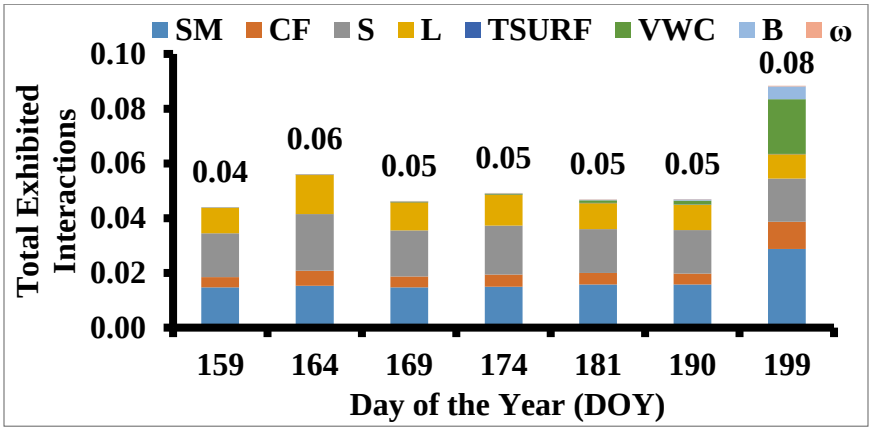

Figure 2.6 SMAPVEX12 Soybean fields A) First Order S_i (left) and Total Sensitivity S_{Ti} (right), B) Second Order Sensitivity Measures S_{ij}, C) Parameter interactions, for DOY_178/182/186/188. Sum of sensitivity indices are mentioned on top of bars.

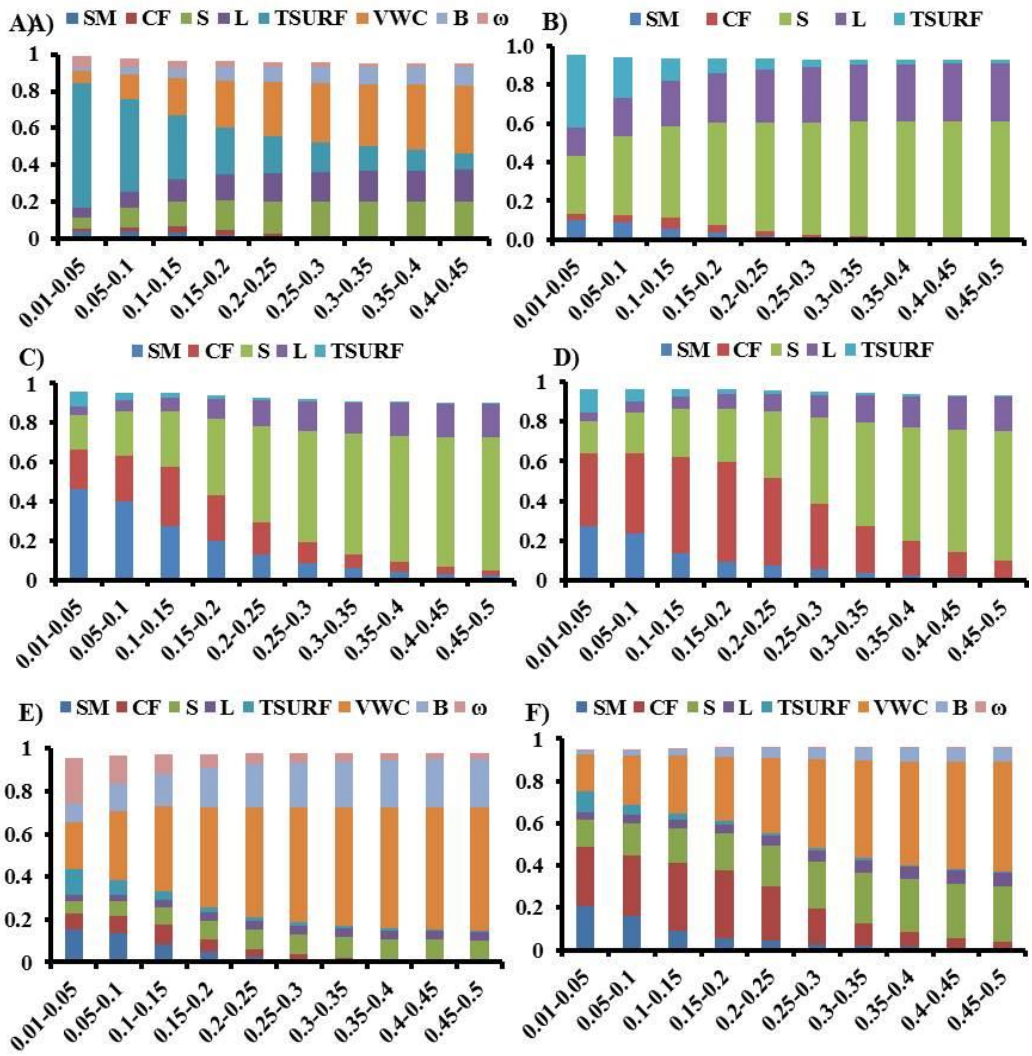

Figure 2.7 First Order Sensitivities of Parameters (S_i) on Y-axis and Soil Moisture (SM) ranges on X-axis, A) SMEX02 Corn DOY: 178, B) SMEX02 Soybean DOY: 178, C) SMAPVEX12 Corn DOY: 159, D) SMAPVEX12 Soybean DOY: 159, E) SMAPVEX12 Corn DOY: 199, F) SMAPVEX12 Soyeban DOY: 199.

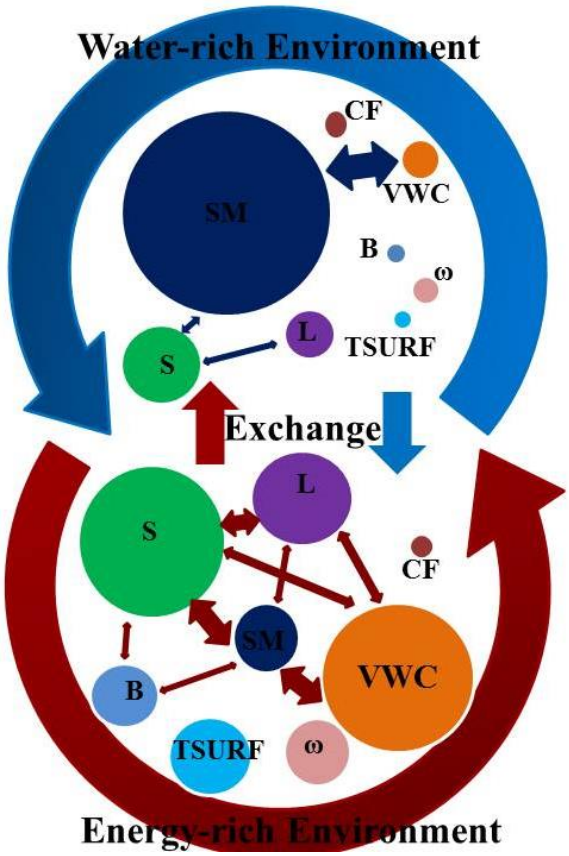

Figure 2.8 Proposed conceptual diagram, where interactions observed in the Energy rich environments are different and higher than those observed in Water rich environments. Different parameters are represented by different colors, where parameter's contribution is represented by circle size and parameter interactions by the arrow thickness.

2.7.2.2 Interactions of Surface Roughness (S, L), (S, VWC), (S, B) and (L, VWC)

An interaction of (S, B), (S, VWC) and (L, VWC) are noticed only in corn (SMEX02) which are otherwise not noticed in soybean (Iowa), due to prominent vegetation structure and higher VWC observed in corn plants which participate in scattering soil radiations. However, none of these interactions are observed in SMAPVEX12 fields due to small VWC and surface roughness. Therefore, we can expect to see interactions between surface roughness and vegetation parameters in structured plants with significant VWC. Also, a consistent (S, L) interaction is realized on all sampling days in SMEX02 and SMAPVEX12 fields emphasizing their underlying correlation.

2.7.3 Total Interactions, Linearity and Non-Linearity

For additive models, first order and total order sensitivity indices are equal and sum to 1 [Satelli et al., 2004]. In SMAPVEX12 fields, ZRT model behave almost linearly with non-linearity increasing with growing canopy displaying lower and higher order interactions. Higher and lower order interactions of almost ~ 2% each are seen on all sampling days, and increasing up to ~ 6 % at the end of field campaign (Fig. 2.5 and 2.6 (B)). Total interactions of ~ 5% are seen on almost all days but increases up to ~10 % on DOY_199 in SMAPVEX12 fields (Fig. 2.5 and 2.6 (C)). In case of SMEX02 fields, ZRT model behaves a lot more nonlinearly, because of higher VWC and roughness conditions. In case of corn fields, first order effects are contributed by vegetation whereas in soybean fields first order effects are contributed by roughness conditions, which are otherwise shielded by corn plants and displayed through second order interactions (Fig. 2.3 and 2.4 (B)). Higher and lower order interactions of 7% each are noticed with total interactions of ~15 % in SMEX02 fields (Fig. 2.3 and 2.4 (C)), that is quite significant in the context of soil moisture retrieval.

2.8 Summary and Conclusions

GSA method is particularly useful for non-linear models with higher order interactions. Using GSA for Zero-Order Radiative Transfer (ZRT) model resulted in primarily four parameters (SM, VWC, S and L) in Iowa region and one parameter (SM) in Winnipeg region to be sensitive to brightness temperature, with temporal variation. Also, parameter interactions increased with VWC and roughness conditions. An interception of soil emissions by growing vegetation are realized through interactions of (SM, VWC), (SM, B) and (S, VWC). A clear distinction between the similar influence of surface roughness and vegetation parameters are achieved along with spatio-temporally varying parameter interactions which can enhance our understanding of ZRT and improve soil moisture retrievals. Based on our analysis of GSA for ZRT model under different spatio-temporal conditions, we have proposed a conceptual model (Fig. 2.8). Considering the SMAPVEX12 fields to be water rich environment (due to higher observed SM) and SMEX02 fields to be energy rich environment (due to lower SM and wide ranges of TSURF), our results indicate that first order effects of parameters changes with water and energy rich environments. Particularly, parameter interactions were observed to be higher and diverse in energy rich environments (SMEX02) than water rich environments (SMAPVEX12). Even under the similar vegetation effects, DOY_199 (SMAPVEX12) and DOY_168 (SMEX02) we observe reduced parameter interactions in water rich fields (SMAPVEX12) than SMEX02 fields. Accounting for observed parameter interactions in *tau-omega* model and its contribution towards improving retrieved soil moisture accuracy is beyond the scope of this paper. Future work can include developing an environment based (water or energy rich) *tau-omega* model, with evolving first order and higher order interaction effects. In summary:

1) Attenuation of soil emission by vegetation (VWC, B) can be significant in structured plants (corn). And, this attenuation/scattering appears to increase with roughness and SM conditions.
2) The effects of B and albedo are not realized in soybean plants but show significant contribution in structured vegetation such as corn plants. These parameters show increasing sensitivity with increasing VWC and SM. Thus, assuming a constant value of B under all SM and VWC conditions will affect soil moisture retrieval accuracy.
3) For similar surface roughness conditions, sensitivity to roughness parameters is higher in wet soils than dry soils. Because of only skin depth emission in case of moist soils, radiations are more perturbed due to surface roughness in wet soils than in dry soils.
4) SM and TSURF show a monotonically decreasing sensitivity function, whereas VWC, S, L and B show a monotonically increasing sensitivity function with increase in SM. CF sensitivity shows an increasing function up to the transition SM, after which it drops exponentially with increase in SM. This peak observed at the transition SM changes with the percentage of clay fraction.
5) SM derived from brightness temperature pixels representative of wide SM conditions are more accurate than pixels representative of narrow(&higher) range of SM conditions, since SM retrieval accuracy will be compromised due to higher sensitivity to other parameters at narrow SM ranges.

3 UNDERSTANDING RADIATIVE TRANSFER MODEL ACROSS SPACE, TIME AND HYDRO-CLIMATES

3.1 Synopsis

A framework is proposed for understanding the efficacy of a radiative transfer model (RTM) with different support scales, and hydro-climates and aggregation (scaling) methods. In this paper, the sensitivity of brightness temperature T_B (H- and V-polarization) to physical variables (soil moisture, soil texture, surface roughness, surface temperature, and vegetation characteristics) is studied using global spatial sensitivity analysis (GSSA). The impact of upscaling from 800 m to 1.6 km, 3.2 km, 6.4 km, and 12.8 km on radiative transfer model (RTM) is illustrated using linear and inverse distance weighted upscaling methods for four different soil moisture field campaigns. Our results indicate that the sensitivity of brightness temperature (V- or H-polarization) is determined by the upscaling method and heterogeneity observed in the physical variables. Under higher heterogeneity, the T_B sensitivity to vegetation and roughness followed a logarithmic function with increasing support scale, while an exponential function is followed under lower heterogeneity. The sensitivity to surface temperature always followed an exponential function with support scale under all heterogeneity conditions. The sensitivity of T_B at H- or V-polarization to soil and vegetation characteristics varied with the spatial scale (extent and support) and the amount of biomass observed. Thus, choosing H- or V-polarization algorithm for soil moisture retrieval is a tradeoff between support scales, and land surface heterogeneity. For undisturbed natural environments such as SGP'97 and SMEX04, the sensitivity of T_B to variables remain nearly uniform and are not influenced by extent, support scales or upscaling method. On the contrary, for anthropogenically-manipulated environments such as SMEX02 and

SMAPVEX12, the sensitivity to variables are highly influenced by the distribution of land surface heterogeneity and upscaling methods.

3.2 Introduction

The remote sensing community aims to develop soil moisture products at various resolutions, as soil moisture finds application from local (e.g., crop water management), regional (e.g., flood and drought forecasting) to global scale (e.g., meteorology, climate dynamics) [Moran et al., 2015]. The active or passive sensors used for estimating soil moisture come with their own challenges such as accuracy, coarse resolution, Radio Frequency Interference (RFI), high sensitivity to vegetation/roughness, spatio-temporal coverage, big data challenges, etc., [Spencer et al., 2010, Mecklenburg et al., 2016]. Developing fine resolution soil moisture products can be achieved either by downscaling retrieved coarse-resolution soil moisture or downscaling observed brightness temperature (T_B) followed by soil moisture retrieval [Merlin et al., 2012, Das et al., 2014, Wu et al., 2014, Molero et al., 2016]. Several scaling algorithms have been developed in past using data fusion techniques integrating information from various scales (point/airborne/satellite), platforms (MODIS/LANDSAT/AVHRR etc.) sensors (active/passive), frequencies (P, L, C, and X), and land surface variables (surface temperature, NDVI etc.) [Piles et al., 2009, 2011, Shin et al., 2013, Song et al., 2014, Djamai et al., 2015]. For most cases, coarse-scale knowledge is estimated from smaller spatial scale features in which upscaling has reduced to the problem of change of support scale. Western and Bloschl [1999] defined the scale triplet (support, spacing, and extent) where, support is referred to area (or volume) integrated by individual soil moisture measurements. The scaling methods incorporate their own conceptual model uncertainties apart from the uncertainties of products used for downscaling/upscaling [Van de Griend et al., 2003, Dorigo et al., 2010, Merlin et al., 2015, Das et al., 2016]. Thus, for

downscaling/upscaling of either soil moisture or T_B, it first calls for understanding the propagation of errors/uncertainties through scale and heterogeneity of land surface variables.

The two main issues that still undermine large scale monitoring of soil moisture are scaling and land surface heterogeneity [Njoku et al., 1996, Western et al., 2002, Entekhabi et al., 2010]. Scaling of microwave theory/models developed over small spatial scales to coarser spatial scales has been a subject of research for the past three decades. Most environmental processes are non-linear in nature and the land surface variables (and their interactions) responsible for these processes vary across scales (space and time) [Ryu and Famiglietti 2006] resulting in complex scaling relationships. The sub-footprint landscape heterogeneity compromises the satellite-based soil moisture retrieval accuracy [Burke and Simmonds, 2003, Lakhankar et al., 2009, Roy et al., 2016]. For example, within a hydroclimate, the heterogeneity in land surface variables observed at 30 m resolution will be different from 100 m, 1 km, 5 km, and so on, and will be different if observed at different time periods, frequencies, polarizations etc,. There can also be considerable effects on retrieved soil moisture if the extent of the analysis or footprint shape/size varies, changing the range of heterogeneity observed for land surface variables. Thus, model calibration of soil-vegetation parameters across land surface heterogeneity and scale pose a challenge for remote sensing retrieval of soil moisture.

We hypothesize that, the varying heterogeneity in land surface variables (soil moisture, soil texture, surface roughness, surface temperature and vegetation characteristics i.e., vegetation water content, vegetation structure, and scattering albedo) through support scales, and different hydroclimates (across the USA) influence sensitivity of brightness temperature at V- and H-polarization. Thus, our objective is to propose a framework for understanding the efficacy of a radiative transfer model (RTM) for soil moisture retrieval with different support scales, and under

land surface heterogeneity. We performed the analysis using two-dimensional spatial maps of land surface variables as model inputs beginning from airborne 800 m and 1.5 km support scale. These variables are then upscaled to various supports (1.6 km, 3.2 km, 6.4 km, and 12.8 km) using two different averaging methodologies, to study the influence of upscaling methods on an RTM performance. Adopting global spatial sensitivity analysis (GSSA) [Lilburne and Tarantola , 2009, Saint-Geours et al., 2011, Sarrazin et al., 2016, Pianosi et al., 2016], the sensitivity to soil and vegetation characteristics across scales are evaluated.

3.3 Materials and Methods

3.3.1 Heterogeneity Observed in Various Hydro climates

The effects of varying heterogeneity on brightness temperature are studied in four different hydroclimates using data from field campaigns namely, SGP97 (Southern Great Plains'1997), SMEX02 (Soil Moisture Experiments'2002), SMEX04 (Soil Moisture Experiments'2004) and SMAPVEX12 (Soil Moisture Active Passive Experiments'2012)**.** These field campaigns were conducted approximately over 4-8 weeks window, primarily to validate soil moisture retrieval algorithms over a wide range of soil and vegetation conditions [Cosh et al., 2008, Jackson et al., 2010, McNairn et al., 2015, Moran et al., 2015]. The airborne remote sensing data for these field campaigns were observed at either 800 m or 1.5 km resolution, which is the base resolution for our analysis. The 800 m pixels are upscaled to support scales of 1.6 km, 3.2 km, 6.4 km, 12.8 km, and 1.5 km pixels are upscaled to 3 km and 9 km to coincide with Soil Moisture Active Passive (SMAP) target products. The variables such as soil moisture, surface temperature, vegetation water content, and soil texture are obtained from various sources, which are discussed under each field campaign. Variables such as surface roughness, vegetation structure, and single scattering albedo,

which are available only at sparse locations, are assumed to be scalars with a uniform probability distribution whose ranges are estimated from extensive field measurements.

3.3.1.1 Southern Great Plains Experiment'1997 (SGP'97), Oklahoma

The SGP'97 hydrology experiment was conducted in the sub-humid (Köppen climate classification-Cfa) region of central Oklahoma from June 18 through July 17, 1997. The topography of the region is moderately rolling and soils vary with a wide range of textures with large regions of both coarse and fine textures with an average annual rainfall and temperature of 750 mm and 288.85 K, respectively. The land use is dominated by rangeland and pasture with significant areas of winter wheat and other crops. The L-band Electronically Scanned Thinned Array Radiometer (ESTAR) was used to measure soil moisture at 800 m × 800 m resolution. An 800 m resolution daily effective soil temperature maps were generated using the ground based soil temperatures and grid based resampling program. The vegetation water content (VWC) map at 800 m resolution was developed from normalized difference vegetation index (NDVI) values computed using the Landsat TM imagery collected on July 25, 1997 [Jackson et al., 1999]. A combination of soil geographic database (STATSGO) and soil texture samples were used to develop resampled texture map at 800 m resolution [Lakhankar et al., 2009].

3.3.1.2 Soil Moisture Experiment'2002 (SMEX02), Iowa

SMEX02 experiment was conducted in Walnut Creek watershed, Iowa from June 23 through July 12, 2002. This region is classified as humid climate (Köppen climate classification-Dfa) with average annual rainfall of 835 mm and temperature 283 K. Considerable amount of variability in soil texture is observed in the region ranging from fine sandy loam to clay with the majority classified as silt loam with relatively low permeability [Jacobs et al., 2004]. Corn and soybean crops are the two dominant land covers of Iowa, covering approximately 50 % and 40 %,

respectively. The C- band Polarimeteric Scanning Radiometer (PSR-C) retrieved soil moisture at 800 m × 800 m resolutions [Bindlish et al., 2006] was used for the analysis. A total of four days (DOY 178, 182, 186, and 188) are selected to capture the temporal variability in land surface heterogeneity due to crop growth, temperature, and soil moisture changes. The Soil Survey Geographic Database (SSURGO) and Landsat-7/5 E/TM derived vegetation water content at 30m were resampled to 800 m × 800 m grids. The average of surface and 1-cm depth soil temperature are interpolated through kriging to obtain coverage for a grid size of 800 m.

3.3.1.3 Soil Moisture Experiment'2004 (SMEX04), Arizona

The SMEX04 field campaign was conducted with a primary focus on Walnut Gulch (WC) Experimental Watershed near Tombstone, operated by the Agriculture Research Service (ARS), U.S. Department of Agriculture (USDA) between August 2 and August 27, 2004 [Cosh et al., 2008]. The climate of this region is classified as semi-arid (Köppen climate classification- BSh), with mean annual temperature 290.85 K and receiving an average annual precipitation of 350 mm. The soils are generally well drained calcareous and gravelly loam with large percentages of rock ranging from nearly 0 % on shallow slopes to over 70 % on the very steep slopes. Vegetation of this region mainly comprises two-thirds of shrubs and remaining one-third is grassland. The polarimetric scanning radiometer (PSR) C-band retrieved soil moisture at regularly spaced grid of 800 m resolution was used. The ground based temperatures (surface and 5 cm temperatures are averaged) and MODIS (MOD11A1) surface temperature product are interpolated (kriging) to generate 800 m resolution surface temperature map. The 800 m resolution vegetation water content map was developed by interpolating high resolution Landsat TM and regularly ground sampled VWC [Yilmaz et al., 2008]. The SSURGO data at 30 m was resampled to obtain soil texture map at 800 m resolution. A total of four days (DOY 221, 222, 225, and 226) are selected based on the

availability of datasets and to study temporal variability in land surface heterogeneity. The surface roughness data was collected extensively over the Walnut Gulch (WG) watershed and sparely over the entire SMEX04 region using a pin board.

3.3.1.4 Soil Moisture Active Passive Validation Experiment'2012 (SMAPVEX12), Winnipeg

SMAPVEX12 was conducted from June 6th to July 17th 2012 in Winnipeg, Manitoba (Canada) which is classified as having extreme humid climate (Köppen climate classification-Dfb) [Peel et al., 2007], with average annual precipitation and temperature of 521 mm and 289 K respectively. The region captures wide variety of variability in land cover and soil texture within few kilometers while moving from southeast to northwest [McNairn et al., 2015]. The agricultural crops (mainly cereals, soybeans, canola, and corn) dominate southeast with heavy clay soils, whereas the north and east see more of lighter sandy and loamy soils with mixed land cover including forest, perennial pastures along with few crop fields. The analysis is conducted for all days (DOY 164, 167, 169, 174, 177, 179, 181, 185, 187, 192, 195, 196, and 199) using Passive Active L-band System (PALS) derived soil moisture and surface temperature at 1.5 km resolution [Colliander et al., 2015]. The VWC available at 5 m resolution estimated from Normalized Difference Water Index (NDWI) using SPOT and RapidEye satellite overpasses were resampled to 1.5 km grids.

3.3.2 Soil Moisture Retrieval Algorithm

The approach followed in this study was based on forward modeling using a first-order radiative transfer model also called as tau-omega (τ-ω) model [Mo et al., 1982] described in equation (3.1).

$$T_{B(p,f,\theta)} = e_{p,\theta,f}.T_{eff}.\exp\left(-\frac{\tau_{p,f}}{\cos\theta}\right) + T_c.\left(1-\omega_{p,f,\theta}\right).\left(1-\exp\left(-\frac{\tau_{p,f}}{cos\theta}\right)\right) +$$

$$T_c.\exp\left(-\frac{\tau_{p,f}}{cos\theta}\right).\left(1-\omega_{p,f,\theta}\right).\left(1-\exp\left(-\frac{\tau_{p,f}}{cos\theta}\right)\right).r_{p,f,\theta} \quad (3.1)$$

where $T_{B(p,f,\theta)}$ is brightness temperature [K]; T_{eff} is effective surface temperature [K]; T_c is effective vegetation temperature [K]; $e_{p,\theta}$ is the emissivity of the (rough) soil surface; $r_{p,f,\theta}$ is the rough surface reflectivity; $\tau_{p,f}$ is the nadir optical depth; $\omega_{p,f,\theta}$ is the single scattering albedo. The subscripts *p,* θ and *f* denote the polarization, angle of incidence, and frequency of measurement respectively. It is assumed that the canopy and soil temperature to be equal during morning thermal crossover which also corresponds to the planned time of observation for` SMAP around 6:00 h local sun time. The radiative transfer (equation 3.1) is essentially approximated as a summation of three components; *1)* the direct emission by soil and one-way attenuation by canopy (the first term), *2)* direct upward emission by canopies (the second term), and *3)* emission by plants and reflected by soil and thereafter attenuated by vegetation (the third term). The formulation in equation (1) is based on the assumptions that; a) the single scattering albedo is small (less than 0.2), and thus diffuse scattering is ignored; b) the air-vegetation reflectivity is assumed zero, thus ignoring losses at the boundary, and c) the refractive index of vegetation is approximately equal to air, which allows using the air-soil reflectivity in equation (3.1). The amount of soil microwave emission that is absorbed and scattered as propagated through canopy is given by the transmissivity of the vegetation and scattering albedo. The loss factor is dependent on the volume fraction of water in the canopy and the architecture of the vegetation. The extinction optical thickness τ_p is estimated as a product of vegetation water content (VWC) and structure of the canopy (*b*). Due to the complex geometry of the natural canopies, approximate values are estimated for canopy structure (*b*) from land cover data. The canopy water content is estimated using the Normalized Difference Vegetation Index (NDVI) and regression with ground sample vegetation data [Jackson

et al., 2004]. The τ_p and ω_p are polarization dependent because there may be differences in propagation of H-polarized and V-polarized wave under different canopy structures [Brunfeldt and Ulaby, 1986; Wigneron et al., 2011].

3.3.3 Global Spatial Sensitivity Analysis: Sobol Method

Global Spatial Sensitivity Analysis (GSSA) [Crosetto et al., 2000, Lilburne and Tarantola, 2009, Saint-Geours et al., 2011] relies on Sobol methods [Sobol, 1993], which can deal with nonlinear and non-monotonic relationships between inputs and output [Saltelli, 2002, Saltelli, et al., 2004, 2008, 2010]. These methods are based on the functional decomposition of variance (ANOVA) of the model prediction (**Y**) into partial variances caused due to each model inputs (**X**) (either considered singularly or in combination) i.e.,

$$V(Y) = \sum_{i=1}^{k} V_i(Y) + \sum_{i<j}^{k} V_{ij}(Y) + \ldots + V_{12..k}(Y) \quad (3.2)$$

where $V_i(Y)$ is the share of the output variance explained by the i^{th} model input; $V_{ij}(Y)$ is the share of the output variance explained by the interaction of the i^{th} and j^{th} inputs, and k is the total number of inputs. The partial variances are explained as $V_i(Y) = V[E(Y|X_i)]$, $V_{ij}(Y) = V\left[E\left(Y\middle|X_i, X_j\right)\right] - V_i(Y) - V_j(Y)$ and so on for higher order interactions, where $\boldsymbol{E}$ and $\boldsymbol{V}$ are the expectation and variance operators, refer appendix for more details. The so-called "Sobol" indices or "variance-based sensitivity indices" are obtained as follows:

First Order Sensitivity Index $\boldsymbol{S_i} = \frac{V_i(Y)}{V(Y)}$, the amount of variance of Y explained by input variable X_i; **Second Order Sensitivity Index** $\boldsymbol{S_{ij}} = \frac{V_{ij}(Y)}{V(Y)}$, the amount of variance of Y explained by the interaction of the factors X_i and X_j (i.e. sensitivity to X_i and X_j not expressed in V_i nor V_j); **Total Sensitivity Index** $\boldsymbol{S_{Ti}} = S_i + \sum_{i<j} S_{ij} + \sum_{i<j<l} S_{ijl} + \ldots S_{1,2,..k}$ it accounts for all the contributions to the output variation due to factor X_i (i.e. first-order index plus all its interactions). In other words,

S_{Ti} index is defined as a summation of main, second, and higher order effects which involves the evaluation over a full range of parameter space. If S_i and S_{Ti} are equal and sum of S_i(and thus S_{Ti}) is 1, then the model is additive (linear) in nature, otherwise S_{Ti} is greater than S_i and $\sum S_i < 1$ or $\sum S_{Ti} > 1$, then the model exhibit non-linearity. Thus, linearity or non-linearity of model through time, scale and hydroclimate can be determined from summation of S_{Ti}'s indices.

Let $\boldsymbol{Y}=f(\boldsymbol{X})$ be a spatial model, then Y is the model output and $\boldsymbol{X}$ are random independent model inputs, where $\boldsymbol{X}$ is composed of $\boldsymbol{U}$ and $\boldsymbol{W}$ with $\boldsymbol{U}$ defined as random vectors and $\boldsymbol{W}$ defined as two-dimensional spatial maps. Using the similar configuration, $\mathbf{Y}$ is the simulated brightness temperature, f is the radiative transfer model, and $\mathbf{X_K}$ is the input parameter vector with K= [X_1, X_2, X_3, X_4] as [Surface Roughness- RMS height (S), Surface Roughness- Correlation length (L), Vegetation Structure (B), Scattering Albedo (ω)] and $\boldsymbol{W}$ as spatial maps [Soil Moisture (SM), Clay Fraction (CF), Surface Temperature (TSURF), Vegetation Water Content (VWC)]. The steps used to carry out the analysis are described in Figure 3.1. The variables such as RMS height (S) and correlation length (L) are sampled from a uniform distribution whose ranges are estimated from field measurements, Table 2.1. The variables such as vegetation structure (B) and scattering albedo (ω) are also sampled from a uniform distribution whose ranges are defined based on vegetation type. However, experimental data for these variables are limited and are obtained from past literature [Jackson et al., 1991, Choudhury et al., 1995]. The range of variability in surface roughness, vegetation parameter, and scattering albedo are assumed to remain constant at all scales. This assumption limits the extent of the study. However, there are no means to obtain and ascertain how those vary with scale. The spatial input variable at each support scale is defined as a real random variable with a uniform range for the number of pixels developed at that scale. That is, the numbers of pixels 'n' at each support scale are considered as equiprobable with each pixel

labeled with a unique integer in the set *{1, ..., n}*. The number of pixels decreases with increasing support scale, for example, the numbers of pixels at 800 m support scale are more than 4000, and at 12.6 km support scale there are about 50 pixels. The first order and total Sobol sensitivity indices are estimated with confidence intervals using the bootstrap technique with resampling [Efron and Tibshirani, 1994]. The number of samples N = 55,000 are used for model evaluations. Here, we discuss and present only total sensitivity indices.

Current SMAP Level 2 and 3 radiometer based soil moisture algorithm [O'Neill et al., 2015] uses vegetation and surface roughness parameters from the look up table by IGBP class, assuming sub footprint-scale homogeneity for vegetation and roughness parameters. However, surface roughness parameters change with soil type, vegetation conditions, wind speed, amount of precipitation etc. Similarly, vegetation parameters vary with growing season, vegetation type and structure. Due to the heterogeneous and dynamic nature of these land surface variables (varying with space and time), assuming them to be fixed parameters will introduce high errors into soil moisture retrievals. Since the range for vegetation and roughness variables are obtained from the respective field campaign conducted over few weeks, larger heterogeneities of land surface variables are possible to occur in real time as we have considered in our analysis.

3.3.4 Upscaling methods: Linear Upscaling vs Inverse Distance Weighted (IDW) Upscaling

Scaling is an important aspect, and is studied in various disciplines including hydrology [Bloschl and Sivapalan, 1995, Bloschl, 1999], meteorology [Raupach and Finnigan, 1995], ecology [Xie et al., 2007] and geography [Malenovský, et al., 2007]. The upscaling and validation of satellite soil moisture products are discussed in Crow et al. [2012], Qin et al. [2015], Chen et al. [2016], Chen et al. [2017], and Colliander et al. [2017]. The upscaling technique for any remotely sensed land surface variable depends on the heterogeneity exhibited by the variable and antenna

gain function, which plays a significant role in capturing the heterogeneity. In this paper, we investigate the difference in sensitivity of retrieval model to the land surface variables, when the variables are upscaled linearly and through Inverse Distance Weighted (IDW) to various support scales (0.8 km, 1.6 km, 3.2 km, 6.4 km, and 12.8 km). This is important because of three main reasons: 1) as the support scale changes (upscaling or downscaling) the heterogeneity of the landscape also varies. Thus, the processes which appear linear may become non-linear and vice-versa. The variables that are important at one scale and hydro-climate may become trivial at other scale and hydro-climate, 2) the non-linearity of the radiative transfer model varies with heterogeneity observed for the retrieval scale. The non-linear retrieval model may show no scale effect, when the scale of analysis (support) is homogeneous [Hu and Islam, 1997, Garrigues et al., 2006], and 3) the upscaling techniques become significant in heterogeneous landscapes to represent the non-linear effects [Drusch et al., 1999, Pachepsky et al., 2003, Jacobs et al., 2004, Famiglietti et al., 2008, Zhan et al., 2008, Brocca et al., 2010]. In case of homogeneous environment, the scaling methods do not significantly influence the output, as also validated in Wu and Liang Li [2009]. The use of an unsuitable upscaling method or inappropriate representation of spatial distribution can lead to potentially wrong decisions. An inappropriate upscaling can have even more profound impact if the result is used as an input for simulations, where a small error or distortion can cause models to produce false estimation.

IDW is a deterministic nonlinear interpolation technique that uses the weighted upscaling of the attribute values from the nearby sample sub-grid to estimate the magnitude of the attribute at a higher support scale. The superior performance of IDW in comparison to other scaling methods are also discussed in Weber and Englund [1994], Moyeed and Papritz [2002], and Babak and Deutsch [2009]. The weight a particular sub-grid is assigned in the averaging scheme depends on

the distance of the sub-grid from the center of the coarser grid. It is an averaging method based on the principle that sample closer to the prediction location has more influence on prediction than sample farther apart. For gridded data, IDW approach can be realized as a-3dB function where higher weights are given to grid cells closer to the center of the pixel than grid cells further apart. This incorporates neighboring heterogeneity, which changes with support scale. For this analysis, the weight of the point changes with the inverse square of the distance known as Inverse Distance Squared (IDS) upscaling. This technique is also used in SMAP L1C [Chan et al., 2014] radiometer data product to average non-uniformly all the brightness temperature data samples that fall within the grid cell.

3.4 Results and Discussion

The spatiotemporal sensitivity of brightness temperature at V-polarization and H-polarization to different land surface variables are observed to be similar in trend but with different intensities and rate. It is observed that the brightness temperature at V-polarization is more sensitive to soil moisture, soil texture (clay fraction), and surface temperature than H-polarization under all conditions (space and time). On the other hand, H-polarization is always observed to be more sensitive to surface roughness variables (S and L) than V-polarization under all conditions. The SMEX02 and SMEX04 field campaigns were conducted using Polarimetric Scanning Radiometer C-band (PSR/C), whereas SGP'97 and SMAPVEX12 were conducted using Passive Active L-band System (PALS) radiometer, as mentioned earlier. To evaluate the effect of frequency, the analysis was conducted for L-band and C-band simulated brightness temperature. However, only ~ 0.5 - 1 % difference in sensitivities to land surface variables was observed between L- and C-band simulated brightness temperatures. In the following sections we discuss the variability observed in sensitivity of L-band brightness temperature at V- and H-polarization

under: 1) Plant Structure, 2) Spatio-Temporal Scales, and 3) Upscaling and Environmental Heterogeneity.

Table 3.1 The mean values of land surface variables used in the analysis for various field campaigns.

Variables	SGP97	SMEX02	SMEX04	SMAPVEX12
	Oklahoma (Sub-Humid)	Iowa (Dfa-Humid)	Arizona (Semi-Arid)	Winnipeg (Dfb-Humid)
Mean Soil Moisture **(**v/v**)**	0.14	0.19	0.07	0.25
Mean Soil Temperature (K)	298	315	319	290
Mean Vegetation Water Content **(**kg/m^2**)**	0.32	1.9	0.09	1.4
Root Mean Square height (cm)	0.27-1.73	0.19-3.05	0.71-23.28	0.23-3.21
Correlation length (cm)	3.4-32.18	0.43-26.95	8.7-119.5	2.5-24.5
Vegetation structure (unit less)	0-0.15	0-0.15	0-0.15	0-0.15
Scattering albedo (unit less)	0-0.05	0-0.05	0-0.05	0-0.05
Support scales (km)	ESTAR: 0.8, 1.6, 3.2, 6.4, 12.8	PSR/C: 0.8, 1.6, 3.2, 6.4, 12.8	PALS : 0.8, 1.6, 3.2, 6.4, 12.8	PALS : 1.5, 3, 9

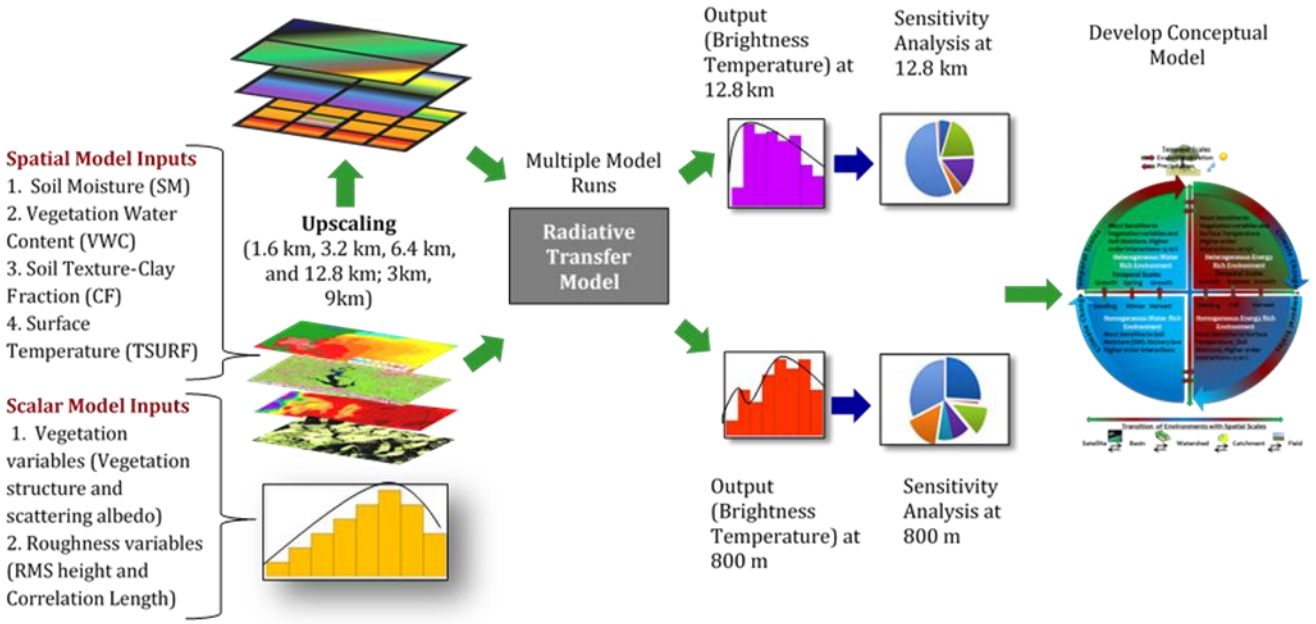

Figure 3.1 Methodology flowchart for implanting global spatial sensitivity analysis.

3.4.1 Plant Structure

It is well understood that vegetation attenuates the microwave emission from the soil, and adds its own radiative flux to the total emission. The extent of attenuation depends on the amount of vegetation and its structure. A crop canopy may be divided into three main components: 1) leaves, 2) stalks, and 3) heads. The attenuation of radiation may thus occur at two layers, the upper layer consisting of heads, and a lower layer composed of leaves and stalks. The propagation characteristics are different for different canopies depending on the emission and scattering properties of these layers. Therefore, assuming polarization-independence may not be true especially for plants where vegetation biomass is concentrated in vertically oriented dipole-like stalks and row crops. For the zero order radiative transfer model (tau-omega model), the effects of vegetation are represented by vegetation water content (VWC), single scattering albedo (ω) and vegetation structure parameter (B), where VWC captures the amount of water content in biomass, 'B' represents the canopy architecture, and ω represents scattering within the canopy.

In canopies with vertical stalks, the attenuation will be smaller for horizontally polarized waves than vertically polarized waves except at a nadir incidence angle, where stalks are not visible, and appear only as small randomly oriented disks. [Fig 3.2]. For a horizontally polarized incident wave, the electric field vector **E** is normal to the axis of the stalk at all incidence angles, and for vertically polarized wave **E** is parallel to stalk thereby coupling strongly [Ulaby et al., 1981]. This difference will be significant mainly over vegetation that exhibits some preferential orientation such as vertical stalks noticed for tall grasses, grains, wheat, corn, maize, forest etc. For vegetation with near horizontally oriented primary branches or broad leaf plants (soybean, bean, canola, sunflower etc.,) there is stronger attenuation for horizontally polarized wave than vertically polarized waves. It is reasonable to assume that the absorption/scattering loss factor will

be approximately polarization independent for canopy components whose sizes are much smaller than the wavelength of observation.

For example, for SMEX04 (Arizona) the vegetation is mainly shrub dominated (whitethorn acacia, creosote bush etc.,) covering two-thirds of the watershed and grass (sideoats grama, lehmann lovegrass etc.,) occupying the rest with a total mean vegetation water content 0.087 kg/m^2. Due to the low vegetation and primarily random vegetation structure, the sensitivity to vegetation variables is insignificant for this region temporally, at all support scales and polarizations [Fig 3.3]. Similarly, SGP97 region (Oklahoma) which has dominantly rangeland and significant occupation of winter wheat crops with total mean vegetation water content 0.323 kg/m^2 shows the insignificant contribution of vegetation variables towards brightness temperature (V- and H-polarization) at all spatial scales [Fig 3.4]. SMEX02 (Iowa) has a total mean vegetation water content of 1.9 kg/m^2. At 800 m scale, H-polarization was observed to be (~ 1- 4 %) more sensitive than V-polarization. With increasing support scale, V-polarization was observed to be ~ 2 % (at 1.6 km) and ~ 15 % (at 12.8 km) more sensitive than H-polarization for vegetation water content (VWC) and vegetation structure (B) [Fig 3.5 (A)]. Under IDW analysis, H-polarization was always temporally more sensitive than V-polarization to vegetation water content by ~ 2 - 3 % and vegetation structure (B) by ~ 3 - 9 %, except on DOY 188, where V- and H-polarization show same sensitivities [Fig 3.5 (B)]. That is, at lower vegetation water content (DOY 178, 182) and support scale of 800 m under linear upscaling and at all support scales under IDW where the heterogeneity in VWC is maintained, a higher sensitivity to VWC and B at H-polarization is noticed. For DOY 188, with higher vegetation water content and higher support scales under linear upscaling where the heterogeneity disappeared with support scales (moving towards extent mean value), a higher sensitivity to vegetation structure (B) at V-polarization is observed. This

confirmed that there is a stronger coupling with plants exhibiting definite vertical structures, and the coupling increasing with increasing vegetation water content and decreasing heterogeneity. SMAPVEX12 region shows a wide variety of agricultural crops such as cereals, soybeans, canola, corn etc., with total mean vegetation content water 1.4 kg/m^2. Unlike in SMEX02, the sensitivity to vegetation structure (B) was always observed to be higher for H-polarization at all scales. We hypothesize that the amount of vegetation water content determines the sensitivity of H- and V-polarization to B variable. To test the hypothesis, the analysis was conducted including pixels with higher vegetation water content than the observed within the SMAPVEX12 extent, which resulted in higher sensitivity to vegetation structure (B) at V-polarization. This may occur because with increasing VWC the dielectric constant of vegetation also increases thereby increasing the sensitivity to V-polarization due to stronger coupling as mentioned earlier. Thus, vegetation variable 'B' is a complex function of plant geometry and vegetation water content.

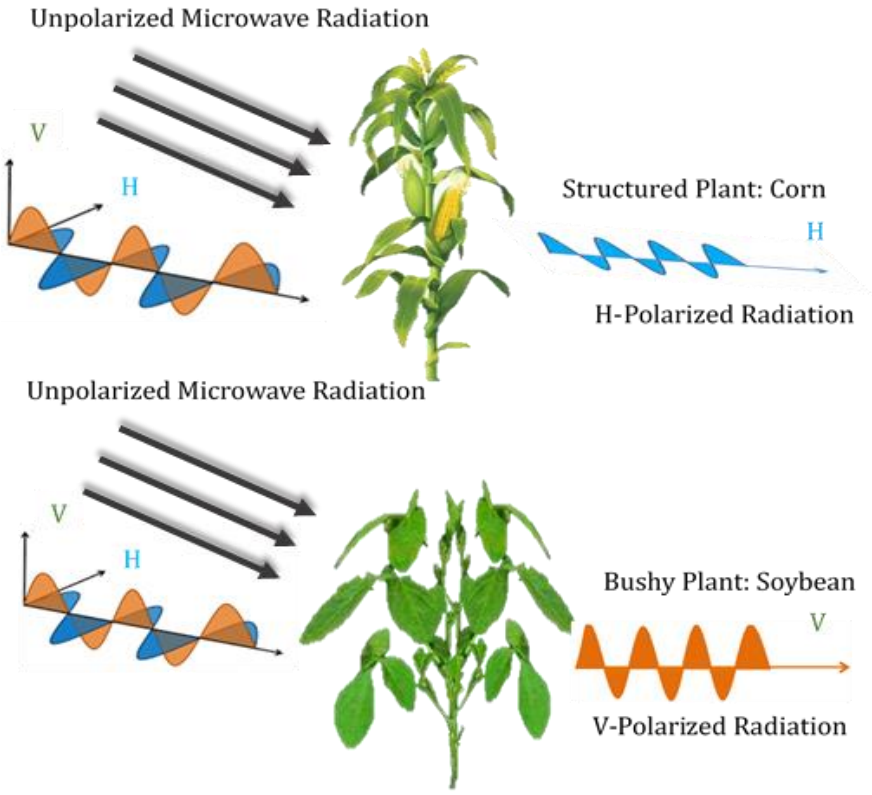

Figure 3.2 Propagation of an unpolarized microwave radiation incident on a lossy dielectric structured vegetation (top) and unstructured/bushy (bottom) vegetation. The unpolarized incident wave propagates through structured vegetation emitting H-polarized wave and V-polarized radiation through bushy vegetation.

3.4.2 Spatio-Temporal Scales in Different Hydro Climates

3.4.2.1 Semi-Arid (SMEX04) Hydro Climate

For semi-arid regions with low vegetation and lower evapotranspiration (lower latent heat flux and higher sensible heat flux), an increase in air and surface temperatures are observed, resulting in higher sensitivity to surface temperature. However, the heterogeneity in temperature is lost with upscaling due to lumped fluxes resulting in exponential (R^2=0.99) decrease in sensitivity to surface temperature with support scale. Due to the rocky topography of SMEX04 region, the observed surface roughness is highly random emphasizing the higher sensitivity to RMS height (S), which increased from ~ 11 % (~ 63 %) to ~ 38 % (~ 87 %) for V-polarization (H-polarization), and correlation length (L) increased from ~ 1 % (~ 7 %) to ~ 5 % (~ 10 %). This is in contrast to SMAPVEX12 and SMEX02, where the surface roughness are more correlated due to regular agricultural practices resulting in higher sensitivity to correlation length (L) as well. The sensitivity to vegetation variables (VWC, B, and ω) and clay fraction are negligible across both polarizations (H and V), upscaling methods and spatio-temporal scales.

3.4.2.2 Sub-Humid (SGP97) Hydro Climate

For a more natural landscape with low density biomass as observed for SGP97, soil moisture is the most sensitive variable for V-polarization (H-polarization) ~ 96 % (~ 83 %) at all support scales under both linear and IDW upscaling. Due to the lower variability of roughness in SGP97 and lower biomass content, incorporating neighboring pixels via IDW or using linear upscaling did not influence the sensitivity measures with support scales. The sensitivity to land surface variables (clay, surface temperature, and scattering albedo) are insignificant (~1 %) at V-polarization, whereas the sensitivity to surface roughness variables (S and L) at H-polarization are observed at ~ 8 % each and sensitivity to vegetation variables (VWC and B) are observed at ~ 2

% each [Fig 3.4]. To further explore the influence of varying extent, the analysis is repeated for a smaller extent over Little Washita (LW) watershed. To maintain statistically significant data points, the upscaling is conducted only up to 3.2 km support scale. Results indicated soil moisture (in both V- and H-polarization) to be still the most sensitive variable at all scales, however its magnitude has decreased slightly to ~ 94 % for V- polarization and ~ 80 % for H- polarization. Sensitivity to vegetation structure (B) increased to ~ 4 % and ~ 2 % for H- and V-polarization respectively at smaller extent than the sensitivities observed at larger extent. This could be due to the increased attenuation caused by higher biomass content (~ 0.41 kg/m^2) for smaller extent than observed at larger extent (SM ~ 0.14 v/v and VWC ~ 0.32 kg/m^2).

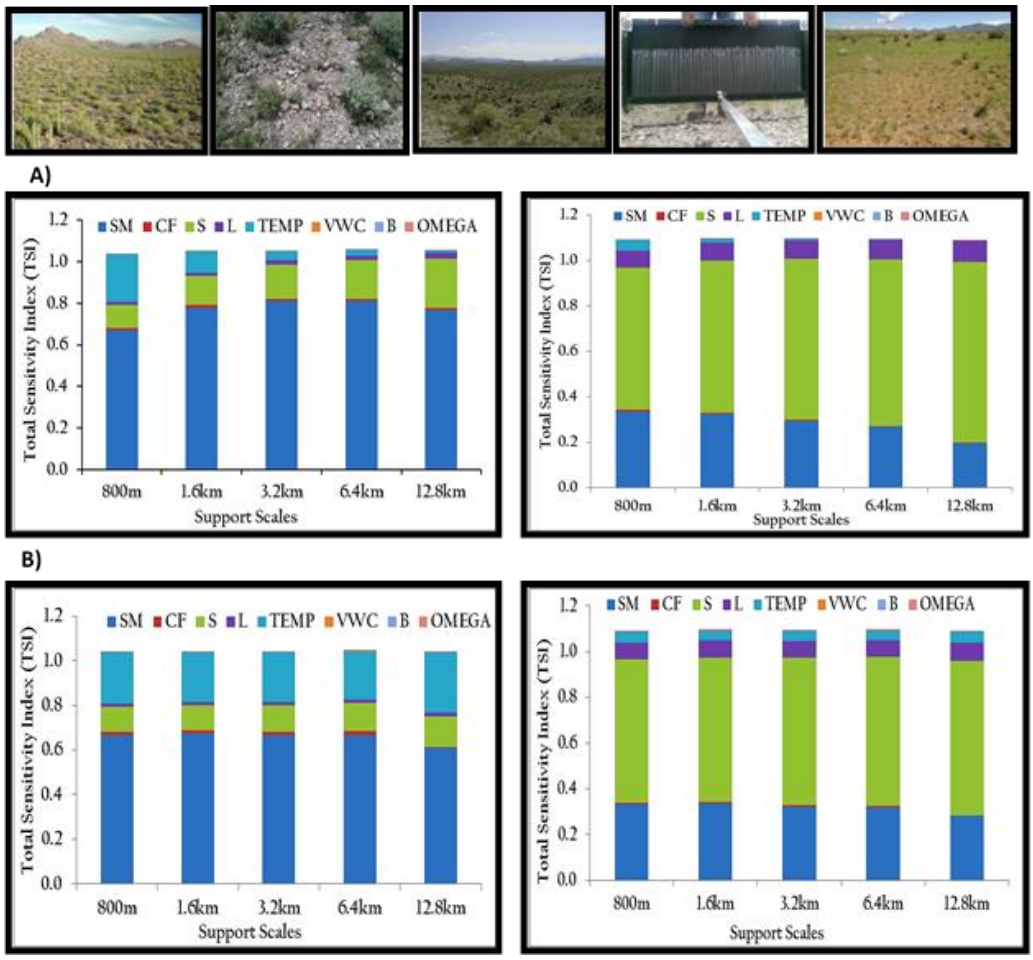

Figure 3.3 Scatter Soil Moisture Experiments 2004 (SMEX04), Total Sensitivity Index (TSI) for Brightness Temperature A) Linear Upscaling: V-polarization (left), and H-polarization (right), B) Inverse Distance Weighted (IDW) Upscaling: V-polarization (left) and H-polarization (right). SM: Soil Moisture; CF: Clay Fraction; S: Root Mean Square Height; L: Correlation Length; TSURF: Surface Temperature; VWC: Vegetation Water Content; B: Vegetation Structure; ω: Single Scattering Albedo.

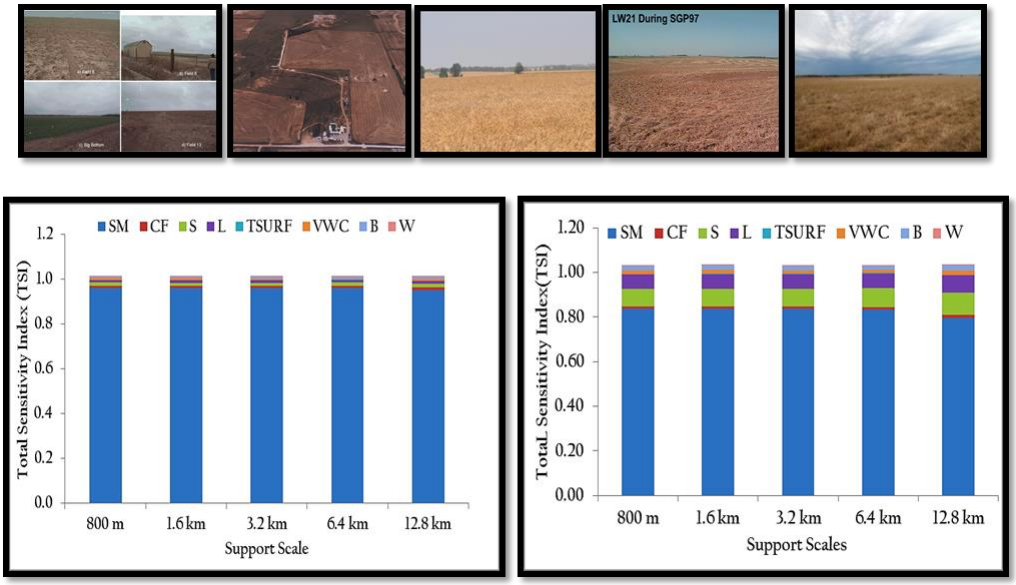

Figure 3.4 Southern Great Plains 1997 (SGP'97), Total Sensitivity Index (TSI) for Brightness Temperature under Linear Upscaling: V-polarization (left), and H-polarization (right). SM: Soil Moisture; CF: Clay Fraction; S: Root Mean Square Height; L: Correlation Length; TSURF: Surface Temperature; VWC: Vegetation Water Content; B: Vegetation Structure; ω: Single Scattering Albedo.

3.4.2.3 Humid-Dfa (SMEX02) Hydro Climate

For SMEX02 the analysis is conducted for DOY 178, 182, 186, and 188, and the soil moisture sensitivity at 800 m followed a similar field scale pattern as observed in Neelam and Mohanty [2015]. Unlike SMEX04 and SGP97, the mean sensitivity to soil moisture across sampling days is ~ 28 % and ~ 13 % for V- and H-polarization respectively at 800 m which decreased to ~ 8 % and ~ 1 % at 6.4 km, and increased by ~ 1 - 2 % at 12.8 km [Fig 3.5 (A)]. Among other land surface variables, sensitivity to surface temperature followed a decreasing exponential function (R^2=0.98) and nearly disappeared at 1.6 km for H- and at 3.2 km for V-polarization. On the other hand, the sensitivity to surface roughness variables (S and L) followed a logarithmic function (R^2=0.97) with increasing support scale. Similarly, vegetation water content (VWC) and vegetation structure (B) followed a decreasing (R^2=0.99) and increasing (R^2=0.94) logarithmic function. This is because of the greater variability in surface roughness, and vegetation variables observed particularly for anthropogenically-modified region such as SMEX02. Thus, the impact of these variables is observed longer with support scale following a logarithmic function compared to surface temperature that followed an exponential function. Under IDW upscaling, the sensitivity to land surface variables with support scales changed by ~ 1 - 2 %. Sensitivity to variables such as soil moisture, surface temperature and surface roughness remained uniform till 6.4 km, which later decreased by ~ 2 % for soil moisture, surface temperature and increased for surface roughness by ~ 2 % at 12.8 km [Fig 3.5 (B)]. The uniformity in sensitivity to these variables till 6.4 km under IDW is similar to reasons explained above. However, for a selected extent the variability in some land surface variables attains saturation at a certain scale (6.4 km) resulting in decrease in sensitivity to those land surface variables upon further upscaling. The support scale at which this saturation is attained is dependent on the heterogeneity and extent of the analysis. The

sensitivity to vegetation water content remained uniform till 3.2 km and decreased ~ 1 % with increasing support scale, and sensitivity to vegetation structure (B) increased linearly (R^2 =0.98) by ~ 6 % with scale. The sensitivity to clay fraction and albedo remained negligible under IDW and linear upscaling. Except for DOY 178 which was a relatively dry day, where the sensitivity to clay fraction increased to ~ 3 % at V-polarization and ~ 1 % at H-polarization till 3.2 km.

It is important to note that we discuss only total sensitivity indices (TSI) of land surface variables. The increased sensitivity of a variable may also be due to increased interaction effects such as (S,B), (S,VWC), (S,SM), (L,VWC), (SM,B) with growing vegetation (increased interception and scattering) [Neelam and Mohanty, 2015]. This may also be one of the contributing factors for the high sensitivity to surface roughness (S and L) and vegetation structure (B). The sensitivity to scattering albedo is observed to be negligible at all scales.

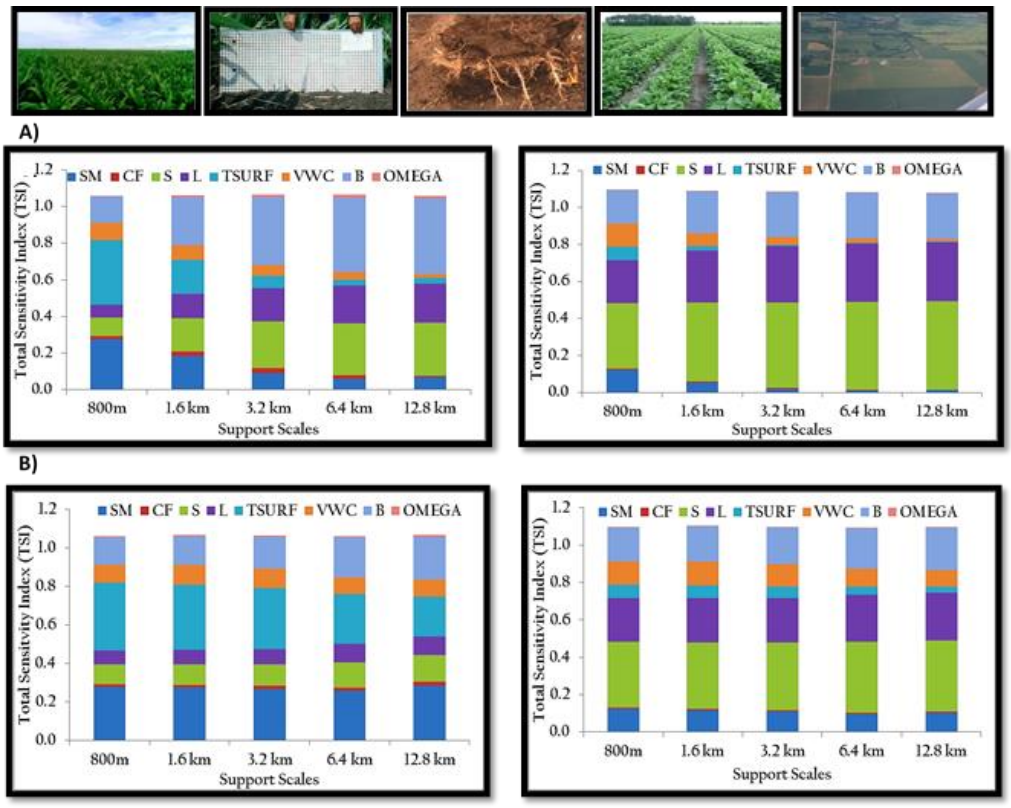

Figure 3.5 Soil Moisture Experiments 2002 (SMEX02), Total Sensitivity Index (TSI) for Brightness Temperature A) Linear Upscaling: V-polarization (left), and H-polarization (right), B) Inverse Distance Weighted (IDW) Upscaling: V-polarization (left) and H-polarization (right). SM: Soil Moisture; CF: Clay Fraction; S: Root Mean Square Height; L: Correlation Length; TSURF: Surface Temperature; VWC: Vegetation Water Content; B: Vegetation Structure; ω: Single Scattering Albedo.

3.4.2.4 Humid-Dfb (SMAPVEX12) Hydro Climate

The SMAPVEX12 region observed lower biomass content and wide heterogeneity in soil moiSture due to which a more gradual variability in sensitivity to land surface variables is noticed, unlike SMEX02. To maintain statistically significant sample points, the upscaling is conducted from 1.5 km to 9 km only. The sensitivity of V-polarization (H-polarization) to soil moisture showed ~ 74 % (~ 52 %) at 1.5 km, which decreased to ~ 61 % (~ 35 %) at 9 km [Fig 3.6]. The sensitivity to clay fraction remained uniform (~ 6 %) spatio-temporally for both V- and H-polarization. A relatively high sensitivity to clay in SMAPVEX12 unlike other regions is due to a wide heterogeneity (~ 5 % to ~ 65 %) in clay fraction observed in this region. The sensitivity to surface roughness variables (S and L) is uniform at ~ 2 – 4 % at all scales unlike in SMEX02 where they increased with scale. This may also be due to higher surface roughness measured for SMEX02 than SMAPVEX12. The sensitivity to vegetation structure and vegetation water content increased exponentially (R^2=0.99) with scale. It is noteworthy that the sensitivity to VWC slightly increased with scale.

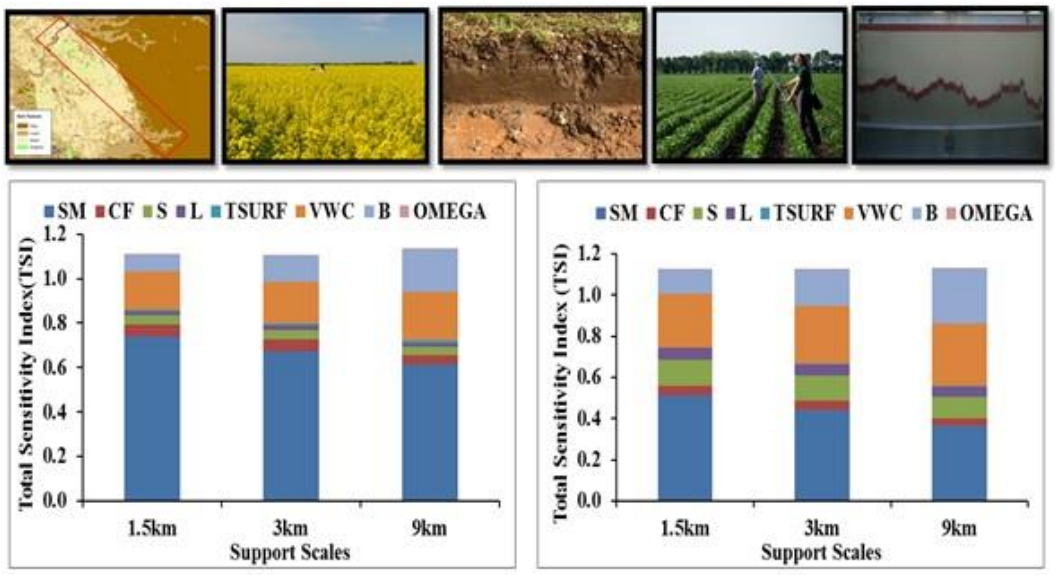

Figure 3.6 Soil Moisture Active Passive Experiments 2012 (SMAPVEX12), Total Sensitivity Index (TSI) for Brightness Temperature under Linear Upscaling: V-polarization (left), and H-polarization (right). SM: Soil Moisture; CF: Clay Fraction; S: Root Mean Square Height; L: Correlation Length; TSURF: Surface Temperature; VWC: Vegetation Water Content; B: Vegetation Structure; ω: Single Scattering Albedo.

3.4.3 Upscaling and Environmental Heterogeneity

The largest up-scaling effects are observed for scenes with high heterogeneity i.e., with strong gradients in land surface variables. The difference between the two (linear and IDW) upscaling methods are therefore more prominent in heterogeneous environments. A high correlation is observed between spatial heterogeneity in soil moisture and density of vegetation [Lakhankar et al., 2009, Said et al., 2012, Ye et al., 2014]. Thus, we classify the hydroclimates as heterogeneous and homogeneous environments based on biomass density. This also complements Mo et al. [1982] and Wigneron et al. [1995, 2017] who suggested that the total amount of biomass within the pixel is important in affecting the microwave response.

3.4.3.1 Homogeneous Environment (Sub-Humid and Semi-Arid)

SGP'97 (Sub-Humid) and SMEX04 (Semi-Arid) are more natural landscapes composed mainly of grasslands and shrubs, with low biomass content. For SGP97, a very small percentage of higher order interactions are observed, ~ 1 % for V- polarization and ~ 3 % for H- polarization. SMEX04 observed higher order interactions of ~ 5 % for V-polarization and ~ 9 % for H-polarization. Due to the rough topography of SMEX04, a higher sensitivity to roughness variables (S and L) for H-polarization is observed which also led to increased higher order interactions than SGP97. Because of higher sensitivity to soil moisture and nearly linear (additive) behavior of radiative transfer model, these regions can be classified as homogenous environments. Due to the homogeneous environment, we do not observe large variabilities in sensitivity measures between linear and non-linear (IDW) upscaling methods [Fig 3.3 and Fig 3.4]. This allows, the land surface variables to be scaled linearly, which is also consistent with studies of Drusch et al. [1999], Crow et al. [2000]. Under homogeneous environments, SMEX04 and SGP97 can further be classified as energy rich and water rich environments respectively. SMEX04 that observed total mean soil

moisture ~ 0.07 v/v and higher surface temperatures ~ 319 K is classified as the energy rich environment and SGP97 that observed a relatively higher total mean soil moisture ~ 0.15 v/v and lower surface temperatures ~ 298 K can be classified as water rich environment. For homogeneous water rich environment, the sensitivity to land surface variables did not vary with either support scale or upscaling methods and but varied only by small percentages due to polarization differences. The sensitivity to land surface variables under homogeneous energy rich environments followed an exponential function with support scale and attained uniformity by ~ 3.2 km, emphasizing the linearity/homogeneity of the region.

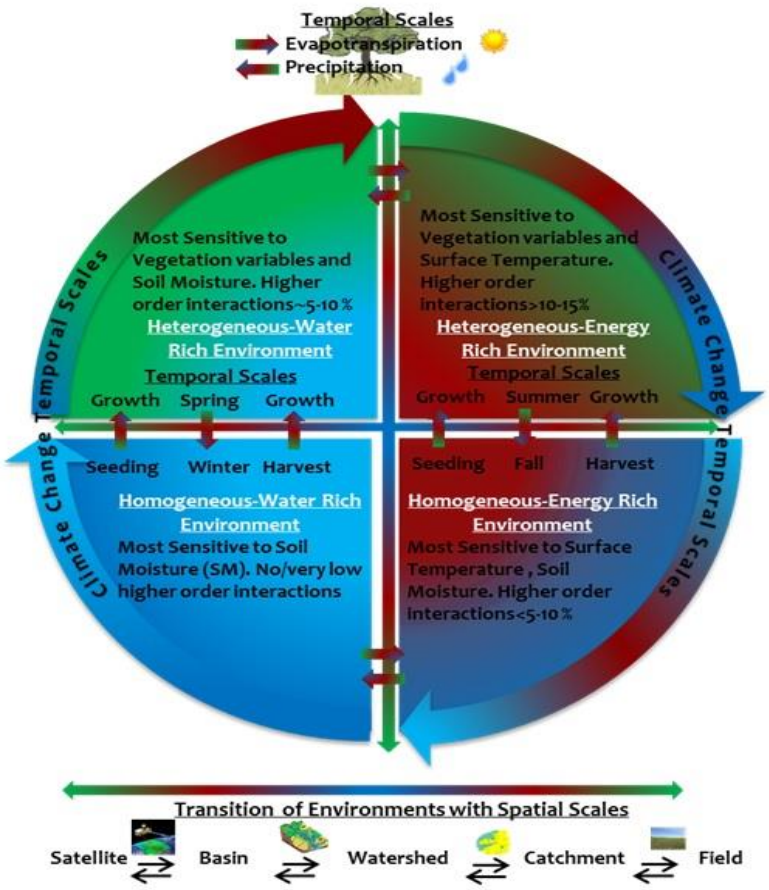

Figure 3.7 The conceptual model describes the classification of environments as homogenous and heterogeneous environments based on density and heterogeneity in biomass (green). Each of these environments can further be classified as water (blue) and energy (red) rich environments. Top-Left quadrant represents heterogeneous water rich environment, where brightness temperature is most sensitive to vegetation and soil moisture with higher order interactions of ~5-10 %; Top-Right quadrant represents heterogeneous energy rich environment, where brightness temperature is most sensitive to vegetation and temperature with higher order interactions of > 10-15 %; Bottom-Left quadrant represents homogeneous water rich environment, where brightness temperature is most sensitive to soil moisture with no or very low higher order interactions; Bottom-Right quadrant represents homogeneous energy rich environment, where brightness temperature is most sensitive to soil moisture and temperature with higher order interactions of < 5-10 %. The transition from homogenous to heterogeneous, energy rich to water rich and vice versa can occur through spatio-temporal scales (spatial: extent and support, time: day, month, seasonality, climate change etc.,) following land-use/land-cover change and events such as precipitation, evapotranspiration etc. The lasting transition from homogeneous to heterogeneous and vice-versa can also occur at the climate change temporal scales.

3.4.3.2 Heterogeneous Environment (Humid Dfa and Humid Dfb)

SMEX02 (Humid Dfa) and SMAPVEX12 (Humid Dfb) are agricultural landscapes with a wide range of biomass content and observe tillage practices on a regular basis. In these regions, the sensitivity to land surface variables are complex and exhibited considerable higher order interactions (nonlinearities). SMAPVEX12 observed higher order interactions of ~ 6 % for V-polarization and ~ 10 % for H- polarization, whereas SMEX02 observed ~ 10 % for V-polarization and ~ 13 % for H-polarization. Because of lower sensitivity to soil moisture and higher non-linear behavior of radiative transfer model, these regions can be classified as heterogeneous environments. Due to the heterogeneous environment, there is significant gradient observed in the sensitivity of land surface variables as they are upscaled linearly from 800 m to 12.8 km. However, as they are upscaled non-linearly the gradient in sensitivity measures decreases [Fig 3.5 and Fig 3.6]. Under heterogeneous environments, SMEX02 and SMAPVEX12 can further be classified as energy rich and water rich environments respectively. SMEX02 which observed mean soil moisture ~ 0.19 v/v and mean surface temperatures of ~ 315 K are classified as energy rich environment. On the other hand, SMAPVEX12 which observed a relatively higher mean soil moisture ~ 0.25 v/v and lower mean surface temperatures ~ 290 K is classified as water rich environment. For heterogeneous water rich environment (SMAPVEX12), the sensitivity to land surface variables followed exponential function with support scale, and for heterogeneous energy rich environment (SMEX02) the sensitivity to land surface variables followed a logarithmic function emphasizing the non-linearity/interactions of the region. Therefore, under heterogeneous environments upscaling method also determined the sensitivity to land surface variables.

In this study, a comprehensive framework is proposed based on the preliminary work presented by Neelam and Mohanty [2015] [Fig 3.7] where the regions can primarily be classified

as homogenous and heterogeneous environments based on density and heterogeneity in biomass. Each of these environments can further be classified as water and energy rich environments. The transition from homogenous to heterogeneous, energy rich to water rich and vice versa can occur through spatial parameters (extent and support), time (day, month, seasonality etc.,) and hydroclimates. For example, with a gradual increase in spatial scale (support, extent, and spacing) there will be a gradual change in land-cover/land-use thereby changing heterogeneity in land surface variables captured with varying spatial scale. Similarly, heterogeneity in land surface variables changes with temporal scales. For example, activities at monthly temporal scales such as seeding, irrigation, crop growth, harvesting, etc., and at seasonal scales such as spring, summer, fall etc., effects heterogeneity in biomass, water, temperature etc. Thus, the transitioning of environments occurs through spatio-temporal scales thereby changing the heterogeneity in land surface variables and their sensitivities to soil moisture retrieval algorithm.

3.5 Summary and conclusion

A comprehensive sensitivity analysis to study radiative transfer model using spatial maps is conducted for various field campaigns in multiple hydroclimates. The primary contribution of this work is to demonstrate how the sensitivity to spatial maps of land surface variables change under various hydroclimates (Arizona, Oklahoma, Iowa, and Winnipeg) and evolving scales (0.8km, 1.6 km, 3.2 km, 6.4 km and 12.8 km) for a given extent. The impact of non-linear upscaling is illustrated by comparison between linear and inverse distance weighted methods. The analysis resulted in environment specific most sensitive variables, SM in homogeneous, and VWC, B in heterogeneous environments. Though the magnitude of sensitivity varied temporally, the ranking among the variables did not change within the study period. The sensitivity to land surface variables in SMEX04 and SMAPVEX12 increased or decreased gradually following an

exponential function with increasing scale. While, for SMEX02 the sensitivities changed rapidly following a logarithmic function. The study emphasized that the observed heterogeneity and upscaling method will determine the sensitivity to land surface variables. This study is particularly relevant to establish the significant variables that can be used for downscaling and upscaling algorithms to various scales and under heterogeneous landscapes.

The analysis assumed independence among the inputs variables which might not be true under natural environments. However, there are very limited studies in past that established a correlation among land surface variables. The future scope of this work can include analyzing the sensitivity of correlated land surface variables and its development with hydro-climates and scales. In summary:

1) For vegetation with dominant vertical stalks, the attenuation will be smaller for horizontally polarized waves than vertically polarized waves except at a nadir incidence angle, due to stronger signal coupling.
2) Both the degree of variability of the land surface variables, the model used to assess flux variability, and the upscaling technique will have an effect on the resolution – spatial variability relationship.
3) No vegetation or low density vegetation regions followed an exponential function for sensitivity of land surface variables with linear upscaling, whereas high vegetation density regions followed a logarithmic function with spatial scale.

The proposed generic model provides a basis to understand the soil moisture-vegetation coupling which varies through spatial parameters (extent and support), time (day, month, seasonality etc.,) and hydroclimates.

4 MULTI SCALE SURFACE ROUGHNESS FOR IMPROVED SOIL MOISTURE

4.1 Synopsis

Surface roughness parameterization plays an important role in passive microwave soil moisture retrieval. This paper proposes a new formulation for estimating surface roughness. The proposed model incorporates the field-scale (micro) roughness, as well as topographic (macro) roughness. The performance of the model was evaluated by inverting the traditional tau-omega model for retrieving soil moisture. The study focused on the PALS (Passive Active L-band System) radiometer data collected as a part of two Soil Moisture Active Passive Validation Experiments (SMAPVEX) i.e., SMAPVEX12 (humid Manitoba, Canada) and SMAPVEX15 (semi-arid Arizona, USA) with highly different topography. The measured surface roughness and derived micro-roughness were observed to increase exponentially with clay fraction. This behavior was minimized with increase in Leaf Area Index (LAI). In the absence of vegetation, the contribution of topography towards surface roughness were observed. A higher surface roughness values were estimated for SMAPVEX12, which positively correlate with LAI and clay fraction and negatively correlate with wetness conditions. On the other hand, due to the high topographic variability in SMAPVEX15 region, the contribution of surface curvature (macro-topography) towards total surface roughness was significant. The consistently dry soil moisture conditions in this domain resulted in high micro roughness for SMAPVEX15. Nevertheless, a total surface roughness estimated for SMAPVEX15 region was less than for SMAPVEX12. The surface roughness formulation presented in this study can be extrapolated to any spatial resolution for improved soil moisture retrievals.

4.2 Introduction

Passive microwave remote sensing is an established technique for monitoring large-scale soil moisture [Mohanty et al., 2017, Wigneron et al., 2017]. ESA's Soil Moisture Ocean Salinity (SMOS launched in 2009) and NASA's Soil Moisture Active Passive (SMAP launched in 2015) are currently two dedicated L-band satellite missions for mapping global soil moisture at resolution ~ 40 km every 2-3 days. The passive microwave soil moisture retrieval algorithms were originally developed and validated using the aircraft and truck based field experiments at L-band frequency conducted over various geographic domains [Schmugge et al., 1992; Jackson et al., 1991, 1999]. At L-band frequencies, vegetation water content (VWC) and soil surface roughness are found to be the most sensitive land surface variables influencing soil moisture retrieval [Neelam and Mohanty, 2015]. In the past, many semi-empirical models [Wegmuller and Matzler, 1999; Wigneron et al., 2011; Wang and Choudhury, 1981] were developed to characterize the soil surface roughness at a plot/field scale using root mean square RMS height (σ) and/or correlation length (l) parameters. These surface roughness parameters were evaluated using pin/grid board measured during field campaigns [i.e. Choudhury et al., 1982; Wang et al., 1982; Wigneron et al., 2001, 2012; Panciera et al., 2009a; McNairn et al., 2015; among others]. In more recent studies [Kerr et al., 2012; Wang et al., 2015; Parrens et al., 2016; Colliander et al., 2016], the roughness parameter is represented as a function of moisture, vegetation cover, and precipitation, but did not incorporate the effect of topography. However, characterizing the dynamic aspects of surface roughness is complicated, due to its variability with agricultural practices, wind speed, organic debris, precipitation rate etc. that vary spatio-temporally.

In this study we hypothesized that, at spatial scales of 1.5 km and 3 km the observed surface roughness is a combination of field-scale (micro) and surface topography (macro) roughness. The

inclusion of macro features in estimation of surface roughness is based on studies, that have shown the importance of topography in altering the measured brightness temperature in several ways [Talone, et al., 2007; Kerr et al., 2003; Sandells et al., 2008; Flores et al., 2009]. For example, topography can vary the optical depth of the atmosphere with elevation, as well as the path length through vegetation and surface emissivity according to gradient of the surfaces. The soil moisture redistribution is also linked with topographic features (elevation, slope, curvature) [Burt and Butcher, 1985; Humphries, 1996], and this may influence its retrieval accuracy. Nevertheless, no consensus was established on parameterization of effective surface roughness which incorporates both field-scale roughness and topographic roughness from different spatial scales.

Therefore, the aim of this study was to develop and evaluate a new comprehensive surface roughness model with geophysical variables obtained from different spatial and temporal scales, Fig 4.1. The new model defined the micro-scale roughness as a function of soil moisture, soil texture, and Leaf Area Index (LAI) and macro-scale roughness as a function of topography (curvature). This comprehensive surface roughness model was evaluated in a soil moisture retrieval algorithm with traditional models for vegetation and soil permittivity. The data from two field campaigns, the Soil Moisture Active Passive Validation Experiment (SMAPVEX) 2012 (Manitoba, Canada) and 2015 (Arizona, USA) were used for validation purposes. The data collected during SMAPVEX12 was used in several earlier studies involving soil moisture retrieval algorithm development [e.g., Martens et al., 2015; Manns et al. 2015; Colliander et al., 2016; Barber et al., 2016]. The study site and data for SMAPVEX15 is also discussed in the works of Colliander et al. [2017] and Cai et al. [2017].

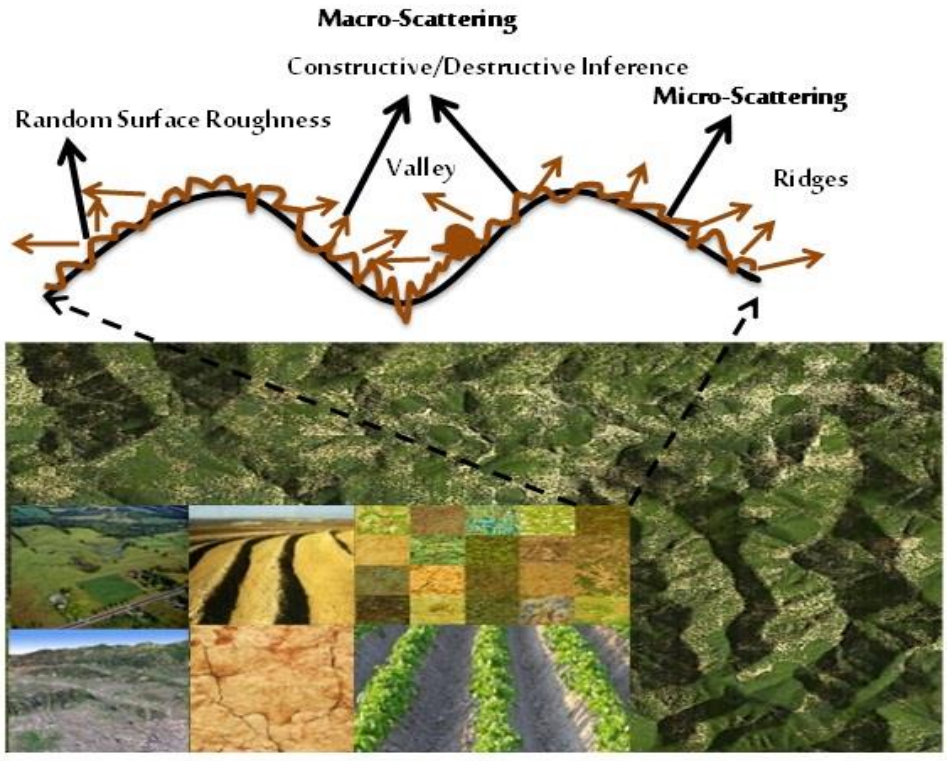

Figure 4.1 Conceptual figure describing the multi-scale surface roughness. The microwave radiation scattered through micro-roughness undergoes further constructive or destructive interference due to macro roughness (topography).

4.3 Materials and Methods

4.3.1 Soil Moisture Active Passive Validation Experiments 2012 (SMAPVEX12)

The SMAPVEX12 experiment was conducted in southern Manitoba (Canada) from June 7th to July 19th, 2012 [McNairn et al., 2015]. The study domain was 12.8 km wide and 70 km long covering a variety of land covers and soil textures, Fig 4.2. The climate of this region is classified as humid continental (Köppen climate classification-Dfb) [Peel et al., 2007] with mean annual precipitation and temperature of 521 mm and 289 K respectively. The agricultural crops (mainly cereals, soybeans, canola, and corn) dominate the southeast portion that has heavy clay soils, whereas the north and east have more sandy and loamy soils with mixed land cover including forest, perennial pastures along with few row crop fields. The southern edge of the study area is more influenced by glacial till deposition with heavy clay soils (~ 65 %), dividing it from sandy (~ 90 %) soils to the west. The soil moisture stations were operated and maintained by Agriculture and Agri-Food Canada, the United States Department of Agriculture (USDA), Manitoba Agriculture Food and Rural Initiatives (MAFRI) and Sustainable Agriculture Environment Systems (SAGES). Along with station data, teams were deployed to collect soil moisture data manually in the fields (0-5 cm depth). The soil moisture sampling strategy was designed to collect measurements at 16 locations along two parallel transects across the field. Along with soil moisture measurements, ancillary variables such as surface roughness and vegetation were measured manually on non-flight days. The surface roughness parameters i.e., RMS height (σ) and the correlation length (l) were measured in the look direction of the UAVSAR (Uninhabited Aerial Vehicle Synthetic Aperture Radar), PALS (Passive Active L-band System), and RADARSAT-2 sensors at two locations per field using a pin board (~ 1 m in length). Vegetation water content (VWC) was measured via destructive sampling of vegetation above the soil surface collected at 3

of the 16 soil moisture sampling points in each field. The surface temperature was estimated using both in-situ sensors and an infrared (IR) sensor onboard PALS. The Leaf Area Index (LAI) data for the region was obtained from the combined Terra and Aqua MODIS (MCD15A3) product composited every 4-day at 1000 m resolution. The LAI data was divided by 10 to rescale between 0 and 1 to obtain normalized LAI (NLAI). During SMAPVEX12, LAI was obtained for 11 days i.e., DOY 161, 165, 169, 173, 177, 181, 185, 189, 193, 197, and 201. Topography for the SMAPVEX12 experimental region was obtained from Shuttle Radar Topography Mission (SRTM) elevation data at a 30 m resolution. The topography of the SMAPVEX12 region was relatively flat; with elevation varying gently over ~ 80 m from north-west to south-east, Fig 4.2.

The PALS (Passive Active L-band System) instrument [Wilson et al., 2001] was used to measure L-band brightness temperature on 17 days of the study. The instrument has a long history of providing L-band brightness temperature measurements in soil moisture field experiments [e.g., Njoku et al., 2002; Narayan, Lakshmi, & Njoku, 2004; Bindlish et al., 2009; Colliander et al., 2012]. The measurements were conducted at low (1200 m) and high (2750 m) altitudes. The analysis is conducted using the measurements from the high altitude flights lines which mapped the whole experimental domain at about 1500 m resolution. The incidence angle of the instrument was fixed at 40° to match the SMAP observation angle [McNairn et al., 2015]. Pixels with more than 10 in-situ measurements and where the nearest measurement is no further than 500 m from the center of the pixel were selected for validation. This criterion avoids non-representative pixels from being used for soil moisture validation.

Table 4.1 Land cover categorization with respect to the original classes in the Agriculture and Agri-Food Canada (AAFC).

No	Land cover	AAFC Class
1	Unclassified	Unclassified
2	Water	Water
3	Urban	Urban
4	Shrub	Shrub
5	Wetlands	Wetlands
6	Pasture	Grass, forage, crops, fallow, barren
7	Cereals	Barley, oats, rye, triticale, wheat
8	Corn	Corn, sunflower
9	Canola	Canola, flaxseed
10	Soybean	Soybeans, peas, potatoes, other vegetables, berries
11	Broadleaf	Broadleaf, nursery

4.3.2 Soil Moisture Active Passive Validation Experiments 2015 (SMAPVEX15)

The SMAPVEX15 field campaign was conducted in a domain that included the Walnut Gulch (WC) Experimental Watershed near Tombstone, Arizona operated by the Agriculture Research Service (ARS), U.S. Department of Agriculture (USDA) and University of Arizona between August 2nd and August 17th, 2015 [Colliander et al., 2017]. The climate of this region is classified as semi-arid (Köppen climate classification- BSh), with mean annual temperature 290.85 K and receiving an average annual precipitation of 312 mm. The data was collected over three main regions, the Walnut Gulch (WC) watershed in the east, Empire Ranch at the center, and the Santa Rita experimental range located in the western part of the study domain, Fig 4.3. The vegetation of Walnut Gulch (WC) is comprised of two-thirds shrubs and one-third of grassland. The Santa Rita Experimental Range has a traditional desert landscape dominated by cactus and large shrubs (whitethorn acacia, creosote bush etc.). Empire Ranch on the other hand, is an active cattle ranch region dominated by grassland (sideoats, grama, lehmann, lovegrass, etc.). A unique feature of arid and semi-arid soils is the presence of whitish layers called calcic horizons. These horizons may be very thin (~ 15 cm) in some soils, or thick (greater than 1 m) in others. Some of these soils may also contain layers of clayey soils above the white calcic horizon. These clay rich layers are called argillic horizons, which may be visible up to 50 cm deep, and contain more than fifty percent clay. While the top soil of these regions was mostly sandy and gravelly, and contain large percentages of rock that range from nearly 0 % on shallow slopes to over 70 % on the very steep slopes. The topography of this region varied largely i.e., Empire Ranch has rolling topography (elevation: 1372 m-1884 m), Santa Rita has an elevation variation from 645 m-1170 m, and elevations at Walnut Gulch varied from 1170 m-1884 m, Fig 4.3. The Leaf Area Index (LAI) for the experimental region varied spatially within 0.12 - 0.53. However, there was only a

small and gradual change in Leaf Area Index (~ 0.014) from DOY 214 to 230. Since no significant change was observed in LAI, it was considered to be constant during the SMAPVEX15.

The PALS was used to measure brightness temperature on 7 days i.e., DOY 214, 217, 220, 222, 225, 228, and 230 at an effective resolution of about 1200 m for flights at an altitude of 2300 m. The data was regridded to 500 m based on a 1 km SMAP EASE ver. 2 grid satisfying Nyquist sampling criterion as described in Colliander et al. [2017]. A criterion of at least 3 in-situ measurements was established for soil moisture retrieval validation. The brightness temperature was upscaled to 3 km support scales to satisfy this criterion. Surface temperature was estimated using in-situ sensors and the infrared (IR) sensor onboard PALS. The vegetation water content was estimated using destructive sampling during non-flight days.

4.4 Soil Moisture Retrieval Algorithm

The tau-omega model, an approximation of the non-linear radiative transfer theory is used to simulate brightness temperature (T_B) under vegetation [Njoku and Entekhabi, 1996]:

$$T_{B(p,f,\theta)} = e_{p,f,\theta}.T_{eff}.\Upsilon_{p,f,\theta} + T_c.\left(1-\omega_{p,f,\theta}\right).\left(1-\Upsilon_{p,f,\theta}\right) + T_c.\Upsilon_{p,f,\theta}.\left(1-\omega_{p,f,\theta}\right)\left(1-\Upsilon_{p,f,\theta}\right).r_{p,f,\theta} \quad (4.1)$$

$$\Upsilon_{p,f,\theta} = \exp\left(-\frac{\tau_{p,f}}{\cos\theta}\right) \quad (4.2)$$

where p, θ and f denote polarization, look angle and frequency respectively. This study considers, p = V-polarization, with constant look angle of 40º at 1.4 GHz frequency. The radiative transfer (equation 4.1) is essentially approximated as a summation of three components 1) the direct emission by soil and one-way attenuation by canopy (the first term), 2) direct upward emission by canopies (the second term), and 3) emission by plants and reflected by soil and thereafter attenuated by vegetation (the third term).

4.4.1 Vegetation

The physical attributes of the vegetation that influence the soil emissivity are: the transmissivity of the vegetation $\Upsilon_{p,f,\theta}$, the single scattering albedo $\omega_{p,f,\theta}$ and the physical temperature of the canopy T_c. The transmissivity of vegetation at a constant look angle is given by equation (4.2) where, $\tau_{p,f}$ is the optical thickness of the vegetation. The formulation in equation (4.1) is based on the assumptions that; a) the single scattering albedo is small (less than 0.2), and thus diffuse scattering is ignored; b) the air-vegetation reflectivity is assumed zero, thus ignoring losses at the boundary, and c) the refractive index of vegetation is approximately equal to air, which allows using the air-soil reflectivity in equation (4.1). The amount of soil microwave emission that is absorbed and scattered as propagated through canopy is given by the transmissivity of the vegetation and scattering albedo. The loss factor is dependent on the volume fraction of water in the canopy and the architecture of the vegetation. The extinction optical thickness τ_p is estimated as a product of vegetation water content (VWC) and structure of the canopy (b). Due to the complex geometry of the natural canopies, approximate values are estimated for canopy structure (b) from land cover data. The canopy water content is estimated using the Normalized Difference Vegetation Index (NDVI) and regression with ground sample vegetation data [Jackson et al., 2004]. The τ_p and ω_p are polarization dependent because there may be differences in propagation of H-polarized and V-polarized wave under different canopy structures [Brunfeldt and Ulaby, 1986; Van de Griend et al., 2004; Wigneron et al., 2011]. For this study, it is assumed that b = 0.1 and ω = 0.05 for SMAPVEX12 and SMAPVEX15

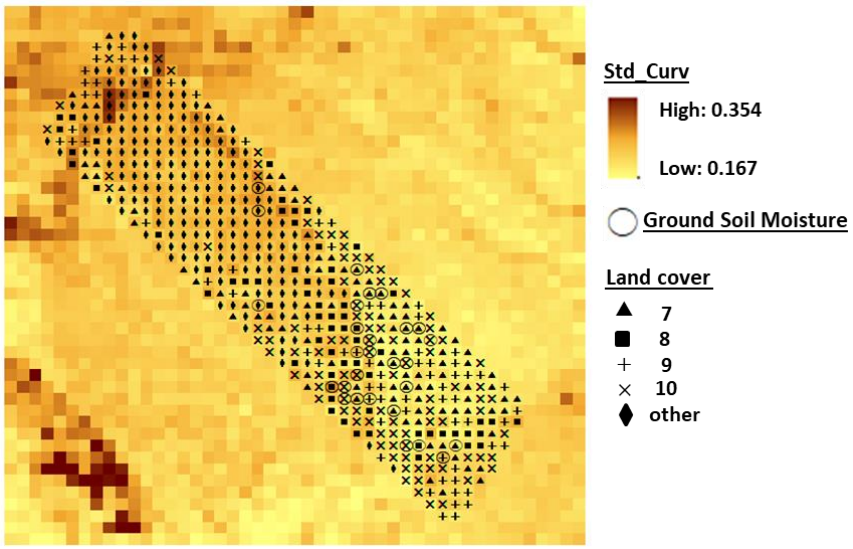

Figure 4.2 SMAPVEX12 field campaign domain and PALS flight lines. The ground truth soil moisture (represented by black dots) sampling strategy was designed to collect measurements at 16 locations along two parallel transects across the field. The variability of soil texture across the study region is represented by circles of different sizes. The gradient in elevation is represented through different colors. The land covers selected for analysis in section 5.1 is represented by different symbols (star, triangle, and pentagon).

4.4.2 Soil

The physical attributes that influence the microwave emissions from soils are surface reflectivity $r_{p,f,\theta}$ and effective soil temperature T_{eff} as given in equation (4.1). The reflectivity of soil can also be represented as $(1 - e_{p,f,\theta})$, where $e_{p,f,\theta}$is the soil emissivity. Soil surface reflectivity is determined by the dielectric constant (ϵ) of soil and the above surface geometric roughness parameters. The dielectric constant (ϵ) of soil is a non-linear function of several quantities including soil water content, bulk density, textural composition, and salinity, and of which soil water content is major determinant. The soil dielectric constant is estimated using the Mironov model [Mironov et al., 2009], due to its better performance under most soil textures [Bircher et al., 2012; Srivastava et al., 2015]. In practice, soil layers exhibit heterogeneity and non-isothermal properties with depth [Njoku and Kong, 1977; Wilheit, 1978; Schmugge and Choudhury, 1981]. Thus, estimating non-uniform temperatures and dielectric properties of vertical soil profiles is complex. Hence, an average of the skin temperature (measured using hand-held sensors) and temperature at 5-cm depth (measured with permanently installed network) is used as T_{eff} for SMAPVEX12 and SMAPVEX15. It is acknowledged that the deviation from actual temperature and texture profile up to L-band penetration depth may introduce an error in modeled brightness temperature.

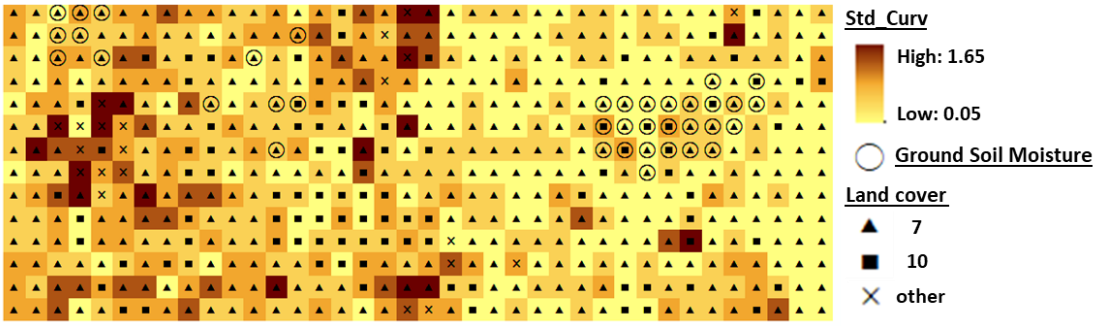

Figure 4.3 SMAPVEX15 field campaign domain and PALS flight lines. The ground truth soil moisture (represented by white dots) data was collected over three main regions, the Walnut Gulch (WC) watershed in the east, Empire Ranch at the center, and the Santa Rita experimental range located in the western part of the study domain. The variability in soil clay fraction across the study region is represented by circles of different sizes. The gradient in elevation is represented through different colors.

4.4.3 Surface Roughness

Equation (4.1) is based on the assumption that scattering (multiple reflections) within the soil medium is negligible and includes only surface reflection at transition layer of thickness *h* [Njoku and Entekhabi, 1979]. The surface roughness formulation that translates smooth reflection (Frensel reflectivity) to rough surface reflection combines statistical surface height variation parameters defined by standard deviation of surface height (σ) and surface correlation length (*l*) [Mo, Schmugge and Wang, 1987].

A simple roughness model was first introduced by Choudhury et al. [1979], which involved a single roughness parameter, the root mean square (RMS) height 'σ' given as;

$$R_r = R_s \, e^{(-H_r cos^2(\theta))} \tag{4.3}$$

$$H_r = 4 \, k^2 \sigma^2 \tag{4.4}$$

where R_r is the effective rough surface reflectivity, $R_s$is smooth surface reflectivity, H_r is the roughness parameter, λ is the wavelength of observation and $k = \frac{2\pi}{\lambda}$ is the wavenumber. The single parameter H_r was unable to match the measured angular variation in T_B. Thus, an extended two parameter model was proposed by Wang and Choudhury [1981] that introduced the polarization mixing parameter, *Q*, which has been refined by other investigators [Shi et al., 2005; Wigneron et al., 2011; Lawrence et al., 2013];

$$R_{r(p)} = [(1 - Q)R_{s(p)} + QR_{s(q)}]e^{(-H_r(SM)cos^n(\theta))} \tag{4.5}$$

where *p* and *q* denote horizontal and vertical linear polarizations respectively or vice-versa. *Q* is the polarization mixing factor. In some studies, *Q* is found to be equal to 0 at L-Band and increases moderately with frequency [Escorihuela et al., 2007; Montpetit et al., 2015; Saleh et al., 2007; Wigneron et al., 2001, 2007, 2011]. The factor *n* ranges from -2 to 2, and describes the dependence of roughness on incidence angle. The H_r is an effective roughness parameter that accounts for; (1)

the spatial variations on the surface of the soil and, (2) the spatial variations in the dielectric constant of the soil layer (upto L-band penetration) which can be caused by non-uniformities in the soil moisture content, texture, density, etc. [Kerr et al., 2012]. The equation (4.4) is currently used by SMAP mission and during field campaigns to estimate surface roughness. Therefore, the surface roughness H_r estimated using equation (4.4) according to each IGBP land cover class [O'Neill et al., 2015] Table 4.1, was used as an alternative to evaluate the performance of the proposed roughness model.

4.5 Proposed Surface Roughness Formulation

According to the Fraunhofer criterion a surface (an interface between two homogeneous non-scattering media in this case) may be considered as smooth in the microwave range if it satisfies [Ulaby, Moore and Fung, 2015];

$$\sigma < \frac{\lambda}{32\cos(\theta)} \tag{4.6}$$

where λ is wavelength of observation, σ is standard deviation of the surface height distribution, and θ is the angle of observation. However, the criterion is limited as it considers only the vertical roughness dimension "σ" and assumes that the horizontal wavelength "Λ" of the soil features is larger than the observation wavelength, thus restricting validity of this criterion by Bragg limit:

$$\Lambda < \frac{\lambda}{2\sin(\theta)} \tag{4.7}$$

For L-band (wavelength = 21 cm), a surface is considered smooth if $\sigma < 0.85\ cm$ and $\Lambda < 16.33\ cm$. However, Bragg's limit is not fulfilled for surfaces composed of stones, cracks, organic matter, and clods at small-scale or when there is topographic variability at large-scale. Thus, a comprehensive roughness model is proposed that encompasses roughness features ($\sigma\ and\ \Lambda$), which occur at small-scale (micro-) and large-scale (macro-) that influence surface reflectivity.

The proposed model is developed using proxy variables that control surface roughness variability at small-scale (micro) and large-scale (macro).

4.5.1 Macro-Roughness (Large-Scale Roughness)

The macro-roughness was described as the large scale undulations of the terrain observed within a footprint. These large scale undulations satisfy the Fraunhofer criteria (and Bragg limit). It is these large-scale deviations (elevated horizons) from the horizontal surface that contribute towards "roughness". Furthermore, in the presence of topographic undulations there are different types of influences on the measured signal; (1) alteration of the incidence and polarization angles and thus the brightness temperature, (2) some facets could be hidden, (3) slopes, valleys, and ridges can interact radiatively, (4) with altitude the influence of the atmosphere is reduced, and (5) topography influences the hydrology and vegetation characteristics of the region resulting in different roughness. For example, water on steeper slopes reduces frictional and cohesive forces among the soil particles, thereby increasing soil water run-off along with other materials such as crumbs, stones, organic debris etc., and thereby changing small-scale (micro) roughness locally. Additionally, topography plays an important role in soil moisture distribution, i.e., the topographic convergence (curvature) or divergence determines variability in wetness conditions. In this study, the topographic roughness (macro-roughness) was defined as the standard deviation of curvature, i.e., the second derivative of a surface, or slope of the slope. It was used to describe the shape of the slope, i.e., whether the surface profile is concave or convex. The curvature estimated in this study was a combination of profile and planform curvatures. The profile curvature affects the acceleration and deceleration of the flow, representing erosional and depositional activities. On the other hand, the plan curvature describes the convergence and divergence of the flow. Thus, considering plan and profile curvature together describes the flow more accurately. A positive

curvature indicates the surface is upwardly convex at that cell, whereas negative curvature indicates the surface is upwardly concave at that cell. For SMAPVEX12, 50 neighboring pixels, and for SMAPVEX15, 17 neighboring pixels were used to calculate the standard deviation in curvature.

4.5.2 Micro-Roughness (Small-Scale Roughness)

The micro-roughness was defined similar to the small-scale surface undulations. These surface undulations are typically measured using a pin-board or a grid board, where the variation in elevations of metal pins are considered due to rough surface underneath. However, due to the infeasibility to do these measurements operationally at airborne footprints (~ 1.5 - 3 km), proxy physical variables were used in defining surface roughness. Several factors such as the amount and rate of precipitation, soil water content, bulk density, composition of the soil, organic debris, wind speed, land cover, and tillage practices etc., influence soil roughness to various degrees. Of these factors, soil texture, wetness conditions and vegetation were used in this study due to their availability during the field campaigns. Starting with soil texture, if the composition of the soil is more clayey then the possibility of forming soil structures such as “peds” and “clods” occur more easily [Lyles and Woodruff, 1961; Allmaras et al., 1967]. This can occur either naturally or artificially based on wetness conditions. The high surface area and surface charge of clay particles play key roles in the formation of soil aggregates that otherwise would not occur in sand and silt soils with very low adhesion and cohesion powers. Additionally, clayey soils exhibit high swell-shrink potential that varies with soil wetness conditions. Under dry conditions, these soils can develop deep cracks and shear planes. All these features may contribute towards surface roughness. Leaf Area Index (LAI) is another proxy variable that was used in determining soil surface roughness dynamically. Precipitation that controls roughness variability is intercepted by

canopy cover (LAI). This reduces the precipitation intensity before it reaches the soil surface as stem flow, canopy drip or through fall. LAI also controls the rate of evapotranspiration, subsequently changing soil wetness conditions. For example, for landscapes with high LAI the surface roughness is higher due to reduced run-off and higher organic debris. In addition, as organic matter decomposes to humus, a variety of compounds are released which "glue" soil particles together, thereby changing soil composition over time. Under low LAI, the impact of a precipitation event on run-off is higher with low organic debris. Previous studies by Escorihuela et al. [2007], Saleh et al. [2006], Wigneron et al. [2001], and Kerr et al. [2012], have shown the influence of soil moisture on the roughness H_r parameter. Surface scattering has been observed to decrease with wetness conditions. Therefore, the influence of wetness conditions is incorporated through field sampled soil moisture collected using theta probes on flight days.

Thus, the new total surface roughness H_{new} formulation is composed of two roughness parameters 'H_{micro}' and 'H_{macro}' as defined in equations 4.8-4.10.

$$H_{new}(i) = H_{micro}(i) \times H_{macro}(i) \quad (4.8)$$

$$H_{micro}(i) = \exp(-\frac{SM(i) \times (1-NLAI(i))}{CF(i)}) \quad (4.9)$$

$$H_{macro}(i) = (std.curv(i))^a \quad (4.10)$$

where, the micro (small-scale) 'H_{micro}' roughness parameter was defined as an exponential function of soil moisture (SM), clay % and normalized leaf area index (NLAI) and the macro-(large-scale) 'H_{macro}' roughness parameter as the standard deviation of curvature, whereas 'i' is per pixel. The calibration parameter 'a' determines the scale of macro-roughness contributing to total surface roughness, and this parameter varies with environmental conditions (wetness, texture, topography, LAI).

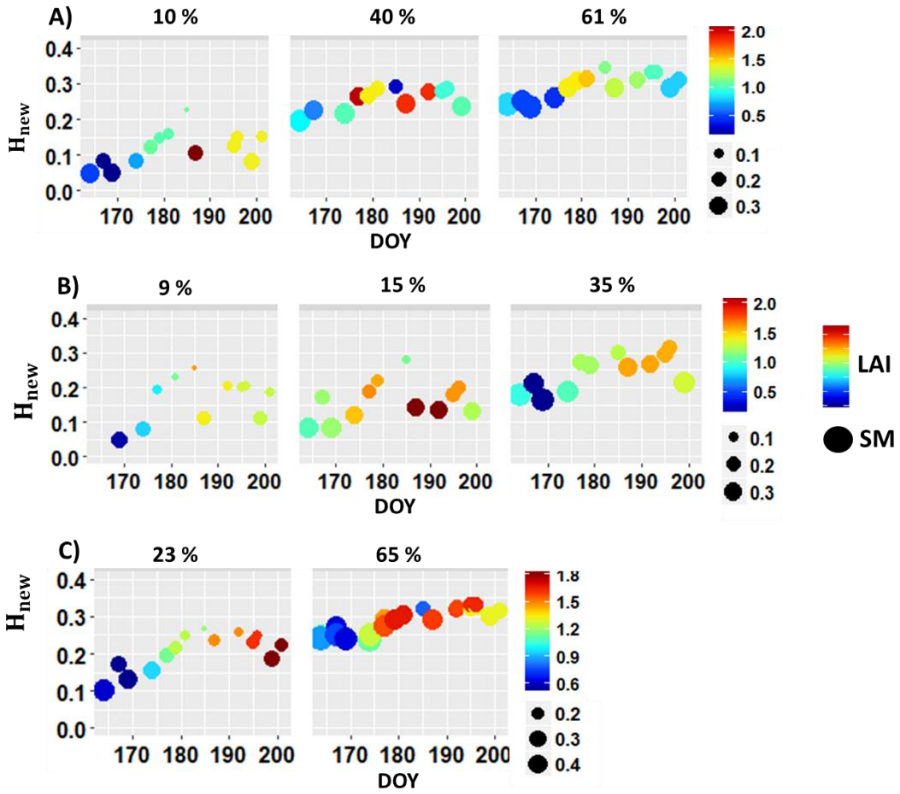

Figure 4.4 The temporal dynamics of derived total-surface roughness (micro-roughness) with soil moisture (SM), clay percentage and Leaf Area Index (LAI) for SMAPVEX12. The Y-axis represents the magnitude of micro-roughness, X-axis represents time (Day of the Year- DOY), size of the circle represents the magnitude of soil moisture (SM), and color bar represents magnitude of LAI. At the top of each subplot, clay percentage and standard deviation in curvature for that pixel is shown A): Land cover 7, Middle: Land cover-9, Bottom: Land cover 10.

4.6 Results and Discussion

The brightness temperature observed during the SMAPVEX12 and SMAPVEX15 field campaigns showed high temporal variability. The soil moisture was retrieved from V-polarization brightness temperature for pixels with vegetation water contents (VWC) ≤ 5kg/m^2 using the algorithm. The performance of the new roughness model (H_{new}) was evaluated with land cover specific roughness (H_LC) estimates (Table 4.1) by comparing the Root Mean Square Error (RMSE), unbiased (mean centered) Root Mean Square Error (ubRMSE), bias and Pearson correlation coefficient (R). The analysis was conducted w.r.t Day of the Year (DOY) and land cover (LC). As observed from Table 4.2 (A, B), the new surface roughness model significantly reduced soil moisture bias.

The lowest RMSE's for soil moisture retrieval was obtained using the new surface roughness [equations (4.8-4.10)] Table 4.2, with $a = 2$ for SMAPVEX15 and $a = 0.5$ for SMAPVEX12. In contrast, during SMAPVEX12 there was a consistent increase in LAI, Fig 4.4. The topography of SMAPVEX12 varied spatially, which resulted in a total surface roughness that is dominated by both micro-roughness and macro-roughness, and that varied spatio-temporally with wetness and vegetation conditions. Conversely, significant contribution of the macro-roughness to total surface roughness was observed for SMAPVEX15.

Table 4.2 Performance metrics of retrieved soil moisture using the new surface roughness model (H_{new}) in comparison with soil moisture retrieved using land cover specific surface roughness (H_LC) analyzed for A) SMAPVEX12 and SMAPVEX15 with DOY and B) SMAPVEX12 and SMAPVEX15 with land cover (LC). RMSE stands for Root Mean Square Error, ubRMSE stands for unbiased RMSE, and R stands for Pearson correlation.

A.1) SMAPVEX12 with DOY

	H_{new}	H_LC	H_{new}	H_LC	H_{new}	H_LC	H_{new}	H_LC
DOY	RMSE		ubRMSE		Bias		R	
164	0.13	0.16	0.10	0.12	-0.08	-0.11	0.41	0.14
167	0.07	0.08	0.07	0.08	0.03	0.02	0.70	0.61
169	0.12	0.14	0.11	0.12	-0.05	-0.07	0.42	0.26
174	0.12	0.14	0.11	0.12	-0.04	-0.06	0.47	0.36
177	0.08	0.09	0.08	0.09	0.01	0.00	0.55	0.44
179	0.08	0.07	0.05	0.05	0.06	0.05	0.65	0.59
181	0.07	0.08	0.07	0.08	-0.01	-0.01	0.42	0.34
185	0.06	0.06	0.06	0.06	0.00	0.00	0.39	0.33
187	0.08	0.10	0.08	0.09	-0.03	-0.04	0.16	0.01
192	0.04	0.05	0.04	0.05	-0.01	-0.01	0.64	0.58
195	0.06	0.07	0.06	0.07	0.02	0.02	0.61	0.55
196	0.05	0.06	0.05	0.05	0.01	0.01	0.63	0.58
199	0.07	0.08	0.07	0.08	-0.01	-0.02	0.64	0.50
201	0.03	0.03	0.03	0.03	0.01	0.01	0.88	0.88

Continued Table 4.2…

A.2) SMAPVEX15 with DOY

	H_{new}	H_LC	H_{new}	H_LC	H_{new}	H_LC	H_{new}	H_LC
DOY	**RMSE**		**ubRMSE**		**Bias**		**R**	
214	0.06	0.08	0.05	0.06	-0.02	-0.05	0.30	0.23
217	0.04	0.04	0.03	0.04	0.02	0.01	0.00	0.00
220	0.04	0.06	0.04	0.05	-0.01	-0.03	0.68	0.67
222	0.06	0.07	0.05	0.06	-0.02	-0.04	0.36	0.38
225	0.04	0.04	0.04	0.04	0.01	-0.01	0.36	0.49
228	0.05	0.06	0.05	0.05	-0.01	-0.04	0.57	0.62
230	0.04	0.04	0.04	0.04	0.01	-0.01	0.00	0.03

B.1) SMAPVEX12 with LC

	H_{new}	H_LC	H_{new}	H_LC	H_{new}	H_LC	H_{new}	H_LC
LC	**RMSE**		**ubRMSE**		**Bias**		**R**	
6	0.11	0.11	0.11	0.11	0.00	-0.01	0.27	0.27
7	0.07	0.08	0.07	0.07	0.01	0.02	0.80	0.79
8	0.12	0.17	0.08	0.10	-0.09	-0.13	0.80	0.77
9	0.12	0.14	0.10	0.11	-0.07	-0.10	0.59	0.60
10	0.05	0.06	0.05	0.06	0.02	0.00	0.83	0.82

B.2) SMAPVEX15 with LC

	H_{new}	H_LC	H_{new}	H_LC	H_{new}	H_LC	H_{new}	H_LC
LC	RMSE		ubRMSE		Bias		R	
7	0.05	0.06	0.05	0.05	0.00	-0.02	0.51	0.53
10	0.04	0.06	0.04	0.05	0.00	-0.04	0.61	0.63

4.6.1 Land cover

The landscape of SMAPVEX12 was dominated by agricultural crops (mainly cereals, soybeans, canola, and corn). The observed mean (standard deviation) of the Leaf Area Index (LAI) varied from ~ 0.81 (~ 0.56) on DOY 164 to ~ 1.41 (~ 0.53) on DOY 201. For similar textural and topographic features, a higher surface roughness was estimated for vegetation with higher LAI and this behavior is consistent across land covers, Fig 4.4 (Top, Middle, Bottom). The increase in canopy interception and stem flow is especially higher among vegetation with broad leaves. This interception by the canopy will determine roughness by altering the surface run-off. In addition, the plant litter, freshly fallen leaves or seasonal leaf off contribute towards organic debris. Thus, vegetation regulates surface (micro) roughness at a field scale through rainfall interception, organic debris, reduced run-off, etc. For SMAPVEX12, three land cover classes (7, 9, 10) are selected to analyze the variability in surface roughness. The cereal crops such as spring wheat, oat, and winter wheat were sampled under land cover 7, whereas canola and flaxseed were sampled under land cover 9. Land cover 10 included soybean, covering ~ 18.5 % of SMAPVEX12 study area. For land cover 10, a consistent increase in LAI with time was noticed which was not the case for land covers 7 and 9 where LAI increased initially and later decreased.

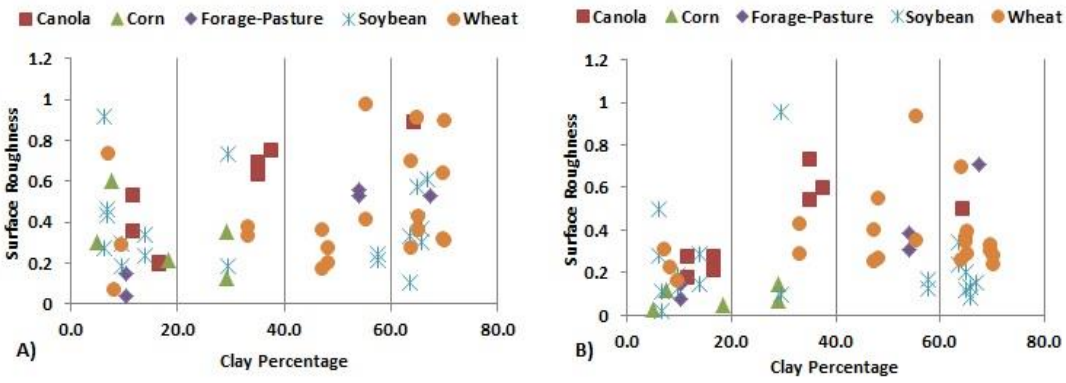

Figure 4.5 The surface roughness measured using grid board in the look direction of, A) PALS (Passive Active L-band System), B) UAVSAR (Uninhabited Aerial Vehicle Synthetic Aperture Radar) during SMAPVEX12, is plotted as a function of clay percentage and crop type.

Typically, the LAI pattern begins with a lag increase early in the season, followed by a rapid increase of LAI until a maximum value is reached, then a decline of LAI is observed as leaves senesce and plants reach physiological maturity. This behavior is more evident in the case of winter wheat (land cover 7), where the LAI is higher before blossoming and decreases after tasseling. As for the soybean fields (land cover 10), the decrease in LAI with senesce is not observed for the duration of field campaign. For soybean, which is a row crop, during the initial stages of the field campaign with low levels of vegetation, a larger portion of the ground surface is exposed to precipitation (increased run-off). This may result in lower surface roughness for land cover 10 than for land covers 7 and 9 initially. However, this changed by the end of the field campaign, when higher surface roughness was estimated for land cover 10, Table 4.3. This may be due to higher LAI for land cover 10 (soybean-broad leaves), than for land covers 7 and 9 where LAI decreased (after tasseling) by the end of field campaign. Therefore, vegetation contributes in regulating surface (micro-) roughness at a field scale through rainfall interception, organic debris, reduced run-off, etc.

Table 4.3 Comparison of pixels selected from three land-cover classes- 7, 9, 10 during SMAPVEX12 to demonstrate the effect of clay %, standard deviation in curvature (std.curv), mean-Leaf Area Index (LAI) in determining the surface roughness. H_LC represents the land cover specific surface roughness.

	Land cover 7			Land cover 9			Land cover 10	
	Pixel-1	Pixel-2	Pixel-3	Pixel-1	Pixel-2	Pixel-3	Pixel-1	Pixel-2
Clay %	61 %	40 %	10 %	35 %	15 %	9 %	65 %	23 %
Std.Curv	0.17	0.17	0.20	0.21	0.19	0.21	0.18	0.18
Mean_LAI	1.30	1.34	1.32	1.13	1.50	1.14	1.49	1.16
H_LC	0.17	0.17	0.17	0.35	0.35	0.35	0.35	0.35
H_{new}	0.23-0.34	0.20-0.30	0.05-0.22	0.16-0.31	0.08-0.28	0.05-0.25	0.24-0.33	0.10-0.27

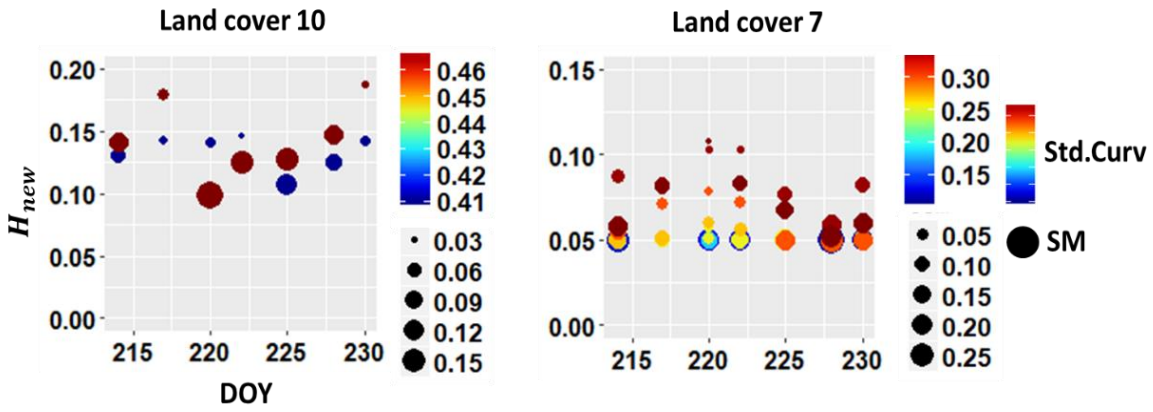

Figure 4.6 The temporal dynamics of new surface roughness (H_{new}) for shrub land (LC-7) (clay % = 16.7) and grassland (LC-10) (clay % = 20 & 18.07) that varied with soil moisture (SM), and std.curv for SMAPVEX15, Table 4. The X-axis represents time (Day of the Year- DOY), color bar and size of the circle represents variability in std.curv and soil moisture respectively.

SMAPVEX15 is a natural landscape dominated by shrub land (LC-7) and grassland (LC-10) land covers as categorized by IGBP with constant roughness parametrizations, Table 4.1B [O'Neill et al., 2015]. Two pixels from each land cover type were selected, Table 4.4. For grasslands, in spite of higher LAI for Pixel 2 than Pixel 1 (other attributes are nearly similar), there was no significant difference in variability of estimated surface roughness. Therefore, for semi-arid regions with low (grass/shrub land) or no vegetation, the control of vegetation in regulating roughness is minimized.

The variability in estimated surface roughness values are also supported by past studies, Wang et al. [2015], Park et al. [2015], and Parrens et al. [2016] who also found a high correlation between surface roughness and vegetation, i.e., higher $H_r$values for higher LAI regions, and lower $H_r$values for shrubs, bare soils and deserts.

4.6.2 Soil Texture

In Table 4.3, two pixels from soybeans (LC-10), and three pixels from cereals (LC-7) and canola (LC-9) land cover category were selected from SMAPVEX12 to depict the effect of clay % on surface roughness. For soils with a high clay %, the ability to form aggregated structures (peds, clods) increased, which contributed towards regulating surface (micro) roughness, Fig 4.4 (Top, Middle, Bottom). To confirm this behavior, the surface roughness measured under different soil textures was analyzed. From Fig 4.5 (A, B) it is apparent that, for crops with lower LAI values (i.e., winter wheat, wheat, canola, pasture, oats, and forage) the micro-surface roughness increased exponentially with the clay %. However, this behavior was not consistent for crops with higher LAI values (i.e., soybean and corn). A higher micro-roughness estimated for soybean and corn (higher LAI) in spite of low clay %, is attributed towards factors such as rainfall interception, and higher organic debris. The soil texture for SMAPVEX12 varied significantly, which also contributed towards wide range of estimated surface roughness. This is in contrast to land cover

specific roughness (H_LC) values which are constant, Table 4.3. For SMAPVEX15, the clay % for the validation pixels varied from 16 % - 25 %, which in addition to dry soil moisture conditions resulted in high micro-roughness for SMAPVEX15, Table 4.4.

4.6.3 Soil Moisture

The observed surface roughness is generally perceived as a combination of surface and volume scattering. The surface scattering is higher than volume scattering under high soil moisture conditions. But as soil dries, there will be an increase in both volume and non-specular surface scattering. This may be because of increase in the penetration depth of the signal under dry conditions at L-band, which enables both volume and multiple scattering in sub-surface. Therefore, decreasing soil moisture increases total surface roughness, as also shown in Figs 4.4, 4.5, 4.6. The effects of soil moisture on surface roughness was also discussed previously in, e.g., Potter, [1990], Zobeck and Onstad, [1987], Escorihuela et al. [2007], Panciera et al. [2009b] and Colliander et al. [2016].

In Fig 4.7 and Table 4.5, two pixels are considered from SMAPVEX12 and SMAPVEX15 with similar clay % (Pixel 1) and macro-roughness (std.curv) (Pixel 2), but different SM and LAI conditions. In spite of low SM and high std.curv, SMAPVEX15 showed smaller roughness variability compared to SMAPVEX12 for both Pixel 1 and Pixel 2 because of higher LAI.

Table 4.4 Comparison of four different pixels selected during SMAPVEX15 to demonstrate the effect of clay percentage, standard deviation in curvature (Std.Curv), mean-Leaf Area Index (LAI) in determining the micro-, macro- and total surface roughness.

	Land cover 7		Land cover 10	
	Pixel-3	Pixel-4	Pixel-1	Pixel-2
Clay %	16.7 %	16.7 %	20 %	18.07 %
Std. Curv	0.35	0.27	0.41	0.47
Mean LAI	0.50	0.70	0.28	0.71
H_LC	0.42	0.42	0.85	0.85
$\mathbf{H}_{\mathbf{new}}$	0.05-0.11	0.05	0.11-0.15	0.10-0.19

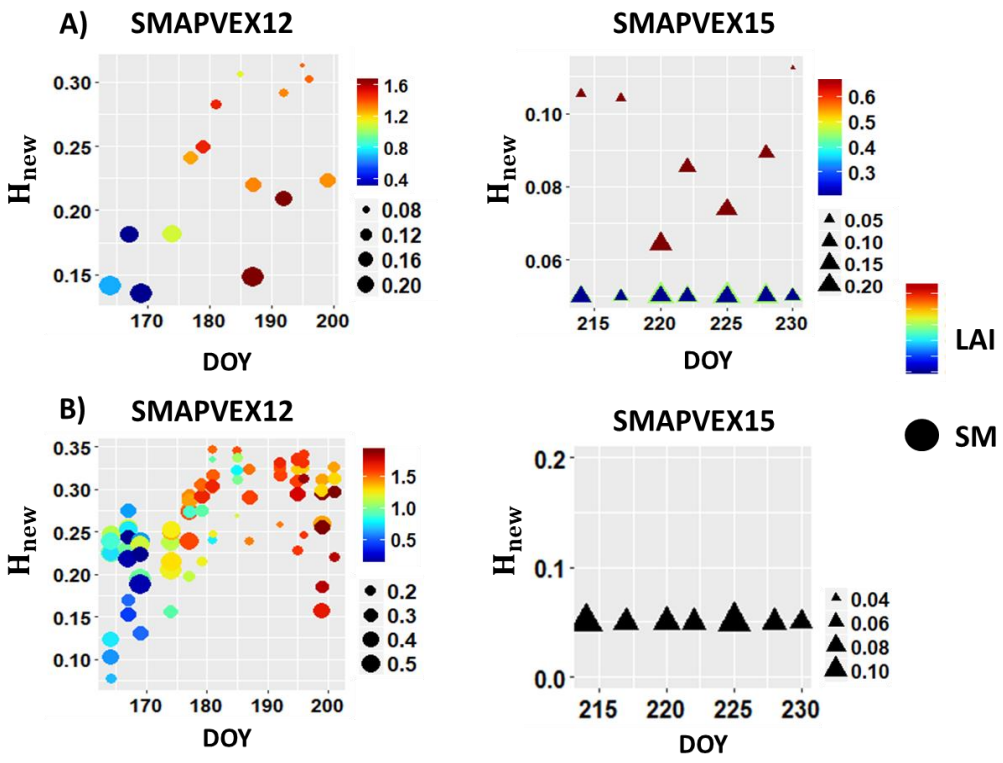

Figure 4.7 The temporal dynamics of derived total and micro-surface roughness for four different pixels (A, B, C, and D) that varied in soil moisture (SM), clay percentage and Leaf Area Index (LAI) for SMAPVEX15. The Y-axis represents the magnitude of land surface variables (total-roughness, micro-roughness, soil moisture, clay percentage and Leaf Area Index), while X-axis represents time (Day of the Year- DOY).

Table 4.5 Comparison of pixels similar in geophysical attributes (clay percentage and macro-roughness) from SMAPVEX12 and SMAPVEX15. Pixel-1 is similar in clay percentage and different macro-roughness, whereas Pixel-2 shows similar macro-roughness and different clay percentages, resulting in different ranges of total surface roughness.

	SMAPVEX12	SMAPVEX15	SMAPVEX12	SMAPVEX15
	Pixel-1		Pixel-2	
Clay %	23	20	10	16.7
Mean LAI	1.23	0.28	0.74	0.70
Mean SM	0.20	0.05	0.20	0.08
Std.Curv	0.18	0.41	0.21	0.27
H_LC	0.35	0.85	~ 0.35	0.42
$\mathbf{H}_{\mathbf{new}}$	0.10-0.26	0.11-0.15	0.05-0.15	~ 0.05

4.6.4 Topography

SMAPVEX15 region with undulating topography showed higher variability in standard deviation of curvature (std.curv), than in SMAPVEX12. A pixel with a higher std.curv was assumed as a rough surface bouncing radiation in all directions as opposed to a pixel with lower std.curv surface (see Fig 4.1). Because of low or no vegetation in SMAPVEX15, the disaggregation of rocky hilltop occurs more easily under the topographic influence. For example, water tends to run-off higher areas and collect in lower areas more easily in the absence of vegetation, which leaves knolls dry with easily erodible topsoil. The disintegrated rocky debris will eventually level out to gravelly topsoil creating new micro-surface roughness.

From Table 4.4, where Pixel 2 and Pixel 4 show nearly similar attributes (i.e., clay % and LAI), Pixel 2 exhibited higher surface roughness variability because of high std.curv. It is observed from the analysis, that the total variability in surface roughness is determined according to the variability in micro-roughness, with magnitudes scaled by macro-roughness. This may be attributed towards enhanced destructive interference of diffused scattering due to micro-roughness reducing the impact of roughness. In addition, regions with high topographic variability and low/no vegetation are generally associated with low soil moisture conditions, which result in high brightness temperatures. While, the ability of tau-omega transfer model to retrieve soil moisture from tau-omega model under dry conditions and its validation with ground truth data require lower H_r surface roughness values, which may otherwise result in saturated soil moisture values during optimization. The $H_r$values found in this study were found to be in agreement with measurements made in other studies [Mo et al., 1982; Wigneron et al., 2012; Wang et al., 2015; McNair et al., 2015; Parrens et al., 2016], where low roughness values are obtained over shrubs, bare ground, and desert, and higher values are obtained for higher vegetation covers.

4.7 Conclusion

A multi-scale roughness model was proposed to estimate surface roughness at different spatial scales using proxy variables (e.g., soil moisture, texture, topography, LAI). The novelty of this study, is it demonstrated the variability in surface roughness and defined the proxy land surface variables which can be used to map roughness dynamically. The performance of the model developed was evaluated by inverting the traditional tau-omega model for retrieving soil moisture from PALS data collected during two field experiments SMAPVEX12 and SMAPVEX15. This investigation validated that incorporating micro and macro-roughness in estimating total surface roughness improves passive microwave soil moisture retrieval. The degree of macro-roughness (a) contributing towards total surface roughness varies with local topography. The study corroborated that the micro-scale roughness increased exponentially with clay fraction under no or low vegetation, and decreased with wetness conditions. However, under higher LAI the effect of soil texture was not obvious and the micro-roughness increased with LAI under all soil textures. Thus, it may no longer be necessary to assume a constant H_r specific to a land. The future work of this analysis can be extended to satellite scale, and can incorporate soil moisture or precipitation data from satellite or ground stations (SMAP/SMOS/GPM/SCAN).

5 ON RADIATIVE TRANSFER MODEL AND ITS RELATIONSHIP WITH THERMAL FLUXES THROUGH SPACE, TIME, AND HYDROCLIMATES

5.1 Synopsis

The spatio-temporal variability in terrestrial biosphere is found to contribute significantly towards uncertainty in microwave radiative transfer model (RTM) due to land surface (soil-vegetation) interactions. In this work, we propose scaling of vegetation optical depth (VOD) based on the coefficient of variation (CV) observed for vegetation water content (VWC) within a pixel. The efficacy of VOD scaling on the retrieved soil moisture accuracy is explored using, i) ground soil moisture observations; ii) soil moisture estimated using a simple water balance; iii) Taylor's Error Propagation (TEP) technique to estimate soil moisture errors. It is found that the soil moisture errors are reduced using scaled VOD especially over croplands (during growing season) and forest land cover classes. The TEP technique is further explored to classify the soil moisture errors into the first order (principal) errors due to the uncertainty in the land surface variables and into their interactions errors (second order). Because these interactions are also the critical drivers of hydrological and metrological processes, we explored their relationship with evaporative fraction (EF), sensible heat (H), and vapor pressure deficit (VPD) analyzed over multiple land covers, hydroclimates, and temporal scales. It is found that, the land surface interactions increased with EF, and decreased with H and VPD. This relationship varied with availability of soil moisture. The effect of VPD on land surface interactions was significant under arid climate than compared to the temperate or continental climates. Generally, the land surface interactions were higher under temperate climate than other climate classes.

5.2 Introduction

Vegetation plays a fundamental role in water, and carbon cycle sustaining biological productivity. The microwave remote sensing of soil moisture is affected due to the high sensitivity of brightness temperature to vegetation optical depth (VOD) which causes systematic and/or random errors in retrieved soil moisture (Wigneron et al., 2017). In addition to this, it still remains a challenge to account for the subfootprint-scale heterogeneity in vegetation water content (VWC) and obtain representative footprint-scale VOD values. VOD is directly proportional to VWC with a proportionality constant which is dependent on vegetation geometry. Currently, the soil moisture active passive (SMAP) mission uses VOD estimated through a non-linear aggregation of fine resolution of VWC [Zhan et al., 2008] upto ~ 9 km on EASE grid, beyond which the VOD is simply averaged to 36 km. Several past studies [Chehbouni et al., 1995; Shuttleworth et al., 1997; O'Neill et al., 2006] found that simple average of VWC within a pixel may overestimate the effective VWC and demonstrated that empirically corrected VWC can improve soil moisture retrievals. Despite these advances, past work has not generally accounted for within pixel variability of VWC. In this study, we explored the coefficient of variation (CV) used in many ecological studies (Taylor, 1961) as a dominant diagnostic tool to quantify variability in VWC within a pixel. This metric conflates the separate patterns of mean and standard deviation in the face of spatial and temporal change in VWC.

In addition to, the importance of mapping vegetation heterogeneity for soil moisture retrieval accuracy, the spatial and temporal variability in vegetation also plays a crucial role in the redistribution of water and energy fluxes (Koster and Suarez, 1992) mainly through, *i*) increase in direct transpiration; *ii*) evaporation from plants surfaces due to intercepted precipitation; *iii*) reduces runoff and increases water holding capacity of soils, leading to increased direct

evaporation from the soils. For example, evapotranspiration (ET) estimated for mean density of vegetation for a coarse pixel, will most likely be different from ET averaged using two adjacent fine resolution pixels with different vegetation densities (Rowe, 1993; Wood, 1997). Also, the temporal (seasonal) changes in vegetation (*i.e.*, dormancy, leaf emergence, mid-season, and senescence) alter the canopy (and stomatal) conductance, that leads to non-linear redistribution of water and energy fluxes at the ground surface.

Therefore, the natural environment is an intricate system formed of mutually interlinked components (soil, water, vegetation, and atmosphere). Understanding the whole ecosystem functionality depends on our capacity to understand the soil-water-vegetation-climate interactions and their impact on driving the water and energy fluxes (Avissar, 1995; Pielke et al., 1998). For example, plants absorb carbon dioxide through photosynthesis, and release water vapor through evapotranspiration, and influence vapor pressure deficit (VPD), and air temperature through their changing reflectivity (albedo). These feedback mechanisms change with soil wetness conditions, growth stage and density of vegetation, atmospheric gradient etc. Therefore, mapping and quantifying the land surface interactions operating on a wide range of spatial and temporal scales are extremely important. A classic microwave radiative transfer model (RTM) is used to characterize the soil-vegetation properties to estimate soil moisture (Njoku and Kong, 1977; Ulaby et al., 1986). This is a linear model, which ignores higher order non-linear interactions among soil and vegetation properties. A Taylor's error propagation method is used to quantify the soil-vegetation interactions observed in microwave RTM which are then associated with evaporation fraction (EF), sensible heat (H), and VPD. The soil-vegetation interactions are categorized as, *i)* within vegetation variables (e.g., VOD, scattering albedo (ω),); *ii)* vegetation (i.e., VOD) and surface temperature (TS); *iii)* brightness temperature (T_B) and vegetation variable (e.g., VOD or

scattering albedo (ω)); *iv)* between vegetation variables e.g., VOD and scattering albedo (ω). These interaction terms hereafter in the paper are referred to as land surface interactions. Since, vegetation water content and brightness temperature are also an indicator of the availability of soil moisture and fluctuations in surface emissivity, therefore interactions derived here are an indication of all vegetation-soil moisture-temperature-soil components. These interactions are also analyzed with the variability in the coefficient of variation (CV), and found to be strongly correlated. Based on our analysis, the Neelam and Mohanty, 2018 (submitted) model is validated and further extended to incorporate fluxes.

The objectives of this paper are as follows, *i)* To improve the soil moisture retrieval accuracy by incorporating the within-pixel heterogeneity in VWC; *ii)* To map the variability in the soil-vegetation interactions in RTM with respect to hydroclimates, temporal scales, and different land covers; *iii)* To analyze the relationship between the soil-vegetation interactions with EF, H and VPD. In summary, we explore the relationship between land surface interactions observed at the L-band microwave frequencies, and fluxes like EF and H.

5.3 Data

5.3.1 SMAP Satellite Products

The SMAP satellite L-band mission was launched by NASA in 2015 (Entekhabi et al., 2010) to retrieve global soil moisture data (top 0-5 cm surface layer). The SMAP Level-3 (Version 4, SPL3SMP) daily composites which are gridded on 36-km on Equal-Area Scalable Earth grid ver.2 (EASE-2) is used for the analysis (Chan et al., 2018). Currently, the passive soil moisture products are retrieved from SMAP T_B radiometer data using the baseline Single Channel Algorithm (SCA) V-pol. This data is freely available at NASA National Snow, and Ice Data Center Distributed Active Archive Center (NSIDC DAAC) (http://nsidc.org/data/SPL3SMP). The

SPL3SMP product brightness temperature, soil moisture along with ancillary data, *i.e.*, vegetation optical depth, (VOD), albedo (ω), surface roughness (RC), and surface temperature (ST), are used in the soil moisture retrieval. The analysis is conducted according to each land cover class as defined by International Geosphere Biosphere Programme (IGBP), Table 5.1 and Fig 5.1.

Table 5.1 IGBP Land Cover Classifications

ID	*MODIS IGBP Land Classification*	*s*	*h*	*b*	*ω*	*Stem factor*
0	Water	--	0	0	0	--
1	Evergreen needleleaf forest	1.60	0.160	0.100	0.05	15.96
2	Evergreen broadleaf forest	1.60	0.160	0.100	0.05	19.15
3	Deciduous needleleaf forest	1.60	0.160	0.120	0.05	7.98
4	Deciduous needleleaf forest	1.60	0.160	0.120	0.05	12.77
5	Mixed forest	1.00	0.160	0.110	0.05	12.77
6	Closed shrub lands	1.00	0.110	0.110	0.05	3.00
7	Open shrub lands	1.10	0.110	0.110	0.05	1.50
8	Woody savannas	1.00	0.125	0.110	0.05	4.00
9	Savannas	1.56	0.156	0.110	0.080	3.00
10	Grasslands	1.56	0.156	0.130	0.050	0.150
11	Permanent wetlands	1.00	0	0	0	4.00
12	Croplands-Average	1.08	0.108	0.110	0.050	3.50
	Wheat	0.83	0.083	TBD	TBD	TBD
	Mixed (Wheat, Barley, Oats)	1.08	0.108	TBD	TBD	TBD
	Corn	0.94	0.094	TBD	TBD	TBD
	Soybean	1.48	1.48	TBD	TBD	TBD
13	Urban and built-up	--	0	0.100	0.030	6.49
14	Cropland/natural vegetation mosaic	1.30	1.30	0.110	0.065	3.25
15	Snow and ice	--	0	0	0	0
16	Barren or sparely vegetated	1.50	0.150	0	0	0

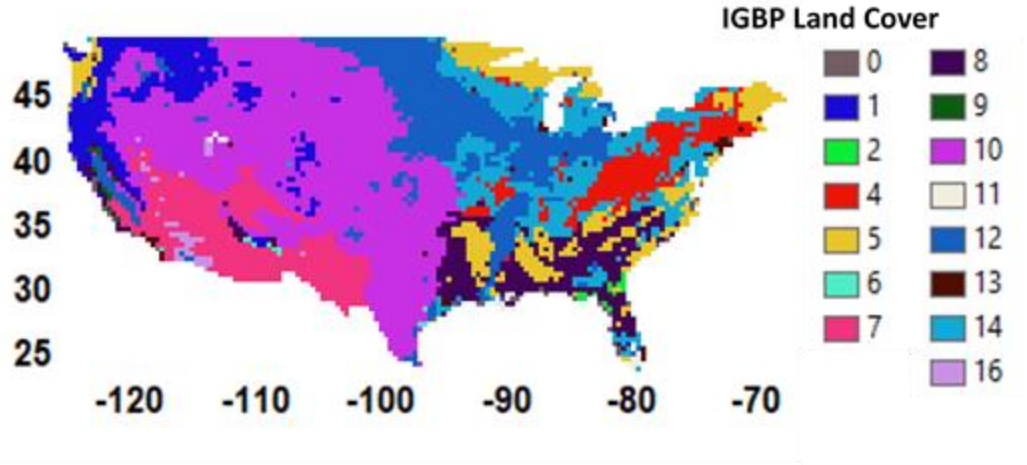

Figure 5.1 The different IGBP land cover classes across continental USA.

5.3.2 Other Remote Sensing Products

The Global Multi-resolution Terrain Elevation Data 2010 (GMTED2010) for topography, the State Soil Geographic (STATSGO) for soil texture and the Moderate Resolution Imaging Spectroradiometer (MODIS) MCD15A3H for Leaf Area Index (LAI) across Conterminous United States (CONUS) at 1 km are used to estimate within pixel (36 km) topographic, textural and vegetation features i.e., mean and standard deviation of elevation, slope, curvature, % sand, % clay and LAI. Terra/MODIS MOD13A3 NDVI data at 1 km and MCD12C1 (Landcover) at 500 m are used to estimate mean and standard deviation of vegetation water content from MODIS NDVI according to the formulation provided in SMAP L2 Algorithm Theoretical Basis Documents (ATBD) Zhan et al., 2008.

5.3.3 Land Surface Models Soil Moisture

The soil moisture simulated from three Land Surface Models (LSMs) (Noah, Mosaic, and VIC) are used for validation purpose. The Noah model has four soil layers: 0–10 cm, 10–40 cm, 40–100 cm, and 100–200 cm. The Mosaic model has three soil layers: 0–10 cm, 10–60 cm, and 60–200 cm. Three soil layers are used in the VIC model, with a 10 cm top layer and spatially varying depths for the other two layers. The topsoil layer 0-10 cm soil moisture from Noah, VIC and Mosaic models are used in the analysis. The first two models (Noah and Mosaic) emerged within the Soil Vegetation Atmosphere Transfer (SVAT) scheme for coupled atmospheric modeling with a focus on the energy and water flux exchange with little calibration. While the VIC model is designed as uncoupled hydrological model with focus on flood simulation and considerable calibration. As a result, all three LSMs are considered as both SVAT and semi-distributed hydrological models (Lohmann et al., 2004).

Table 5.2 The AmeriFlux stations selected across CONUS for soil moisture validation.

Site	Latitude	Longitude	Elevation	IGBP	Climate Koppen
Amargosa Desert Research Site (ADR)	36.7653	-116.6933	842	BSV	Bwh
RCEW Low Sagebrush (Rls)	43.1439	-116.7356	1608	CSH	Bsh
Reynolds Creek Wyoming big sagebrush (Rws)	43.1675	-116.7132	1425	OSH	Bsk
Santa Rita Grassland (SRG)	31.7894	-110.8277	1291	GRA	Bsk
Walnut Gulch Lucky Hills Shrub (Whs)	31.7438	-110.0522	1370	OSH	Bsk
Sierra Critical Zone, Sierra Transect, Sierran Mixed Conifer (CZ3)	37.0674	-119.1951	2015		
RCEW Mountain Big Sagebrush (Rms)	43.0645	-116.7486	2111	CSH	Bsh
Southern California Climate Gradient - Pinyon/Juniper Woodland (SCw)	33.6047	-116.4527	1281	OSH	
Santa Rita Mesquite (SRM)	31.8214	-110.8661	1120	WSA	Bsk
Walnut Gulch Kendall Grasslands (Wkg)	31.7365	-109.9419	1531	GRA	Bsk
Sierra Critical Zone, Subalpine Forest, Shorthair (CZ4)	37.0675	-118.9867	2710	ENF	
Rosemount-C7 (Ro2)	44.7288	-93.0888	292	CRO	Dfa
Valles Caldera Sulphur Springs Mixed Conifer (Vcs)	35.9193	-106.6142	2752	ENF	Dfb
Valles Caldera Mixed Conifer (Vcm)	35.8884	-106.5321	3030	ENF	Dfb

5.3.4 In-Situ Measurements

5.3.4.1 USCRN

The US Climate Reference Network (USCRN; Diamond et al. 2013) encompasses a number of sites located across USA. As these sites are located across a wide range of vegetation types and hydroclimates they are highly suitable for validation purposes. However, to avoid as much uncertainty, we consider stations that are within 10 km from the center of a SMAP pixel. This criterion reduces the number of validation stations from 150 to 20 stations within the CONUS. The soil moisture measurements from top 5 cm of soil profile are used to evaluate the performance of the proposed improved soil moisture product.

5.3.4.2 AmeriFlux

The flux and meteorological data measurements from AmeriFlux stations located spatially across 20 different sites are used in the analysis. Of which only 12 sites listed in Table 5.2 are used to evaluate the performance of improved soil moisture product. The daily and half-hourly data from 06:30 AM to 08:30 AM are used to estimate mean flux observations to be in synchronous with SMAP overpass. The eddy covariance method (EC) was used for flux observations at all sites. The data includes flux measurements (the latent heat (LE), sensible heat (H), and net radiation (Rn)) and meteorological variables (e.g., air temperature, relative humidity, saturated vapor pressure deficit, and precipitation). The AmeriFlux station US-Ro2 located in Minnesota (Latitude = 43.17, and Longitude = -93.09) and Us-Vcs (Latitude = 35.92, and Longitude = -106.61) and Us-Vcm (Latitude = 35.89 and Longitude = -106.53) both located in New Mexico are used to evaluate the transferability of optimized parameters for sites with similar heterogeneity. The US-Ro2 site is located in an agricultural site, farmed in accordance with the dominant farming practice in the region: a corn/soybean/clover rotation with chisel plow tillage in the fall following corn

harvest and in the spring following soybeans. The climate of this location is classified as continental humid (Dfa under Koppen classification). The other two sites, US-Vcm and US-Vcs, are located in 1200 km^2 Jemez River basin with humid climate (Dfb) and landcover classified as Evergreen Needle leaf Forests. The field capacity for continental USA is obtained from NLDAS soil hydraulic parameters.

5.4 Methods

5.4.1 Soil Moisture Retrieval Algorithm

The tau-omega model which is an approximation of the non-linear radiative transfer theory is used to simulate brightness temperature (T_B) under vegetation (Mo et al., 1982):

$$T_{B(p,f,\theta)} = e_{p,f,\theta}.T_{eff}.\Upsilon_{p,f,\theta} + T_c.\left(1-\omega_{p,f,\theta}\right).\left(1-\Upsilon_{p,f,\theta}\right) + T_c.\Upsilon_{p,f,\theta}.\left(1-\omega_{p,f,\theta}\right)\left(1-\Upsilon_{p,f,\theta}\right).r_{p,f,\theta} \quad (5.1)$$

$$\Upsilon_{p,f,\theta} = \exp\left(-\frac{\tau_{p,f}}{\cos\theta}\right) \quad (5.2)$$

where *p*, θ, and *f* denote polarization, look angle and frequency respectively. This study considers, p = V-polarization, with constant look angle of 40º at 1.4 GHz frequency. The radiative transfer (equation 5.1) is essentially approximated as a summation of three components, *i)* the direct emission by soil and one-way attenuation by canopy (the first term); *ii)* direct upward emission by canopies (the second term), and *iii)* emission by plants and reflected by soil and thereafter attenuated by vegetation (the third term). The effective rough surface reflectivity $r_{p,f,\theta}$, hereafter defined as R_r is first modeled using Choudhury et al. [1979], which involved a single roughness parameter, the root mean square (RMS) height 'σ' given as;

$$R_r = R_s\, e^{(-H_r cos^2(\theta))} \quad (5.3)$$

$$H_r = 4\, k^2 \sigma^2 \quad (5.4)$$

where $R_s$is smooth surface reflectivity, H_r is the roughness parameter, λ is the wavelength of observation and $k = \frac{2\pi}{\lambda}$ is the wavenumber. The physical attributes of the vegetation that influence the soil emissivity are: the transmissivity of the vegetation $\Upsilon_{p,f,\theta}$, the single scattering albedo $\omega_{p,f,\theta}$ and the physical temperature of the canopy T_c. The transmissivity of vegetation at a constant look angle is given by equation (5.2) where, $\tau_{p,f}$ is the optical thickness of the vegetation, also referred to as VOD. The amount of soil microwave emission that is absorbed and scattered as propagated through canopy is given by the transmissivity of the vegetation and scattering albedo. The loss factor is dependent on the volume fraction of water in the canopy and the architecture of the vegetation. The extinction optical thickness τ_p is estimated as a product of vegetation water content (VWC) and structure of the canopy (*b*). Due to the complex geometry of the natural canopies, approximate values are estimated for canopy structure (*b*) from land cover data.

The scaling method employed using VWC on vegetation optical depth (VOD) to account for within pixel VWC heterogeneity is,

new VOD = original VOD $^{(SNR)}$ (5.5)

where SNR is signal to noise ratio = $\frac{\mu}{\xi}$, μ is the pixel mean and ξ is the standard deviation of VWC derived from 1 km NDVI (MOD13A3) for each pixel. In addition to scaling VOD, the roughness model proposed by Neelam et al., 2018 is also used in the analysis. Currently for a given landcover, SMAP uses roughness parameter H_r that is constant with spatio-temporal scales (SMAP ATBD, O'Neil., 2018). A brief description of roughness formulation proposed by Neelam et al., 2018 is given in equations 5.6-5.8,

$$H_{new}(i) = H_{micro}(i) \times H_{macro}(i) \quad (5.6)$$

$$H_{micro}(i) = \exp\left(-\frac{SM(i) \times (1 - NLAI(i))}{CF(i)}\right) \quad (5.7)$$

$$H_{macro}(i) = (std.curv(i))^{a} \quad (5.8)$$

where, the micro- (small-scale) 'H_{micro}' roughness parameter is defined as an exponential function of soil moisture (SM), clay fraction (CF) and normalized leaf area index (NLAI) and the macro- (large-scale) 'H_{macro}' roughness parameter as standard deviation of curvature, 'i' is per pixel. The parameter 'a' determines the scale of macro-roughness contributing to total surface roughness which varies from 0-2.

Therefore, in summary, we evaluate, *i)* SMAP soil moisture i.e., using SMAP VOD and SMAP surface roughness (h); *ii)* soil moisture estimated using SMAP VOD and new roughness (equation 5.8); *iii)* soil moisture estimated using new VOD (equation 5.3) and SMAP surface roughness (h) (equation 5.5); *iv)* soil moisture estimated using new VOD (equation 5.3) and new roughness (equation 5.8). The performance of these products are evaluated under different land covers, hydroclimates and temporal scales using three metrics as suggested by Entekhabi et al. (2010), *i)* unbiased root-mean-square error (ubRMSE); *ii)* root-mean-square error (RMSE); and *iii)* correlation coefficient (R).

5.4.2 Error Propagation through Retrieval Algorithm

The errors associated with soil moisture retrievals through remote sensing platforms are mainly contributed by uncertainties in land surface variables/parameters in the retrieval model, apart from shortcomings of theoretical knowledge of microwave theory. Taylor's series expansion for error propagation is analyzed to evaluate the performance of radiative transfer equation. The equation is expanded under first and second order series assuming independence as well as correlations between land surface variables. The correlation between land surface variables *i.e.*, (scattering albedo, vegetation water content), (scattering albedo, brightness temperature), (scattering albedo, roughness), (vegetation water content, brightness temperature), (roughness,

vegetation water content), and (roughness, brightness temperature) estimated within each IGBP classification is used in the analysis. The measurement uncertainties in land surface variables are considered according to the SMAP ATBD algorithm. We consider two cases of vegetation water content uncertainty (sVWC =0.05 kg/m^2, and =0.50 kg/m^2).

5.4.3 Taylor's First and Second Order Propagation of Uncertainty

The Taylor's series expansion is an approximate derivative based technique which renders an analytical expression for the uncertainty of output given the uncertainties in the inputs. The function is assumed to be continuously differentiable up to second order, along with normality assumption for the inputs (Heuvelink and Burrough 1989). This technique provides high level of accuracy, and predicts the entire output distribution. The propagation technique is used to estimate root mean square error (RMSE) spatiotemporally for each soil moisture observation. Consider *y* be some function of *n* inputs x_i with some distribution. Then, the first and second order Taylor series approximation expanded about the input means $\bar{x}_i$ are shown in equation (5.9) and (5.10) below,

$$y \approx f(\bar{x}_1, \dots, \bar{x}_n) + \sum_{i=1}^{n} \frac{\partial f}{\partial x_i} (x_i - \bar{x}_i) + \text{remainder} \quad (5.9)$$

$$y \approx f(\bar{x}) + \sum_{i=1}^{n} \frac{\partial f}{\partial x_i} (x_i - \bar{x}_i) + \frac{1}{2!} \sum_{j=1}^{n} \sum_{i=1}^{n} \frac{\partial^2 f}{\partial x_i \partial x_j} (x_i - \bar{x}_i)(x_j - \bar{x}_j) + \text{remainder} \quad (5.10)$$

Based on Eqn (5.9), the first order Taylor's variance (σ_{FF}^2) is given as,

$$\sigma_{FF}^2 = \sum_{i=1}^{n} \sum_{j=1}^{n} \left\{ \frac{\partial f}{\partial x_i} \frac{\partial f}{\partial x_j} \sigma_{x_i} \sigma_{x_j} \rho_{ij} \right\} \quad (5.11)$$

and the second order Taylor's variance (σ_{SF}^2) is based on Eqn (5.10),

$$\sigma_{SF}^2 = \sum_{k=1}^{n}\sum_{l=1}^{n}\left\{\frac{\partial f}{\partial x_k}\frac{\partial f}{\partial x_l}\sigma_k\sigma_l\rho_{kl}\right\} + \frac{1}{4}\sum_{i=1}^{n}\sum_{j=1}^{n}\sum_{k=1}^{n}\sum_{l=1}^{n}\left\{\left(\rho_{ik}\rho_{jl}\sigma_k\sigma_i\sigma_j\sigma_l + \rho_{il}\rho_{jk}\sigma_i\sigma_j\sigma_l\sigma_k\right)\frac{\partial^2 f}{\partial x_i\,\partial x_j}\frac{\partial^2 f}{\partial x_k\,\partial x_l}\right\} \quad (5.12)$$

where $\frac{\partial f}{\partial x_i}$, $\frac{\partial^2 f}{\partial x_i\,\partial x_j}$, ρ_{ij} are the first, second derivatives and correlation coefficient of f with respect to *i* and *j* inputs respectively, while σ_{x_i} is the standard deviation in *x*. The total *land surface interaction errors* observed using RTM are estimated as the difference between the second (Eqn 5.12) and the first (Eqn 5.11) order errors. They include lower order linear terms $\left(\frac{\partial f}{\partial x_i} \times \frac{\partial f}{\partial x_j}\right)$, pure quadratic terms $\left(\frac{\partial^2 f}{\partial {x_i}^2}\right)$ and higher order interaction terms $\left(\frac{\partial^2 f}{\partial x_i\,\partial x_j}\right)$. These terms are assumed to represent within variable scattering and between variables scattering. The effect of correlation between land surface variables on total errors are analyzed are measured as the difference between the errors calculated with correlation and errors without correlations.

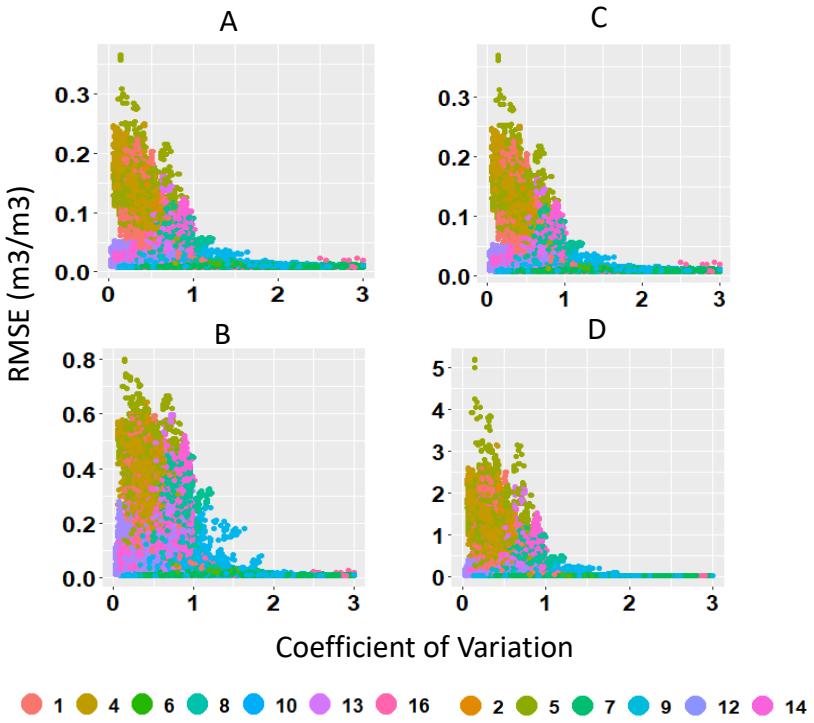

Figure 5.2 Variability in SMAP Soil Moisture Error (Left: First Order (A-B); Right: Second Order(C-D)) with Coefficient of Variation (CV) for two classes of uncertainties (Top: sVWC=0.05 kg/m^2, Bottom: sVWC=0.5 kg/m^2)

5.5 Results and Discussion

The soil moisture error propagates through space and time due to heterogeneity and uncertainty associated with land surface variables used in the retrieval algorithm. As mentioned earlier, VOD (=VWC × B) contributes significantly towards soil moisture errors. And the Coefficient of Variation (CV) which measures the dispersion in data relative to the mean is used to estimate dispersion in VWC. The CV of VWC reflects both the spatial variability and temporal changes (seasonality, annual, human and/or natural interference). A significant trend was observed between total soil moisture errors and the land surface interaction errors (Eqn 5.12 - Eqn 5.11) with CV of VWC. It is observed that, the errors increased exponentially with increase in mean VWC, and followed a curvilinear path for variability in the standard deviation of VWC within a pixel. For CV > 1 the errors reduced rapidly, as shown in Fig 5.2. Therefore, CV =1 is considered as the transitional state to classify ecosystem into regimes based on vegetation density and land surface interactions. Since, CV of VWC is highly correlated with soil moisture errors and associated land surface interactions, it is therefore used to scale VOD. The ecosystem is classified into regimes namely, *i)* homogeneous regime (within pixel CV >1, with low land surface interactions); and *ii)* heterogeneous regime (within pixel CV<1, with high land surface interactions). It was further observed that, the variability in land surface interactions within each regime are controlled by the spatio-temporally evolving soil moisture and temperature dynamics. This led to classification of each homogeneous and heterogeneous regime into water-rich (WR) and water-limited (WL) domain based on soil moisture threshold.

The results are discussed are three sections, *i)* validation; *ii)* land surface interactions. In the validation section, the efficacy of VOD scaling using Eqn 5.5 is discussed. The soil moisture retrieved using scaled VOD is validated using, *i)* reduced RMSE's obtained using Eqn 5.11 and

5.12; *ii)* ground soil moisture from USCRN; *iii)* using soil moisture estimated through a simple water balance. The land surface interactions observed as difference between Eqn 5.12 and 5.11 are analyzed under, *i)* land cover; *ii)* ecosystem: homogeneous and heterogeneous; *iii)* climate: dry, temperate, and continental.

5.5.1 Validation: Taylor's Error Estimates

The soil moisture RMSE's are evaluated for SMAP VOD and scaled VOD (Eqn 5.5) using Taylor's first and second order errors (Eqn's 5.11 and 5.12). The soil moisture obtained using Eqn 5.5 is termed as improved soil moisture (ISM). We consider two levels of VWC uncertainty i.e., sVWC = 0.05 kg/m^2 and sVWC = 0.50 kg/m^2, hereafter they are referred to as *s1* and *s2* respectively. There is no difference between first and second order errors for *s1* whereas, for *s2* these differences increased to an average of ~ 44 % and ~ 28 % with SMAP and ISM respectively, Table 5.1. A significant amount of these difference are due to forests and cropland classes. However, with ISM an average of ~ 40 % improvement in both first and second order errors is estimated for *s1*, whereas, for *s2* an average improvement of ~ 27 % in first and ~ 31 % in second order errors are estimated.

The effect of correlation is similar on first and second order errors with s1 and with s2, the effect becomes significantly different for first and second order errors. The effect of correlation is significant for forest classes (LC-1, 4, 5), and accounting for it reduced total errors during the winter, while increased during summer and no effect during spring and fall, Fig 5.5. For forests classes the seasonality in correlation between VWC and T_B is evident (LC-4, 1, 5 and 2), as it decreased during summer due to increased photosynthetic activity after the winter dormancy and leaf offseason, Fig 5.4. And for land cover classes such as grasslands, croplands, and croplands/natural mosaic, the VWC_T_B decreased twice, once during April to October which is

the growing season, and again during the winter season. The high positive correlation between VWC-TBV during winter for forest classes could be due to snow cover on leaves. The snow-covered vegetation increases the scattering even though vegetation is under dormancy during winter. This also increases H_TBV during winters and decreases during the growing season because of the increased masking effect of vegetation, which reduces the effect of surface roughness on brightness temperature except for LC-10 (grasslands). In case of grasslands, the masking effect by vegetation is reduced due to low VWC (mean = 0.7 kg/m^2) content, because of which the effect of roughness on brightness temperature is high. The evergreen needle forests (LC-1) observe the lowest VWC_TBV correlation among other forest classes, because of its long, thin leaves of conifers shape in contrast to broad leaf vegetation, whereas LC-2 (evergreen broadleaf forests) and LC-4, 5 (deciduous broadleaf and mixed forests respectively) is the highest correlation. The mean variability in correlation and interactions errors are presented according to IGBP land covers in Table 5.2. For mixed forests (LC-5), woody savannas (LC-8) and cropland/natural mosaic (LC-14), behave similarly, though the magnitude of error is smaller for LC-8, and LC-14 due to their low VWC. The high positive correlation between the vegetation variables for these land covers suppresses the scattering error exhibited by VOD, Fig 5.3 and 5.5. Because of which uncorrelated errors are higher than correlated errors. In addition, due to the small effect of seasonality on these classes, when compared to other forest classes the errors remain nearly constant. The deciduous broadleaf forests (LC-4) and evergreen needleleaf forests (LC-1) show a similar trend with seasonality. However, this effect is prominent for LC-4 than perennial LC-1. Due to the flat leaves structure of deciduous broadleaf forests, higher vegetation scattering is observed, because of which the correlation between scattering albedo and brightness temperature (ω_TBV) is significantly negative than coniferous forests with scale/needle like vegetation. Unlike

LC-5 where high positive correlation led to error suppression, in case of LC-1, and LC-4 the high negative and zero correlation (no effect on error) enhances the error because of which correlated errors are higher than uncorrelated errors, Table 5.2.

5.5.2 Validation: Ground and LSM Soil Moisture

The improved soil moisture and SMAP soil moisture are validated using, *i)* using ground soil moisture from USCRN stations; *ii)* LSM's soil moisture *i.e.,* Mosaic, VIC, and Noah. The validation is conducted at two temporal scales, *i)* using daily data for crop growing season, *i.e.,* for June, July, Aug and September; *ii)* the monthly. The performance metrics (unbiased RMSE, RMSE and bias) are evaluated according to different IGBP land covers, and hydroclimates. In addition, SMAP corrected for roughness using Eqns (5.6) and (5.8) is also evaluated. The performance metrics are improved with VOD corrected soil moisture as shown in Fig 5.9. Generally, soil moisture estimation is observed to improve for arid /semi-arid climate with grasslands and croplands land cover classes by refining soil roughness parametrization alone. On the other hand, forest classes and natural vegetation mosaics with temperate and continental climate, correcting for both soil roughness and vegetation improves soil moisture estimation as shown in Table 5.4.

5.5.3 Validation: A Simple Water Balance

A simple water balance model is adapted from Orth and Seneviratne (2015), where a dependency between evapotranspiration (E) and soil moisture (SM) is given as;

$$\frac{\lambda \rho_w E}{R} = \beta_o \left(\frac{SM}{C_s}\right)^{\gamma} \quad \text{with } \gamma > 0 \text{ and } \beta_o \leq 0 \tag{5.13}$$

where λ is the latent heat of vaporization (in J/kg), ρ_w is the density of water (in kg/m^3), and R denotes net radiation. In Eqn (5.13), SM is scaled by soil water- holding capacity C_s (in mm), such that the function operates on the degree of saturation. Another model parameter β_o (unitless), allows to capture the evaporative resistance of the soil and the vegetation, while the parameter γ

(also unitless) ensures a strictly monotonic increasing function of evapotranspiration ratio. The data from 14 AmeriFlux stations (Table 5.2) are used in the analysis. The data from 11 Ameriflux stations are used to optimize the parameters in Eqn (5.13). The measurements which satisfy 50 % $\geq \frac{LE+H}{R-G} \leq 100$ %, where LE, H, R, G represent latent heat, sensible heat, net radiation and ground heat, are selected so they comply as close with energy closure (Wilson et al, 2002). These sites are located in regions are located in regions with VWC CV ranging from 0.3 and 0.6. The parameters β_o and γ optimized in Eqn (5.13) are transferred to sites Vcs, Vcm, and Ro2 with CV in the same range (0.3-0.6), Fig 5.8. The performance metrics in Table 5.4 indicates that, the ISM estimated after scaling VOD according to heterogeneity in VWC matches better with EF estimated SM. This also corroborates our hypothesis that, quantifying and incorporating vegetation heterogeneity (dominant variable) improves representation of soil water dynamics.

5.5.4. Land Surface Interactions: Land Cover

The trend in land surface interactions varies under different land covers, seasons, and hydro climates, however, the trend remains similar for s1 and s2. It is observed that, the mean trend in land surface interactions follow that of VWC, while the variability in trend is caused due to soil moisture, Fig 5.6. An ~ 15 % land surface interactions are reduced for each land cover class (higher for forests) by accounting for heterogeneity in VWC through CV.

The land surface interactions are prominent for IGBP classes in the order of forests (evergreen needle leaf forests LC-1, evergreen broadleaf forests LC-2, deciduous broadleaf forests LC-4, mixed forest LC-5), woody savannas (LC-8) and cropland/natural mosaic (LC-12, 14) as shown in Fig 5.7, where an average of 0.35 m3/m3 interactions were observed with SMAP which reduced to 0.22 m3/m3 with ISM.

As mentioned earlier, a significant correlation between land surface interactions and CV is observed with higher interactions observed for CV < 1. This pattern reflects the signal trapping behavior of dense vegetation, [Dickinson, 1983], where the radiation reflected from soil surface and understory at lower layers of canopy interacts (i.e., absorbed or further scattered) with vegetation at higher levels in the canopy (e.g., trees) and this intensifies the interactions. In regions with high spatial variability in VWC, the signal trapping behavior is reduced which decreases interactions between the soil-vegetation components. These pixels are mostly observed in the mountainous regions ad for with land cover classes of savannas, shrublands and grasslands with VWC ≤ 2-3 kg/m2.

5.5.5. Land Surface Interactions: Partition of Ecosystem

A regime shift can result from a change in dominant feedback occurring at some critical threshold in soil-vegetation-atmosphere system. And these feedback mechanisms evolve spatiotemporally and eventually stabilize for a combination of land-atmosphere components. The significance of vegetation in remote sensing platforms i.e., top-down approaches (truck-based radiometers, airborne, and satellite) and its impact on land surface interactions led to classify the ecosystem into fundamentally two regimes; *i*) homogeneous (CV > 1), and *ii*) heterogeneous (CV < 1). This classification is predominantly proposed on CV of VWC. It was further observed that, the variability in land surface interactions are conditioned on the combination of soil moisture and temperature variability. This led to further classify the regimes mentioned above as water rich (WR) and water limited (WL) based on SM threshold at 0.15 m^3/m^3. Below this SM threshold no land surface interactions are observed. A higher soil moisture increased the nonlinearity of the system through higher land surface interactions, Fig 5.8. A conceptual design was already provided in Neelam and Mohanty, [2015, 2017] based on Monte Carlo Simulations. However, an

quantification of these interactions were not provided. In this paper, in addition to quantification of land surface interactions, their relationship with EF, H, and VPD is also discussed.

5.5.5.1 Homogenous Regime

The homogeneous regime observes negligible land surface interactions implying the environment is nearly linear here, Table 5.2. The grasslands (LC-10) and woody savannas (LC-8) are the only land cover class under this regime with visible land surface interactions. For homogeneous regimes, the interactions are driven by soil moisture and vegetation. This regime also covers shrublands and few pixels of croplands with no land surface interactions.

5.5.5.2 Heterogeneous Regime

The land cover classes for heterogeneous regimes are mainly forest (LC-1, 2, 4, 5), woody savanna (LC-8), and cropland (LC-12, 14). The heterogeneous regimes are characterized by high land surface interactions, which varies with magnitude of VWC, TS, and SM. For example, the effect of TS on land surface interactions are not observed except for mixed forests and croplands. That is, TS decreased land surface interactions for mixed forests and increased for croplands, while it had no effect on other land cover classes. The mixed forests which are predominantly at the border of Appalachian/blue ridge mountains (occupying the piedmont zone) skirting coastal plains show continuous presence of leaves with higher water table, and lower relative humidity. This may be attributed towards, the simultaneous contribution of vegetation, SM, and TS towards land surface interactions for mixed forests. In case of broadleaf forests, the wide leaf structure may result in higher within and with vegetation scattering when compared to coniferous or mixed forests which have needle like leaves. Thus, the land surface interactions for broadleaf forests are more vegetation controlled than SM. The relationship between land surface interactions and atmospheric variables i.e., EF, VPD, and H is unique for each land cover class under this regime.

For example, mixed forests and croplands behave widely different under WR conditions. For mixed forests the land surface interactions and EF (H and VPD) are inversely (directly) proportional. Whereas, for croplands the interactions are directly (inversely) proportional to EF (H and VPD) for croplands, a behavior that is similar to WL conditions. And this difference may be attributed towards the density of biomass, i.e., the high TS and VPD can exert high stress on small plants (VWC ≤ 2 kg/m^2) to transpire beyond its capability which can lead to false stress alert on plants to stop transpiring. However, with increase in VWC this negative stress is removed. Therefore, for less densely vegetated regions, the land surface interactions are primarily controlled by soil moisture followed by a combination of temperature and vegetation. In case of WL regimes (homogeneous and heterogeneous), there are no significant land surface interactions realized.

For heterogeneous WR regimes, EF is governed by vegetation heterogeneity and surface temperature than SM variability. While for homogeneous regimes, EF is observed to be strongly governed by SM variability than heterogeneity in vegetation and surface temperature. The EF, VPD, and H measurements also differ significantly based on regimes, Table 5.6.

5.5.6. Land Surface Interactions: Climate

The impact of SM and VWC variability on land surface interactions under homogeneous regimes is prominent in case of semi-arid climate, while under temperate climate zones no effect of SM on interactions are seen. The increase in VPD and H decreased land surface interactions, and this relationship is more significant under arid climate followed temperate and continental climate. Each of the climate zones covers both homogenous and heterogeneous regimes (and also WR and WL).

5.5.6.1 Dry Climate

The regions under dry climate have high annual temperature with potential evaporation and transpiration higher than precipitation. The dry climate is further classified as dry arid (desert-BW(h,k)) and dry semiarid (steppe-BS(h,k)). This climate mostly observes the land covers such as grasslands, shurblands, barren and some croplands. The land surface interactions are ≤ 0.01 m^3/m^3, and observed mostly for croplands under semi-arid climate. The interactions observed under this climate are soil moisture driven than vegetation. For regions under dry climates, a soil moisture deficit ($SM \leq 0.11$ m^3/m^3) conditions along with high surface temperatures ($TS \approx 285$ K) are observed during summer and spring (fall) season. The soil water in the range of 0.01- 0.1 m^3/m^3 are tightly held by soil particles which restrains movement of water in and through soil matrix due to strong adhesive forces. The SM deficit conditions with high TS creates high VPD conditions which exerts stress on vegetation and soil to conserve water thereby limiting evapotranspiration (ET). As such, the chain of interactions between soil-vegetation-atmosphere is broken resulting in reduced coupled interactions. With increase in soil moisture, and decrease in temperature during winter season ($SM \geq 0.13$ m^3/m^3 and $TS \approx 276$ K), this behavior recedes increasing soil-vegetation-atmosphere interactions. For regions with $VWC \geq 3$ kg/m^2 ($SM \geq 0.13$ m^3/m^3), the exchange of water and energy fluxes are dominated by vegetation, i.e., interactions increased with EF and decreased with H. While, for regions with $VWC \leq 3$ kg/m^2 ($SM \leq 0.11$ m^3/m^3), the exchange of fluxes are driven by soil i.e., interactions decrease with EF and increase slightly with H.

5.5.6.2 Temperate Climate

The regions with temperate climate have warm and humid summers with mild winters observed mainly along the eastern and western borders of USA. The subcategories of this climate are Cfa (humid subtropical) identified in southeastern USA, Cs (Mediterranean) in western coasts,

and Cfb (marine) identified sparely across USA. A wide variety of land cover types are sustained under this climate ranging from grasslands to forest classes.

For humid and marine climate, the effect of temperature on interactions errors remains consistent across seasons for each land cover, while varies within season for Mediterranean climate. For humid subtropical climate (Cfa), the interactions increased with VPD and H, while no effect of EF is noticed. Since this region is not typically WL, the high VPD and H aids in driving the fluxes, increasing the land surface interactions. While for marine climate (Cfb), the land surface interactions decreased with VPD and H, Table 5.6. For regions under Mediterranean climate (Cs), generally, the land surface interactions are both TS and SM driven. All seasons except for winter, the land surface interactions are observed to decrease with TS. Also, the VPD and H are observed to decrease the land surface interactions, while EF increased them.

5.5.6.3 Continental Climate

The continental climate is further classified as hot (Dfa) and warm (Dfb) summers, based on average temperatures observed (Kottek et al., 2006). The land surface interactions under this climate are predominantly SM driven. A relatively higher impact of TS is observed for warm (Dfb). There is no/weak effect of EF and H observed under Dfb, while the interactions decreased with VPD. Whereas, for Dfa the interactions decreased with H and increased with EF, while no effect of VPD is observed.

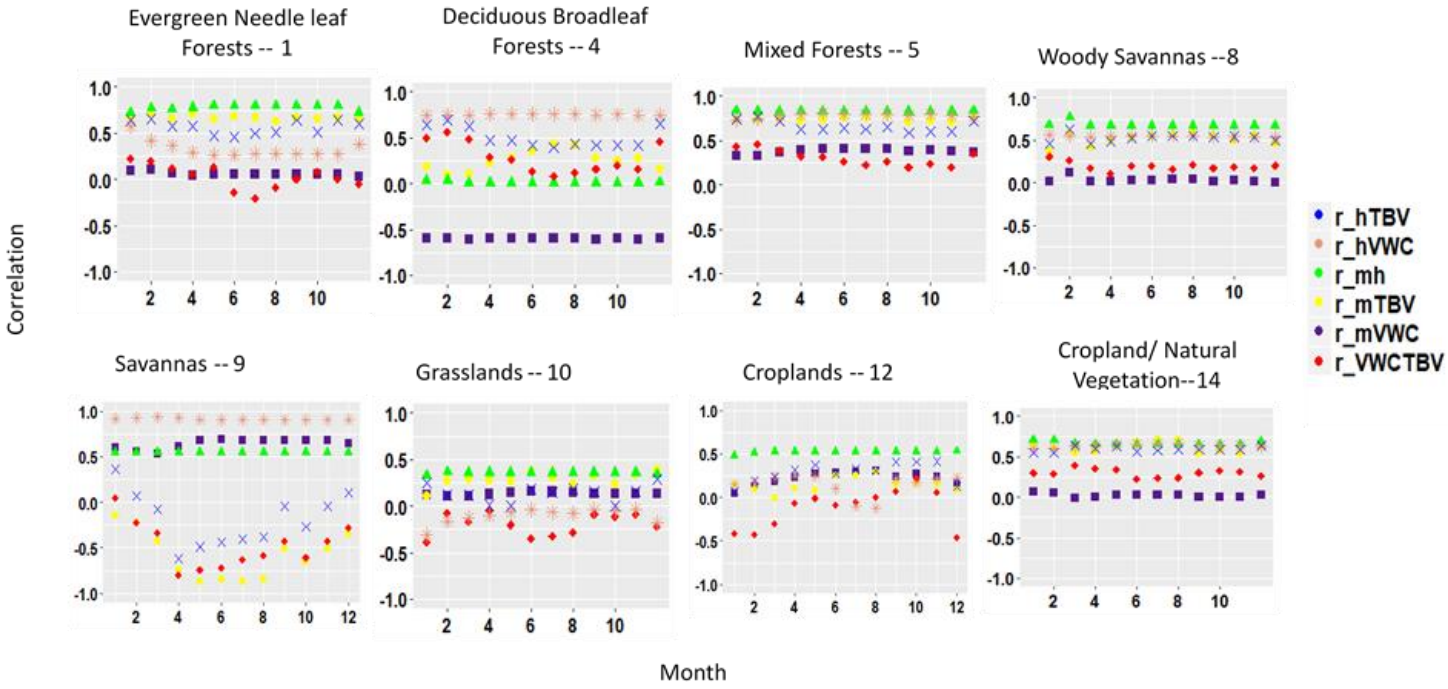

Figure 5.3 Temporal variability in correlation among land surface variables for IGBP Classes that show maximum variability.

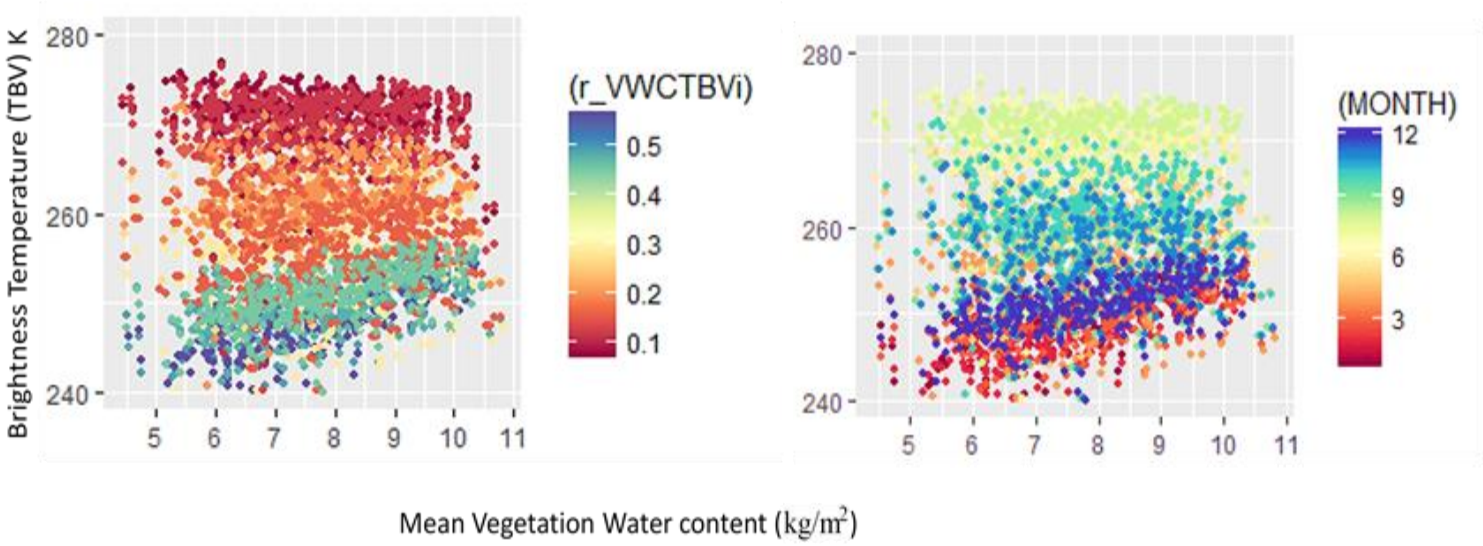

Figure 5.4 The variability in brightness temperature with mean VWC, different colors reflect the correlation between brightness temperature and vegetation water content (left), and monthly change (right).

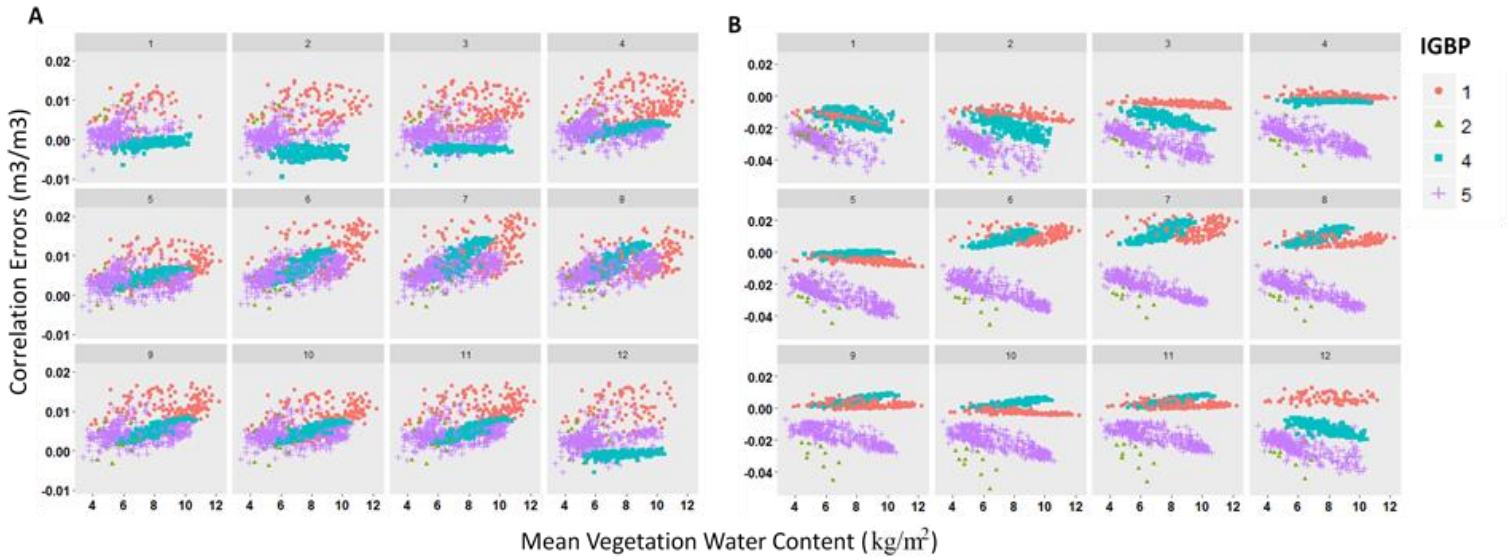

Figure 5.5 The temporal variability in correlation errors for forest classes (IGBP - 1, 2, 4, 5). The small windows represent months, and two sections represent different vegetation uncertainty. Left Panel: for vegetation uncertainty 0.05 kg/m^2, A) the effect of correlation on first order errors, Right Panel: for vegetation uncertainty 0.50 kg/m^2 C) the effect of correlation on first order errors.

Table 5.3 The first and second order RMSE's estimated for SMAP soil moisture and improved soil moisture (ISM**)** according to IGBP land cover class for vegetation uncertainties sVWC = 0.05 kg/m^2 and 0.50 kg/m^2.

	SMAP								ISM							
	First		Second		First Correlated		Second Correlated		First		Second		First Correlated		Second Correlated	
IGBP	***0.05***	***0.5***	***0.05***	***0.5***	***0.05***	***0.5***	***0.05***	***0.5***	***0.05***	***0.5***	***0.05***	***0.5***	***0.05***	***0.5***	**0.05**	0.5
1	0.08	0.24	0.08	0.62	0.08	0.24	0.09	0.62	0.05	0.16	0.05	0.39	0.05	0.16	**0.05**	0.39
2	0.09	0.40	0.10	0.92	0.09	0.37	0.09	0.92	0.07	0.37	0.07	0.76	0.06	0.35	0.07	0.75
4	0.11	0.37	0.11	1.00	0.12	0.37	0.12	1.03	0.07	0.26	0.07	0.61	0.07	0.26	0.07	0.63
5	0.11	0.41	0.11	1.07	0.11	0.38	0.12	1.06	0.07	0.32	0.07	0.74	0.07	0.31	0.07	0.73
6	0.02	0.08	0.02	0.10	0.02	0.08	0.02	0.10	0.02	0.07	0.02	0.09	0.02	0.07	0.02	0.09
7	0.01	0.01	0.01	0.01	0.01	0.01	0.01	0.01	0.00	0.00	0.00	0.00	0.01	0.01	0.01	0.01
8	0.06	0.23	0.06	0.38	0.06	0.22	0.06	0.38	0.04	0.18	0.04	0.27	0.04	0.17	0.04	0.27
9	0.02	0.06	0.02	0.06	0.02	0.06	0.02	0.06	0.01	0.03	0.01	0.04	0.01	0.03	0.01	0.04
10	0.01	0.02	0.01	0.02	0.01	0.02	0.01	0.02	0.00	0.01	0.00	0.02	0.00	0.02	0.00	0.02
11	0.02	0.09	0.02	0.09	0.02	0.08	0.02	0.08	0.02	0.09	0.02	0.09	0.01	0.08	0.01	0.08
12	0.02	0.06	0.02	0.07	0.02	0.06	0.02	0.07	0.01	0.03	0.01	0.04	0.01	0.03	0.01	0.04
13	0.06	0.25	0.06	0.50	0.05	0.25	0.06	0.49	0.04	0.21	0.04	0.39	0.04	0.20	0.04	0.38
14	0.04	0.17	0.04	0.25	0.04	0.16	0.04	0.25	0.03	0.12	0.03	0.17	0.03	0.12	0.03	0.17
16	0.00	0.00	0.00	0.00	0.01	0.01	0.01	0.01	0.00	0.00	0.00	0.00	0.01	0.01	0.01	0.01

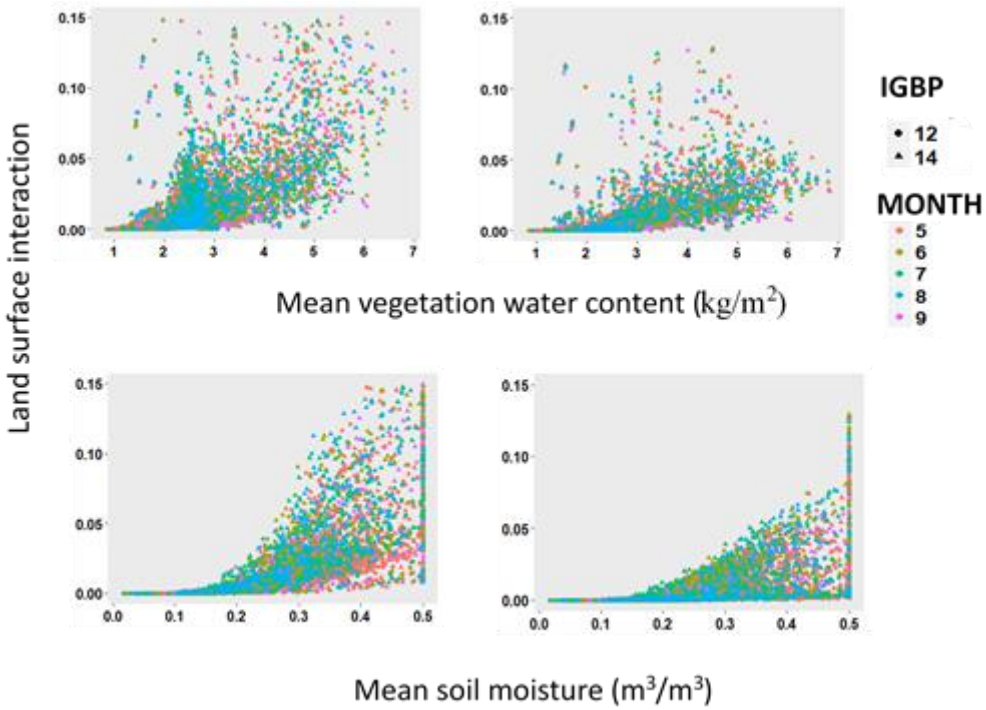

Figure 5.6 The temporal variability in interaction errors with mean vegetation water content (top) and mean soil moisture (bottom) for croplands classes (IGBP – 12 and 14) for vegetation uncertainty of 0.50 kg/m^2 obtained from SMAP VOD (left) and CV scaled VOD (right).

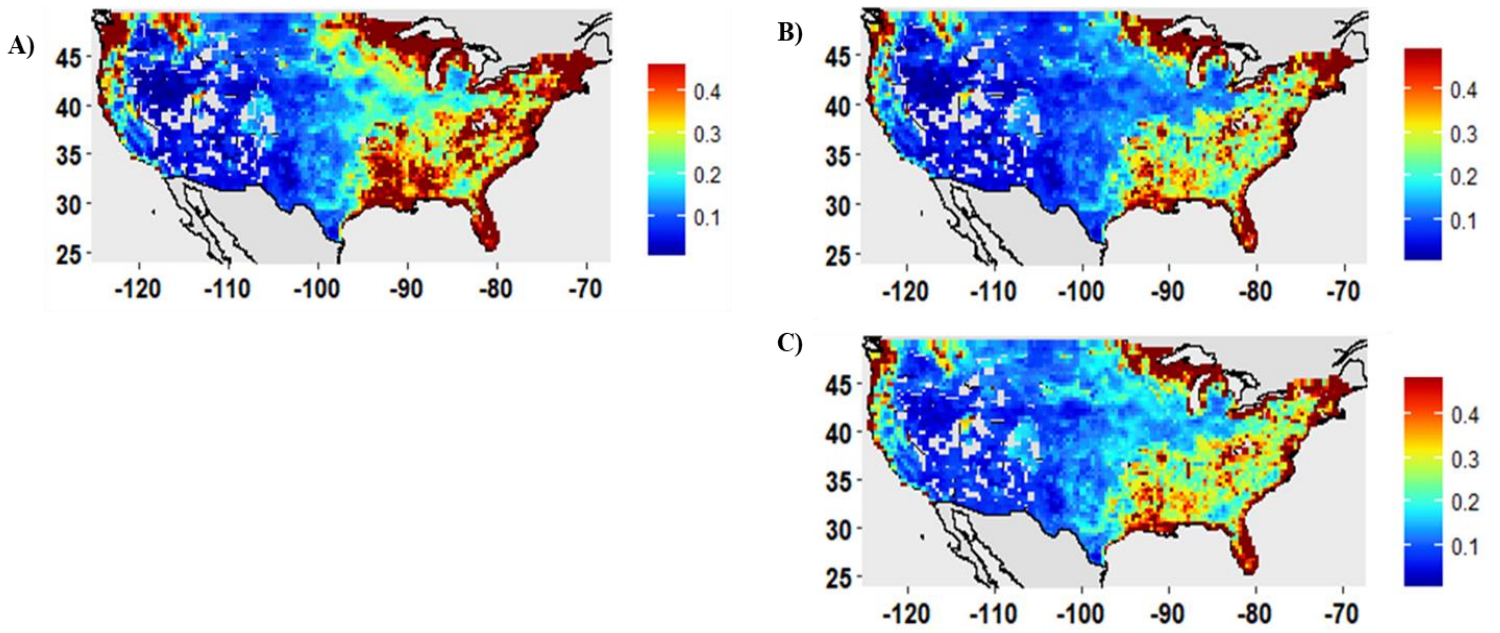

Figure 5.7 The spatial variability of soil moisture for summer (jun-july-aug), A) SMAP soil moisture with H (equation 5.5), B) improved soil moisture (ISM) with H (equation 5.5), C) ISM with (equation 5.6).

Table 5.4 RMSE and unbiased RMSE estimated for SMAP and improved soil moisture (ISM) when EF estimated soil moisture is considered as true soil moisture.

Month	RMSE (Unbiased) SMAP	RMSE (Unbiased) ISM	ID	Climate
Jun	0.10 (0.08)	0.09 (0.03)	US-Ro2	Humid-(Dfa)
Jul	0.07 (0.04)	0.09 (0.02)	US-Ro2	
Aug	0.14 (0.05)	0.07 (0.03)	US-Ro2	
Total	**0.10(0.07)**	**0.08(0.03)**	US-**Ro2**	
Jun	0.13 (0.04)	0.18 (0.03)	US-Vcm	Humid-(Dfb)
Aug	0.13 (0.08)	0.05 (0.06)	US-Vcm	
Sep	0.07 (0.05)	0.11 (0.04)	US-Vcm	
Total	**0.12(0.12)**	**0.12(0.08)**	**US-Vcm**	
Jun	0.09 (0.03)	0.11 (0.02)	US-Vcs	Humid-(Dfb)
Jul	0.12 (0.06)	0.14 (0.04)	US-Vcs	
Aug	0.14 (0.06)	0.05 (0.04)	US-Vcs	
Sep	0.08 (0.08)	0.08 (0.06)	US-Vcs	
Total	**0.11(0.10)**	**0.10(0.07)**	US-Vcs	

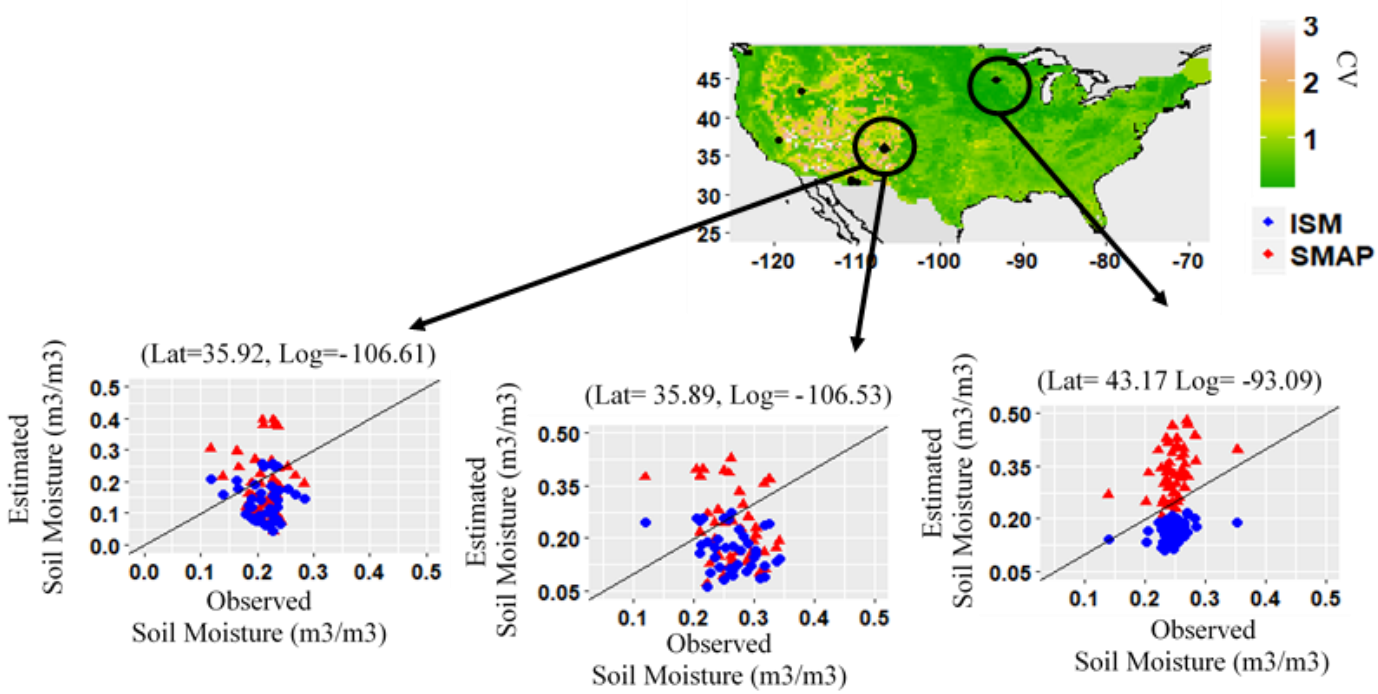

Figure 5.8 The evaporative fraction (EF) estimated soil moisture is evaluated against SMAP and VOD improved soil moisture. The transferability of optimized parameters in equation (5.13) is examined at three AMERIFLUX sites (US-Vcs, US-Vcm, and US-Ro2).

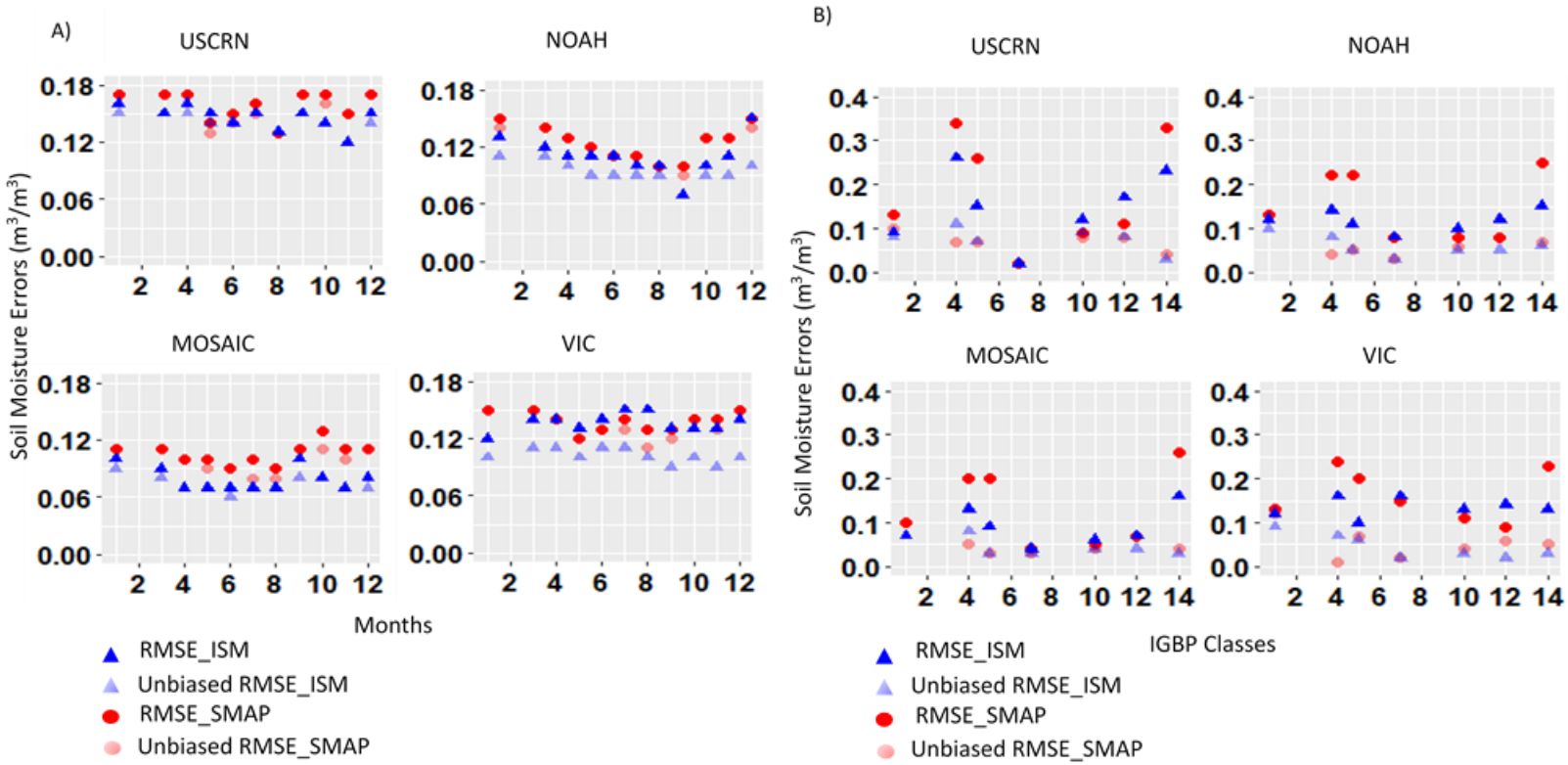

Figure 5.9 The temporal (A) spatial (B) variability of RMSE and unbiased RMSE for SMAP and improved soil moisture (ISM) when USCRN, VIC, NOAH and VIC are assumed to be true soil moisture.

.

Table 5.5 The performance metrics evaluated under different A) hydro climates and B) IGBP land cover classes for, 1) SMAP soil moisture (SMAP R & VOD); 2) soil moisture estimated using SMAP VOD and new roughness (NR); 3) soil moisture estimated using new VOD (NVOD) and SMAP (H); 4) soil moisture estimated using new VOD (NVOD) and new roughness (H_{new}), where α is the macro-roughness scaling parameter.

A) Hydroclimates

Climate	SMAP H & VOD			SMAP VOD & H_{new} (α=0)			SMAP H & NVOD			SMAP H_{new} (α=0) & NVOD			SMAP H_{new} (α=0.5) & NVOD		
	ub RMSE	RMSE	bias	ub RMSE	RMSE	bias	ub RMSE	RMSE	bias	ub RMSE	RMSE	bias	ub RMSE	RMSE	bias
BSk	0.08	0.10	-0.06	0.08	0.09	-0.03	0.09	0.13	-0.09	0.09	0.11	-0.06	0.09	0.14	-0.10
BWh	0.06	0.07	-0.04	0.06	0.06	0.00	0.06	0.09	-0.06	0.06	0.07	-0.03	0.06	0.09	-0.07
BWk	0.08	0.10	-0.05	0.09	0.10	-0.01	0.08	0.11	-0.07	0.08	0.10	-0.04	0.08	0.11	-0.08
Cfa	0.16	0.16	-0.02	0.13	0.13	0.02	0.15	0.17	-0.08	0.13	0.14	-0.06	0.14	0.17	-0.09
Cfb	0.12	0.17	0.12	0.11	0.18	0.14	0.09	0.12	0.07	0.07	0.11	0.09	0.08	0.10	0.06
Csa	0.07	0.09	0.05	0.07	0.10	0.08	0.06	0.07	0.02	0.06	0.08	0.05	0.06	0.06	0.02
Csb	0.12	0.17	0.13	0.10	0.18	0.14	0.09	0.11	0.07	0.07	0.11	0.08	0.08	0.10	0.06
Dfa	0.08	0.34	0.33	0.08	0.34	0.33	0.10	0.24	0.22	0.09	0.22	0.20	0.09	0.22	0.20
Dfb	0.08	0.10	0.05	0.08	0.11	0.06	0.05	0.06	0.03	0.05	0.07	0.04	0.05	0.06	0.02

Table 5.5 Continued…

B) IGBP land cover classes

IGBP Class	SMAP H &VOD			SMAP H &NVOD			SMAP VOD & (H_{new}) (α=0)			SMAP (H_{new}) (α=0) & NVOD		
	ubRMSE	RMSE	bias	ubRMSE	RMSE	bias	ubRMSE	RMSE	bias	ubRMSE	RMSE	bias
1	0.10	0.13	0.08	0.07	0.09	0.05	0.09	0.14	0.11	0.07	0.09	0.06
4	0.07	0.34	0.34	0.11	0.26	0.24	0.07	0.34	0.34	0.10	0.24	0.21
5	0.07	0.26	0.26	0.07	0.16	0.14	0.06	0.27	0.26	0.07	0.15	0.13
7	0.02	0.02	0.01	0.02	0.02	0.01	0.01	0.03	0.03	0.01	0.03	0.02
10	0.08	0.09	-0.05	0.09	0.12	-0.08	0.08	0.08	-0.02	0.09	0.10	-0.10
12	0.08	0.11	-0.08	0.08	0.17	-0.15	0.09	0.09	-0.02	0.08	0.14	-0.10
14	0.04	0.33	0.33	0.03	0.23	0.23	0.04	0.30	0.30	0.03	0.21	0.21

5.6. Summary and Conclusion

In this paper we attempted a technique to improve the soil moisture retrieval accuracy by incorporating the within-pixel heterogeneity in VWC. On observing a high correlation between the non-linear soil moisture errors and heterogeneity in vegetation, an effort was undertaken to map the variability in the non-linearity in RTM with respect to hydroclimates, temporal scales, and different land covers, and importantly with variables such as EF, H and VPD.

1) The effect of the correlation among the land surface variables on soil moisture retrieval accuracy is higher for the first-order errors, and can reduce mean RMSE by 0.032 m^3/m^3 for the pixels with high VWC.
2) Soil moisture retrieval errors are significant under heterogeneous/homogeneous water rich conditions (WR) with mean SM > 0.15 m^3/m^3, and lower for water limited (WL) conditions with mean SM < 0.15 m^3/m^3.
3) The land surface interactions generally decreased with increase in VPD and H. However, this varied with SM, and TS conditions. This relationship is stronger under arid climate than temperate or continental climate. While, the land surface interactions increased with EF, and this relationship is stronger under WR conditions.

Based on this work, we emphasize that the uncertainties and biases in predicted land-atmosphere coupling can be improved with the threshold-based representation of vegetation-soil moisture-thermal fluxes.

6 GENERAL CONCLUSIONS

The improvement in remote sensing of soil moisture is essentially a heterogeneity-scaling issue. Addressing this issue appropriately can better facilitate the research upon hydrological and metrological processes.

The global sensitivity analysis work indicated that the total sensitivity (linear + non-linear) of land surface variables varied with hydro climates and time. In addition, attenuation of soil emission by vegetation (VWC, B, ω) can be significant in structured plants (corn) and not realized in soybean plants. And, this attenuation/scattering appears to increase with roughness, SM and VWC conditions. Also, SM and surface temperature show a monotonically decreasing sensitivity function, whereas VWC, S, L and B show a monotonically increasing sensitivity function with increase in SM. CF sensitivity shows an increasing function up to the transition SM, after which it drops exponentially with increase in SM. This peak observed at the transition SM changes with the percentage of clay fraction.

The impact of non-linear upscaling on the sensitivity of radiative transfer model to evolving spatial maps (0.8 km, 1.6 km, 3.2 km, 6.4 km and 12.8 km) of land surface variables under various hydroclimates (Arizona, Oklahoma, Iowa, and Winnipeg) is illustrated. The analysis resulted in environment specific most sensitive variables, SM in homogeneous, and VWC in heterogeneous environments. The sensitivity to land surface variables in arid and humid-Dfa climate classes, increased or decreased gradually following an exponential function with increasing scale. While, for humid-Dfb the sensitivities changed rapidly following a logarithmic function. The study emphasized that the heterogeneity and upscaling method will determine the sensitivity to land surface variables.

Section 4 describes a new surface roughness model which integrates roughness from different spatial scales i.e., from field-scale (micro-roughness) to foot-print (macro-roughness) scale. The primary contribution of this work is to demonstrate the improvement in soil moisture retrieval with spatio-temporally variable surface roughness over retrieval using constant roughness parameters.

Section 5 explored 1) the effect of vegetation heterogeneity on soil moisture errors, which are found to be significant, 2) the effect of correlation among land surface variables is analyzed. And the correlation effect is observed to be higher for first-order errors, and can reduced mean RMSE by 0.032 m3/m3 for dense vegetation pixels, 3) the natural system can be broadly classified into homogeneous and heterogeneous regimes based on interactions observed. For homogeneous regimes fewer/no interactions are observed, whereas significant interactions are observed for heterogeneous regime, 4) the variability in land surface interactions decreased with increase in VPD and sensible heat. And this relationship is stronger under arid climate than temperate or continental climate. On the other hand, the land surface interactions increased with EF, and this relationship is stronger under WR conditions.

To sum up, the soil moisture retrieval accuracy improved with surface roughness and vegetation optical depth parameterizations and a better physical understanding of land surface interactions and its variability with evaporative fraction (EF) and sensible heat (H) will shed some new insights on land-atmosphere coupling.

The future work should investigate if land atmosphere coupling can be improved with the threshold-based representation of vegetation-soil moisture-energy fluxes in land surface models.

REFERENCES

Allmaras, R. R., Burwell, R. E., and Holt, R. F. (1967). Plow-layer porosity and surface roughness from tillage as affected by initial porosity and soil moisture at tillage time. Soil Science Society of America Journal, 31(4), 550-556.

Alvarez-Mozos, J., Casali, J., González-Audícana, M., and Verhoest, N. E. (2006). Assessment of the operational applicability of RADARSAT-1 data for surface soil moisture estimation, IEEE Trans. Geosci.Remote Sens., 44(4), 913-924.

Avissar, R. (1995). Scaling of land-atmosphere interactions: An atmospheric modelling perspective. Hydrological Processes, 9(5-6), 679-695.

Babak, O., and Deutsch, C. V. (2009). Statistical approach to inverse distance interpolation. Stochastic Environmental Research and Risk Assessment, 23(5), 543-553.

Barber, M., Bruscantini, C., Grings, F. and Karszenbaum, H. (2016). Bayesian combined active/passive (B-CAP) soil moisture retrieval algorithm. IEEE Journal of Selected Topics in Applied Earth Observations and Remote Sensing, 9(12), pp.5449-5460.

Bindlish, R., Jackson, T. J., Gasiewski, A. J., Klein, M., and Njoku, E. G. (2006). Soil moisture mapping and AMSR-E validation using the PSR in SMEX02. Remote Sensing of Environment, 103(2), 127-139.

Bindlish, R., Jackson, T., Sun, R., Cosh, M., Yueh, S. and Dinardo, S. (2009). Combined passive and active microwave observations of soil moisture during CLASIC. IEEE Geoscience and Remote Sensing Letters, 6(4), pp.644-648.

Blöschl, G. (1999). Scaling issues in snow hydrology. Hydrological processes, 13(14-15), 2149-2175.

Blöschl, G., and Sivapalan, M. (1995). Scale issues in hydrological modelling: a review. Hydrological processes, 9(3-4), 251-290.

Brocca, L., Melone, F., Moramarco, T., and Morbidelli, R. (2010). Spatial-temporal variability of soil moisture and its estimation across scales. Water Resources Research, 46(2).

Brunfeldt, D. R., and Ulaby, F. T. (1986). Microwave emission from row crops, IEEE Transactions on Geoscience and Remote Sensing., (3), 353-359.

Burke, E. J., and Simmonds, L. P. (2003). Effects of sub-pixel heterogeneity on the retrieval of soil moisture from passive microwave radiometry. International Journal of Remote Sensing, 24(10), 2085-2104.

Burke, W. J., Schmugge, T., and Paris, J. F. (1979). Comparison of 2.8-and 21-cm microwave radiometer observations over soils with emission model calculations, J. Geophys. Res., 84(C1), 287-294.

Burt, T. P., and Butcher, D. P. (1985). Topographic controls of soil moisture distributions. Journal of Soil Science, 36(3), 469-486.

Cai, X., Pan, M., Chaney, N.W., Colliander, A., Misra, S., Cosh, M.H., Crow, W.T., Jackson, T.J. and Wood, E.F. (2017). Validation of SMAP soil moisture for the SMAPVEX15 field campaign using a hyper-resolution model. Water Resources Research, 53(4), pp.3013-3028.

Calvet, J. C., Wigneron, J. P., Walker, J., Karbou, F., Chanzy, A., and Albergel, C. (2011). Sensitivity of passive microwave observations to soil moisture and vegetation water content: L-band to W-band, IEEE Trans. Geosci. Remote Sens., 49(4), 1190-1199.

Chan, S. K., Bindlish, R., O'Neill, P. E., Njoku, E., Jackson, T., Colliander, A., Chen, F., Burgin, M., Dunbar, S., Piepmeier, J. and Yueh, S. (2016). Assessment of the SMAP passive soil

moisture product. IEEE Transactions on Geoscience and Remote Sensing, 54(8), pp.4994-5007.

Chan, S., Njoku, E. and Colliander, A. (2014). Soil Moisture Active Passive (SMAP) Algorithm Theoretical Basis Document: Level 1C Radiometer Data Product, pp. 1–19, Jet Propul. Lab., Pasadena, Calif. [Available at https://nsidc.org/sites/nsidc.org/files/technical-references/279_L1C_TB_ATBD_RevA_web.pdf.].

Chan, S.K., Bindlish, R., O'Neill, P., Jackson, T., Njoku, E., Dunbar, S., Chaubell, J., Piepmeier, J., Yueh, S., Entekhabi, D. and Colliander, A. (2018). Development and assessment of the SMAP enhanced passive soil moisture product. Remote Sensing of Environment, 204, pp.931-941.

Chauhan, N. S. (2002). Soil moisture inversion at L-band using a dual-polarization technique: a model-based sensitivity analysis,. Int. J. Remote Sens., 23(16), 3209-3227.

Chehbouni, A., Njoku, E.G., Lhomme, J.P. and Kerr, Y.H. (1995). Approaches for averaging surface parameters and fluxes over heterogeneous terrain. Journal of climate, 8(5), pp.1386-1393.

Chen, F., Crow, W.T., Colliander, A., Cosh, M.H., Jackson, T.J., Bindlish, R., Reichle, R.H., Chan, S.K., Bosch, D.D., Starks, P.J. and Goodrich, D.C. (2017). Application of triple collocation in ground-based validation of Soil Moisture Active/Passive (SMAP) level 2 data products. IEEE Journal of Selected Topics in Applied Earth Observations and Remote Sensing, 10(2), pp.489-502.

Chen, J., Wen, J., and Tian, H. (2016). Representativeness of the ground observational sites and up-scaling of the point soil moisture measurements. Journal of Hydrology, 533, 62-73.

Choudhury, B. J., Schmugge, T. J., Chang, A., and Newton, R. W. (1979). Effect of surface roughness on the microwave emission from soils. Journal of Geophysical Research: Oceans (1978–2012), 84(C9), 5699-5706.

Colliander, A., Chan, S., Kim, S.B., Das, N., Yueh, S., Cosh, M., Bindlish, R., Jackson, T. and Njoku, E. (2012). Long term analysis of PALS soil moisture campaign measurements for global soil moisture algorithm development. Remote Sensing of Environment, 121, pp.309-322.

Colliander, A., Cosh, M. H., Misra, S., Jackson, T. J., Crow, W. T., Chan, S., Bindlish, R., Chae, C., Collins, C.H. and Yueh, S. H. (2017). Validation and scaling of soil moisture in a semi-arid environment: SMAP validation experiment 2015 (SMAPVEX15). Remote Sensing of Environment, 196, pp.101-112.

Colliander, A., Jackson, T., McNairn, H., Chazanoff, S., Dinardo, S., Latham, B., O'Dwyer, I., Chun, W., Yueh, S. and Njoku, E. (2015). Comparison of Airborne Passive and Active L-band System (PALS) brightness temperature measurements to SMOS observations during the SMAP Validation Experiment 2012 (SMAPVEX12).Geoscience and Remote Sensing Letters, IEEE 12.4 (2015): 801-805.

Colliander, A., Njoku, E. G., Jackson, T. J., Chazanoff, S., McNairn, H., Powers, J., and Cosh, M. H. (2016). Retrieving soil moisture for non-forested areas using PALS radiometer measurements in SMAPVEX12 field campaign. Remote Sensing of Environment, 184, 86-100.

Colliander, A., Jackson, T. J., Bindlish, R., Chan, S., Das, N., Kim, S. B, Cosh, M. H., Dunbar, R.S., Dang, L., Pashaian, L, and Asanuma, J. (2017). Validation of SMAP surface soil

moisture products with core validation sites. Remote Sensing of Environment, 191, 215-231.

Choudhury, B.J., Schmugge, T.J., Chang, A. and Newton, R.W. (1979). Effect of surface roughness on the microwave emission from soils. Journal of Geophysical Research: Oceans, 84(C9), pp.5699-5706.

Cosh, M. H., Jackson, T. J., Moran, S., and Bindlish, R. (2008). Temporal persistence and stability of surface soil moisture in a semi-arid watershed. Remote Sensing of Environment, 112(2), 304-313.

Crosetto, M., Tarantola, S., and Saltelli, A. (2000). Sensitivity and uncertainty analysis in spatial modelling based on GIS. Agriculture, ecosystems and environment, 81(1), 71-79.

Crosson, W. L., Limaye, A. S., and Laymon, C. A. (2005). Parameter sensitivity of soil moisture retrievals from airborne L-band radiometer measurements in SMEX02, IEEE Trans. Geosci. Remote Sens.,43(7), 1517-1528.

Crow, W. T., Berg, A. A., Cosh, M. H., Loew, A., Mohanty, B. P., Panciera, R., Rosnay, P., Ryu, D., and Walker, J. P. (2012). Upscaling sparse ground-based soil moisture observations for the validation of coarse-resolution satellite soil moisture products. Reviews of Geophysics, 50(2).

Crow, W. T., Wood, E. F., and Dubayah, R. (2000). Potential for downscaling soil moisture maps derived from spaceborne imaging radar data. Journal of Geophysical Research: Atmospheres, 105(D2), 2203-2212.

Crow, W.T., Chan, S., Entekhabi, D., Hsu, A., Jackson, T. J., Njoku, E., O'Neill, P. and Shi, J. (2005). An observing system simulation experiment for Hydros radiometer-only soil

moisture products. IEEE Transactions on Geoscience and Remote Sensing, 43(6), pp.1289-1303.

Crow, W.T., Ryu, D. and Famiglietti, J.S. (2005). Upscaling of field-scale soil moisture measurements using distributed land surface modeling. Advances in Water Resources, 28(1), pp.1-14.

Das, N. N., Entekhabi, D., Dunbar, R. S., Njoku, E. G., and Yueh, S. H. (2016). Uncertainty Estimates in the SMAP Combined Active–Passive Downscaled Brightness Temperature. IEEE Transactions on Geoscience and Remote Sensing, 54(2), 640-650.

Das, N. N., Entekhabi, D., Njoku, E. G., Shi, J. J., Johnson, J. T., and Colliander, A. (2014). Tests of the SMAP combined radar and radiometer algorithm using airborne field campaign observations and simulated data. IEEE Transactions on Geoscience and Remote Sensing, 52(4), 2018-2028.

Davenport, I. J., Fernández-Gálvez, J., and Gurney, R. J. (2005). A sensitivity analysis of soil moisture retrieval from the tau-omega microwave emission model, IEEE Trans. Geosci. Remote Sens.,, 43(6), 1304-1316.

De Jeu, R. A. M., and Owe, M. (2003). Further validation of a new methodology for surface moisture and vegetation optical depth retrieval, Int. J. Remote Sens., 24(22), 4559-4578.

Diamond, H.J., Karl, T.R., Palecki, M.A., Baker, C.B., Bell, J.E., Leeper, R.D., Easterling, D.R., Lawrimore, J.H., Meyers, T.P., Helfert, M.R. and Goodge, G. (2013). US Climate Reference Network after one decade of operations: Status and assessment. Bulletin of the American Meteorological Society, 94(4), pp.485-498.

Dickinson, R. E. (1983). Land surface processes and climate—Surface albedos and energy balance. In Advances in geophysics (Vol. 25, pp. 305-353). Elsevier.

Djamai, N., Magagi, R., Goita, K., Merlin, O., Kerr, Y., and Walker, A. (2015). Disaggregation of SMOS soil moisture over the Canadian Prairies. Remote Sensing of Environment, 170, 255-268.

Dorigo, W. A., Scipal, K., Parinussa, R. M., Liu, Y. Y., Wagner, W., De Jeu, R. A., and Naeimi, V. (2010). Error characterisation of global active and passive microwave soil moisture datasets. Hydrology and Earth System Sciences,14(12), 2605-2616.

Drusch, M., Wood, E. F., and Simmer, C. (1999). Up-scaling effects in passive microwave remote sensing: ESTAR 1.4 GHz measurements during SGP'9. Geophysical Research Letters, 26(7), 879-882.

Efron, B., and Tibshirani, R. J. (1994). An introduction to the bootstrap (Vol. 57). CRC press.

Entekhabi, D., Njoku, E.G., O'Neill, P.E., Kellogg, K.H., Crow, W.T., Edelstein, W.N., Entin, J.K., Goodman, S.D., Jackson, T.J., Johnson, J. and Kimball, J. (2010). The soil moisture active passive (SMAP) mission. Proceedings of the IEEE, 98(5), pp.704-716.

Entekhabi, D., Reichle, R. H., Koster, R. D., and Crow, W. T. (2010). Performance metrics for soil moisture retrievals and application requirements. Journal of Hydrometeorology, 11(3), 832-840.

Entekhabi, D., Rodriguez-Iturbe, I., and Castelli, F. (1996). Mutual interaction of soil moisture state and atmospheric processes. Journal of Hydrology, 184(1-2), 3-17.

Entekhabi, D., Yueh, S., O'Neill, P. E., Kellogg, K.H., Allen, A., Bindlish, R., Brown, M., Chan, S., Colliander, A., Crow, W.T. and Das, N. (2014). SMAP Handbook–Soil Moisture Active Passive: Mapping Soil Moisture and Freeze/Thaw from Space.

Escorihuela, M. J., Kerr, Y. H., de Rosnay, P., Wigneron, J. P., Calvet, J. C., and Lemaitre, F. (2007). A simple model of the bare soil microwave emission. IEEE Transactions on Geoscience and Remote Sensing 45, no. 7 (2007): 1978-1987.

Famiglietti, J. S., Ryu, D., Berg, A. A., Rodell, M., and Jackson, T. J. (2008). Field observations of soil moisture variability across scales. Water Resources Research, 44(1).

Fernandez-Moran, R., Wigneron, J.P., Lopez-Baeza, E., Al-Yaari, A., Coll-Pajaron, A., Mialon, A., Miernecki, M., Parrens, M., Salgado-Hernanz, P.M., Schwank, M. and Wang, S. (2015). Roughness and vegetation parameterizations at L-band for soil moisture retrievals over a vineyard field. Remote Sensing of Environment, 170, pp.269-279.

Flores, A. N., Ivanov, V. Y., Entekhabi, D., and Bras, R. L. (2009). Impact of hillslope-scale organization of topography, soil moisture, soil temperature, and vegetation on modeling surface microwave radiation emission. IEEE Transactions on Geoscience and Remote Sensing, 47(8), 2557-2571.

Garrigues, S., Allard, D., Baret, F., and Weiss, M. (2006). Influence of landscape spatial heterogeneity on the non-linear estimation of leaf area index from moderate spatial resolution remote sensing data. Remote Sensing of Environment, 105(4), 286-298.

Gaur, N., and Mohanty, B. P. (2013). Evolution of physical controls for soil moisture in humid and subhumid watersheds, Water Resour. Res., 49, doi:10.1002/wrcr.20069.

Gentine, P., D'Odorico, P., Lintner, B. R., Sivandran, G., and Salvucci, G. (2012). Interdependence of climate, soil, and vegetation as constrained by the Budyko curve. Geophysical Research Letters, 39(19).

Heather M., et al., (2012). Soil Moisture Active Passive Validation Experiment 2012 (SMAPVEX12) Experimental Plan. (https://smapvex12.espaceweb.usherbrooke.ca/home.php)

Heuvelink, G. B., Brown, J. D., and van Loon, E. E. (2007). A probabilistic framework for representing and simulating uncertain environmental variables. International Journal of Geographical Information Science, 21(5), 497-513.

Heuvelink, G. B., Burrough, P. A., and Stein, A. (1989). Propagation of errors in spatial modelling with GIS. International Journal of Geographical Information System, 3(4), 303-322.

Hu, Z., and Islam, S. (1997). A framework for analyzing and designing scale invariant remote sensing algorithms. IEEE Transactions on Geoscience and Remote Sensing, 35(3), 747-755.

Humphries, E. J. (1996). The relationship between topography and soil moisture distribution (Doctoral dissertation, Massachusetts Institute of Technology).

Jackson, T. J. (1993). III. Measuring surface soil moisture using passive microwave remote sensing, Hydrol. Processes, 7(2), 139-152.

Jackson, T. J., and Le Vine, D. E. (1996). Mapping surface soil moisture using an aircraft-based passive microwave instrument: algorithm and example, J. Hydrol., 184(1), 85-99.

Jackson, T. J., and O'Neill, P. E. (1990). Attenuation of soil microwave emission by corn and soybean at 1.4 and 5 GHz,. IEEE Trans. Geosci. Remote Sens., 28(5), 978-980.

Jackson, T. J., and Schmugge, T. J. (1991). Vegetation effects on the microwave emission of soils. Remote Sensing of Environment, 36(3), 203-212.

Jackson, T. J., Chen, D., Cosh, M., Li, F., Anderson, M., Walthall, C., Doriaswamy, P. and Hunt, E.R. (2004). Vegetation water content mapping using Landsat data derived normalized

difference water index for corn and soybeans. Remote Sensing of Environment, 92(4), pp.475-482.

Jackson, T. J., Le Vine, D. M., Hsu, A.Y., Oldak, A., Starks, P. J., Swift, C. T., Isham, J. D. and Haken, M. (1999). Soil moisture mapping at regional scales using microwave radiometry: The Southern Great Plains Hydrology Experiment. IEEE Transactions on Geoscience and Remote Sensing, 37(5), pp.2136-2151.

Jackson, T.J., Chen, D., Cosh, M., Li, F., Anderson, M., Walthall, C., Doriaswamy, P. and Hunt, E.R. (2004). Vegetation water content mapping using Landsat data derived normalized difference water index for corn and soybeans. Remote Sensing of Environment, 92(4), pp.475-482.

Jackson, T.J., Cosh, M.H., Bindlish, R., Starks, P.J., Bosch, D.D., Seyfried, M., Goodrich, D.C., Moran, M.S. and Du, J. (2010). Validation of advanced microwave scanning radiometer soil moisture products. IEEE Transactions on Geoscience and Remote Sensing, 48(12), pp.4256-4272.

Jackson, T.J., Le Vine, D.M., Hsu, A.Y., Oldak, A., Starks, P.J., Swift, C.T., Isham, J.D. and Haken, M. (1999). Soil moisture mapping at regional scales using microwave radiometry: The Southern Great Plains Hydrology Experiment. IEEE Transactions on Geoscience and Remote Sensing, 37(5), pp.2136-2151.

Jacobs, J. M., Mohanty, B. P., Hsu, E. C., and Miller, D. (2004). SMEX02: Field scale variability, time stability and similarity of soil moisture. Remote Sensing of Environment, 92(4), 436-446.

Jana, R. B., and Mohanty, B. P. (2012). On topographic controls of soil hydraulic parameter scaling at hillslope scales, Water Resour. Res., 48, W02518, doi:10.1029/2011WR011204.

Jones, M. O., Jones, L. A., Kimball, J. S., and McDonald, K. C. (2011). Satellite passive microwave remote sensing for monitoring global land surface phenology, Remote Sens. Environ.,115(4), 1102-1114.

Joshi, C., and Mohanty, B. P. (2010). Physical controls of near-surface soil moisture across varying spatial scales in an agricultural landscape during SMEX02, Water Resour. Res., 46, W12503, doi:10.1029/2010WR009152.

Kerr, Y. H., and Njoku, E. G. (1990). A semiempirical model for interpreting microwave emission from semiarid land surfaces as seen from space, IEEE Trans. Geosci. Remote Sens., 28(3), 384–393.

Kerr, Y. H., Secherre, F., Lastenet, J., and Wigneron, J. P. (2003). SMOS: Analysis of perturbing effects over land surfaces. Proceedings of IEEE Int. Geosci. Remote Sens. Symp. (IGARSS'03), Jul. 21-25 Toulouse, France

Kerr, Y. H., Waldteufel, P., Richaume, P., Wigneron, J. P., Ferrazzoli, P., Mahmoodi, A., Al Bitar, A., Cabot, F., Gruhier, C., Juglea, S.E. and Leroux, D. (2012). The SMOS soil moisture retrieval algorithm. IEEE Transactions on Geoscience and Remote Sensing, 50(5), pp.1384-1403.

Koster, R. D., and Suarez, M. J. (1992). A comparative analysis of two land surface heterogeneity representations. Journal of Climate, 5(12), 1379-1390.

Koster, R.D., Dirmeyer, P.A., Guo, Z., Bonan, G., Chan, E., Cox, P., Gordon, C.T., Kanae, S., Kowalczyk, E., Lawrence, D. and Liu, P. (2004). Regions of strong coupling between soil moisture and precipitation. Science, 305(5687), pp.1138-1140.

Kottek, M., Grieser, J., Beck, C., Rudolf, B. and Rubel, F., 2006. World map of the Köppen-Geiger climate classification updated. Meteorologische Zeitschrift, 15(3), pp.259-263.

Kustas, W. P., and Albertson, J. D. (2003). Effects of surface temperature contrast on land-atmosphere exchange: A case study from Monsoon 90. Water Resources Research, 39(6).

Kustas, W.P., Li, F., Jackson, T.J., Prueger, J.H., MacPherson, J.I. and Wolde, M. (2004). Effects of remote sensing pixel resolution on modeled energy flux variability of croplands in Iowa. Remote sensing of Environment, 92(4), pp.535-547.

Lakhankar, T., Ghedira, H., Temimi, M., Azar, A. E., and Khanbilvardi, R. (2009). Effect of land cover heterogeneity on soil moisture retrieval using active microwave remote sensing data. Remote Sensing, 1(2), 80-91.

Lawrence, H., Wigneron, J. P., Demontoux, F., Mialon, A., and Kerr, Y. H. (2013). Evaluating the Semiempirical H-Q Model Used to Calculate the L-Band Emissivity of a Rough Bare Soil, IEEE Trans. Geosci. Remote Sens., 51(7), 4075-4084.

Lilburne, L., and Tarantola, S. (2009). Sensitivity analysis of spatial models. International Journal of Geographical Information Science, 23(2), 151-168.

Lohmann, D., Mitchell, K.E., Houser, P.R., Wood, E.F., Schaake, J.C., Robock, A., Cosgrove, B.A., Sheffield, J., Duan, Q., Luo, L. and Higgins, R.W. (2004). Streamflow and water balance intercomparisons of four land surface models in the North American Land Data Assimilation System project. Journal of Geophysical Research: Atmospheres, 109(D7).

Lyles, L., and Woodruff, N.P. (1961). Surface Soil Cloddiness in relation to soil density at time of tillage. Soil Science, 91(3), 178-182.

Malenovský, Z., Bartholomeus, H. M., Acerbi-Junior, F. W., Schopfer, J. T., Painter, T. H., Epema, G. F., and Bregt, A. K. (2007). Scaling dimensions in spectroscopy of soil and vegetation. International Journal of Applied Earth Observation and Geoinformation, 9(2), 137-164.

Manns, H. R., Berg, A. A. and Colliander, A. (2015). Soil organic carbon as a factor in passive microwave retrievals of soil water content over agricultural croplands. Journal of Hydrology, 528, pp.643-651.

Martens, B., Lievens, H., Colliander, A., Jackson, T. J. and Verhoest, N. E. (2015). Estimating effective roughness parameters of the L-MEB model for soil moisture retrieval using passive microwave observations from SMAPVEX12. IEEE transactions on geoscience and remote sensing, 53(7), pp.4091-4103.

Mätzler, C., Hiltbrunner, D., and Standley, A. (1998). Relief effects for passive microwave remote sensing, WP330, SNOW-TOOLS, Res (No. 98-3). Report.

McCabe, M. F., Gao, H., and Wood, E. F. (2005). Evaluation of AMSR-E-derived soil moisture retrievals using ground-based and PSR airborne data during SMEX02, J. Hydrometeo., 6(6), 864-877.

McNairn, H., Jackson, T.J., Wiseman, G., Belair, S., Berg, A., Bullock, P., Colliander, A., Cosh, M. H., Kim, S. B., Magagi, R. and Moghaddam, M. (2015). The Soil Moisture Active Passive Validation Experiment 2012 (SMAPVEX12): Prelaunch calibration and validation of the SMAP soil moisture algorithms. IEEE Transactions on Geoscience and Remote Sensing, 53(5), pp.2784-2801.

McNairn, H., Jackson, T.J., Wiseman, G., Belair, S., Berg, A., Bullock, P., Colliander, A., Cosh, M.H., Kim, S.B., Magagi, R. and Moghaddam, M. (2015). The Soil Moisture Active Passive Validation Experiment 2012 (SMAPVEX12): Prelaunch calibration and validation of the SMAP soil moisture algorithms. IEEE Transactions on Geoscience and Remote Sensing, 53(5), pp.2784-2801.

Mecklenburg, S., Drusch, M., Kaleschke, L., Rodriguez-Fernandez, N., Reul, N., Kerr, Y., Font, J., Martin-Neira, M., Oliva, R., Daganzo-Eusebio, E. and Grant, J. (2016). ESA's Soil Moisture and Ocean Salinity mission: From science to operational applications. Remote Sensing of Environment, 180, pp.3-18.

Merlin, O., Malbéteau, Y., Notfi, Y., Bacon, S., Khabba, S. E. R. S., and Jarlan, L. (2015). Performance metrics for soil moisture downscaling methods: Application to DISPATCH data in Central Morocco. Remote Sensing, 7(4), 3783-3807.

Merlin, O., Ruediger, C., Al Bitar, A., Richaume, P., Walker, J. P., and Kerr, Y. H. (2012). Disaggregation of SMOS Soil Moisture in Southeastern Australia. IEEE Transactions on Geoscience and Remote Sensing, 50, 1556-1571.

Mialon, A., Coret, L., Kerr, Y.H., Sécherre, F. and Wigneron, J. P. (2008). Flagging the topographic impact on the SMOS signal. IEEE Transactions on Geoscience and Remote Sensing, 46(3), pp.689-694.

Mironov, V. L., Kosolapova, L. G., and Fomin, S. V. (2009). Physically and mineralogically based spectroscopic dielectric model for moist soils. IEEE Transactions on Geoscience and Remote Sensing, 47(7), 2059-2070.

Mo, T., Choudhury, B., Schmugge, T.,Wang, J., and Jackson, T. (1982). A model for microwave emission from vegetation-covered fields. Journal of Geophysical Research: Oceans (1978–2012), 87, 11229–11237.

Mohanty, B. P., Cosh, M. H., Lakshmi, V. and Montzka, C. (2017). Soil moisture remote sensing: State-of-the-science. Vadose Zone Journal, 16(1).

Molero, B., Merlin, O., Malbeteau, Y., Al Bitar, A., Cabot, F., Stefan, V., Kerr, Y., Bacon, S., Cosh, M.H., Bindlish, R., and Jackson, T.J. (2016). SMOS disaggregated soil moisture

product at 1 km resolution: Processor overview and first validation results. Remote Sensing of Environment, 180, 361-376.

Montpetit, B., Royer, A., Wigneron, J. P., Chanzy, A., and Mialon, A. (2015). Evaluation of multi-frequency bare soil microwave reflectivity models. Remote Sensing of Environment, 162, 186–195.

Mood, A., Graybill, F., and Boes, D. (1974). Introduction to the theory of statistics. 3rd Mcgraw-Hill.

Moran, M. S., Doorn, B., Escobar, V., and Brown, M. E. (2015). Connecting NASA science and engineering with earth science applications. Journal of Hydrometeorology, 16(1), 473-483.

Moyeed, R. A., and Papritz, A. (2002). An empirical comparison of kriging methods for nonlinear spatial point prediction. Mathematical Geology, 34(4), 365-386.

Narayan, U., Lakshmi, V., and Njoku, E. G. (2004). Retrieval of soil moisture from passive and active L/S band sensor (PALS) observations during the Soil Moisture Experiment in 2002 (SMEX02), Remote Sens. Environ.,92(4), 483-496.

Neelam, M., and Mohanty, B. P. (2015). Global sensitivity analysis of the radiative transfer model. Water Resources Research, 51(4), 2428-2443.

Newton, R. W., Black, Q. R., Makanvand, S., Blanchard, A. J., and Jean, B. R. (1982). Soil moisture information and thermal microwave emission, IEEE Trans. Geosci. Remote Sens., (3), 275-281.

Njoku, E. G. and Kong, J. A. (1977). Theory for passive microwave remote sensing of nearsurface soil moisture, J. Geophys. Res., 82, 3108-3118.

Njoku, E. G., and Chan, S. K. (2006). Vegetation and surface roughness effects on AMSR-E land observations, Remote Sens. Environ.,100(2), 190-199.

Njoku, E. G., and Entekhabi, D. (1996). Passive microwave remote sensing of soil moisture. Journal of hydrology, 184 (1-2), 101-129.

Njoku, E. G., Hook, S. J., and Chehbouni, A. (1996). Effects of surface heterogeneity on thermal remote sensing of land parameters, Scaling up in Hydrology using remote sensing. JB Steward ET Engman RA Feddes Y. Kerr, 19-37.

Njoku, E.G., Wilson, W.J., Yueh, S.H., Dinardo, S.J., Li, F.K., Jackson, T.J., Lakshmi, V. and Bolten, J. (2002). Observations of soil moisture using a passive and active low-frequency microwave airborne sensor during SGP99. IEEE Transactions on Geoscience and Remote Sensing, 40 (12), pp.2659-2673.

O'Neill, P. E., Njoku, E. G., Jackson, T. J., Chan, S., and Bindlish, R. (2015). SMAP algorithm theoretical basis document: Level 2 and 3 soil moisture (passive) data products. Jet Propulsion Lab., California Inst. Technol., Pasadena, CA, USA, JPL D-66480.

O'Neill, P., Owe, M., Gouweleeuw, B., Njoku, E., Shi, J. and Wood, E., 2006, July. Hydros soil moisture retrieval algorithms: Status and relevance to future missions. In Geoscience and Remote Sensing Symposium, 2006. IGARSS 2006. IEEE International Conference on (pp. 436-439). IEEE.

Orth, R., and Seneviratne, S. I. (2015). Introduction of a simple-model-based land surface dataset for Europe. Environmental Research Letters, 10(4), 044012.

Owe, M., de Jeu, R., and Walker, J. (2001). A methodology for surface soil moisture and vegetation optical depth retrieval using the microwave polarization difference index, IEEE Trans. Geosci. Remote Sens.,,39(8), 1643-1654.

Pachepsky, Y., Radcliffe, D. E., and Selim, H. M. (Eds.). (2003). Scaling methods in soil physics. CRC press.

Pampaloni, P., and Paloscia, S. (1986). Microwave emission and plant water content: A comparison between field measurements and theory, IEEE Trans. Geosci. Remote Sens., (6), 900-905.

Panciera, R., Walker, J. P., and Merlin, O. (2009b). Improved understanding of soil surface roughness parameterization for L-band passive microwave soil moisture retrieval. IEEE Geoscience and Remote Sensing Letters, 6, 625–629.

Panciera, R., Walker, J. P., Kalma, J. D., Kim, E. J., Saleh, K., and Wigneron, J. P. (2009a). Evaluation of the SMOS L-MEB passive microwave soil moisture retrieval algorithm. Remote Sensing of Environment, 113, 435–444.

Park, S., Kweon, S. K., and Oh, Y. (2015). Validity Regions of Soil Moisture Retrieval on LAI-θ Plane for Agricultural Fields at L-, C-, and X-Bands. IEEE Geoscience and Remote Sensing Letters, 12(6), 1195-1198.

Parrens, M., Wigneron, J.P., Richaume, P., Mialon, A., Al Bitar, A., Fernandez-Moran, R., Al-Yaari, A. and Kerr, Y.H. (2016). Global-scale surface roughness effects at L-band as estimated from SMOS observations. Remote Sensing of Environment, 181, pp.122-136.

Peel, M. C., Finlayson, B. L., and McMahon, T. A. (2007). Updated world map of the Köppen-Geiger climate classification. Hydrology and Earth System Sciences Discussions, 4(2), 439-473.

Pianosi, F., Beven, K., Freer, J., Hall, J. W., Rougier, J., Stephenson, D. B., and Wagener, T. (2016). Sensitivity analysis of environmental models: A systematic review with practical workflow. Environmental Modelling and Software, 79, 214-232.

Pielke, R. A., Avissar, R., Raupach, M., Dolman, A. J., Zeng, X., and Denning, A. S. (1998). Interactions between the atmosphere and terrestrial ecosystems: influence on weather and climate. Global change biology, 4(5), 461-475.

Piles, M., Camps, A., Vall-Llossera, M., Corbella, I., Panciera, R., Rudiger, C., Kerr, Y., and Walker, J. (2011). Downscaling SMOS-derived soil moisture using MODIS visible/infrared data. IEEE Transactions on Geoscience and Remote Sensing, 49(9), 3156-3166.

Piles, M., Entekhabi, D., and Camps, A. (2009). A change detection algorithm for retrieving high-resolution soil moisture from SMAP radar and radiometer observations. IEEE Transactions on Geoscience and Remote Sensing, 47(12), 4125-4131.

Potter, K. N. (1990). Soil properties effect on random roughness decay by rainfall. Transactions of the ASAE, 33(6), 1889-1892.

Qin, J., Zhao, L., Chen, Y., Yang, K., Yang, Y., Chen, Z., and Lu, H. (2015). Inter-comparison of spatial upscaling methods for evaluation of satellite-based soil moisture. Journal of Hydrology, 523, 170-178.

Quattrochi, D. A., Wentz, E., Lam, N. S. N., and Emerson, C. W. (Eds.). (2017). Integrating Scale in Remote Sensing and GIS. CRC Press.

Raupach, M. R., and Finnigan, J. J. (1995). Scale issues in boundary-layer meteorology: Surface energy balances in heterogeneous terrain. Hydrological Processes, 9(5-6), 589-612.

Roy, S.K, Rowlandson, T. L., Berg, A. A., Champagne, C., and Adams, J. R. (2016). Impact of sub-pixel heterogeneity on modelled brightness temperature for an agricultural region." International Journal of Applied Earth Observation and Geoinformation 45 (2016): 212-220.

Ryu, D., and Famiglietti, J. S. (2006). Multi-scale spatial correlation and scaling behavior of surface soil moisture. Geophysical Research Letters, 33(8).

Said, S., Kothyari, U. C., and Arora, M. K. (2012). Vegetation effects on soil moisture estimation from ERS-2 SAR images. Hydrological Sciences Journal, 57(3), 517-534.

Saint-Geours, N., Lavergne, C., Bailly, J. S., and Grelot, F. (2011). Sensitivity analysis of spatial models using geostatistical simulation. Mathematical Geosciences at the Crossroads of Theory and Practice-IAMG 2011 Conference (pp. 178-189).

Saleh, K., Wigneron, J. P., de Rosnay, P., Calvet, J. C., and Kerr, Y. (2006b). Semi-empirical regressions at L-band applied to surface soil moisture retrievals over grass. Remote Sensing of Environment, 101, 415–426.

Saleh, K., Wigneron, J. P., Waldteufel, P., De Rosnay, P., Schwank, M., Calvet, J. C., and Kerr, Y. H. (2007). Estimates of surface soil moisture under grass covers using L-band radiometry, Remote Sens. Environ.,109(1), 42-53.

Saltelli, A. (2002). Making best use of model evaluations to compute sensitivity indices. Computer Physics Communications, 145(2), 280-297.

Saltelli, A., Annoni, P., Azzini, I., Campolongo, F., Ratto, M., and Tarantola, S. (2010). Variance based sensitivity analysis of model output. Design and estimator for the total sensitivity index. Computer Physics Communications, 181(2), 259-270.

Saltelli, A., Ratto, M., Andres, T., Campolongo, F., Cariboni, J., Gatelli, D., Saisana, M. and Tarantola, S. (2008). Global sensitivity analysis: the primer. John Wiley and Sons.

Saltelli, A., Tarantola, S., Campolongo, F., and Ratto, M. (2004). Sensitivity analysis in practice: a guide to assessing scientific models. John Wiley & Sons.

Sandells, M. J., Davenport, I. J., and Gurney, R. J. (2008). Passive L-band microwave soil moisture retrieval error arising from topography in otherwise uniform scenes. Advances in Water Resources, 31(11), 1433-1443.

Santi, E., Pettinato, S., Paloscia, S., Pampaloni, P., Macelloni, G., and Brogioni, M. (2012). An algorithm for generating soil moisture and snow depth maps from microwave spaceborne radiometers: HydroAlgo, Hydrol. Earth Syst. Sci., 9(3), 3851-3900.

Sarrazin, F., Pianosi, F., and Wagener, T. (2016). Global sensitivity analysis of environmental models: convergence and validation. Environmental Modelling and Software, 79, 135-152.

Satelli, A., Tarntola, S., Campolongo, F., and Ratto, M. (2004). Sensitivity Analysis in Practice. John Wiley and Sons, Ltd, 42-49.

Schaefer, G. L., Cosh, M. H., and Jackson, T. J. (2007). The USDA natural resources conservation service soil climate analysis network (SCAN). Journal of Atmospheric and Oceanic Technology, 24(12), 2073-2077.

Schmugge, T. J. (1983). Remote sensing of soil moisture: Recent advances, IEEE Trans. Geosci. Remote Sens., (3), 336-344.

Schmugge, T. J. and Choudhury, B. J. (1981). A comparison of radiative transfer models for predicting the microwave emission from soils. Radio Science, 16(05), pp.927-938.

Schmugge, T. J., Jackson, T. J., Kustas, W. P., Wang, J. R. (1992). Passive microwave remote sensing of soil moisture: Results from HAPEX, FIFE, and MONSOON'90. Internatonal Journal of Photogrammetry and Remote Sensing 47, 127–143.

Schmugge, T., Gloersen, P., Wilheit, T., and Geiger, F. (1974). Remote sensing of soil moisture with microwave radiometers, J. Geophys. Res., 79(2), 317-323.

Schmugge, T., O'Neill, P. E., and Wang, J. R. (1986). Passive microwave soil moisture research. IEEE Trans. Geosci. Remote Sens., (1), 12-22.

Seneviratne, S.I., Corti, T., Davin, E.L., Hirschi, M., Jaeger, E.B., Lehner, I., Orlowsky, B. and Teuling, A.J. (2010). Investigating soil moisture–climate interactions in a changing climate: A review. Earth-Science Reviews, 99(3-4), pp.125-161.

Seo, D., Lakhankar, T., and Khanbilvardi, R. (2010). Sensitivity analysis of b-factor in microwave emission model for soil moisture retrieval: A case study for SMAP mission, Remote Sensing, 2(5), 1273-1286.

Shin, Y., and Mohanty, B. P. (2013). Development of a deterministic downscaling algorithm for remote sensing soil moisture footprint using soil and vegetation classifications. Water Resources Research, 49(10), 6208-6228.

Shuttleworth, W.J., Yang, Z.L. and Arain, M.A. (1997). Aggregation rules for surface parameters in global models. Hydrol. Earth Syst. Sci, 2, pp.217-226.

Sobol, I. M. (1993). Sensitivity estimates for nonlinear mathematical models. Mathematical Modelling and Computational Experiments, 1(4), 407-414.

Song, C., Jia, L., and Menenti, M. (2014). Retrieving high-resolution surface soil moisture by downscaling AMSR-E brightness temperature using MODIS LST and NDVI data. IEEE Journal of Selected Topics in Applied Earth Observations and Remote Sensing, 7(3), 935-942.

Spencer, M., Wheeler, K., White, C., West, R., Piepmeier, J., Hudson, D., and Medeiros, J. (2010). The Soil Moisture Active Passive (SMAP) mission L-band radar/radiometer instrument. Geoscience and Remote Sensing Symposium (IGARSS), 2010 IEEE International (pp. 3240-3243).

Talone, M., Camps, A., Monerris, A., Vall-llossera, M., Ferrazzoli, P., and Piles, M. (2007). Surface topography and mixed-pixel effects on the simulated L-band brightness temperatures. IEEE Transactions on Geoscience and Remote Sensing, 45(7), 1996-2003.

Taylor, L. R. (1961). Aggregation, variance and the mean. Nature, 189(4766), 732-735.

Templeton, R.C., Vivoni, E.R., Méndez-Barroso, L.A., Pierini, N.A., Anderson, C.A., Rango, A., Laliberte, A.S. and Scott, R.L. (2014). High-resolution characterization of a semiarid watershed: Implications on evapotranspiration estimates. Journal of hydrology, 509, pp.306-319.

Ulaby, F. T., Moore, R. K. and Fung, A. K. (2015). Microwave remote sensing active and passive.

Ulaby, F. T., Moore, R. K., and Fung, A. K. (1981). Microwave Remote Sensing, 48, Addison-Wesley, Reading, Mass., 1981.

Ulaby, F. T., Moore, R. K., and Fung, A. K. (1986). Microwave Remote Sensing Active and Passive-Volume III: From Theory to Applications. Addison-Wesley Publishing Company

Ulaby, F. T., Razani, M., and Dobson, M. C. (1983). Effects of vegetation cover on the microwave radiometric sensitivity to soil moisture, IEEE Trans. Geosci. Remote Sens., (1), 51-61.

Van de Griend, A. A., and Owe, M. (1994). Microwave vegetation optical depth and signal scattering albedo from large scale soil moisture and Nimbus/SMMR Satellite observations, Meteorol. Atmos. Phys., 54, pp. 225-239.

Van de Griend, A. A., and Wigneron, J. P. (2004). The b-factor as a function of frequency and canopy type at H-polarization. IEEE Transactions on Geoscience and Remote Sensing, 42(4), 786-794.

Van de Griend, A. A., Wigneron, J. P., and Waldteufel, P. (2003). Consequences of surface heterogeneity for parameter retrieval from 1.4-GHz multiangle SMOS observations. IEEE Transactions on Geoscience and Remote Sensing, 41(4), 803-811.

Van Dijk, A. I. J. M., and Bruijnzeel, L. A. (2001). Modelling rainfall interception by vegetation of variable density using an adapted analytical model. Part 1. Model description. Journal of Hydrology, 247(3), 230-238.

Wang, J. R., McMurtrey, J. E., Engman, E. T., Jackson, T. J., Schmugge, T. J., Gould, W. I., Fuchs, J. E. and Glazar, W. S. (1982). Radiometric measurements over bare and vegetated fields at 1.4-GHz and 5-GHz frequencies. Remote Sensing of Environment, 12(4), pp.295-311.

Wang, J. R., O'Neill, P. E., Jackson, T. J., and Engman, E. T. (1983). Multifrequency measurements of the effects of soil moisture, soil texture, and surface roughness, IEEE Trans. Geosci. Remote Sens., (1), 44-51.

Wang, J., and Choudhury, B. (1981). Remote sensing of soil moisture content, over bare field at 1.4 GHz frequency. Journal of Geophysical Research: Oceans (1978–2012), 86, 5277–5282.

Wang, S., Wigneron, J.P., Jiang, L.M., Parrens, M., Yu, X.Y., Al-Yaari, A., Ye, Q.Y., Fernandez-Moran, R., Ji, W. and Kerr, Y. (2015). Global-scale evaluation of roughness effects on C-band AMSR-E observations. Remote Sensing, 7(5), pp.5734-5757.

Weber, D. D., and Englund, E. J. (1994). Evaluation and comparison of spatial interpolators II. Mathematical Geology, 26(5), 589-603.

Wegmuller, U., and Matzler, C. (1999). Rough bare soil reflectivity model. IEEE Transactions on Geoscience and Remote Sensing, 37, 1391–1395.

Western, A. W., and Blöschl, G. (1999). On the spatial scaling of soil moisture. Journal of hydrology, 217(3), 203-224.

Western, A. W., Grayson, R. B., and Blöschl, G. (2002). Scaling of soil moisture: A hydrologic perspective. Annual Review of Earth and Planetary Sciences, 30(1), 149-180.

Wigneron, J. P., Chanzy, A., Calvet, J. C., and Bruguier, N. (1995). A simple algorithm to retrieve soil moisture and vegetation biomass using passive microwave measurements over crop fields. Remote Sensing of Environment, 51 (3), 331-341.

Wigneron, J. P., Chanzy, A., Kerr, Y. H., Lawrence, H., Shi, J., Escorihuela, M. J., Mironov, V., Mialon, A., Demontoux, F., De Rosnay, P. and Saleh-Contell, K. (2011). Evaluating an improved parameterization of the soil emission in L-MEB. IEEE Transactions on Geoscience and Remote Sensing, 49(4), pp.1177-1189.

Wigneron, J. P., Jackson, T. J., O'neill, P., De Lannoy, G., De Rosnay, P., Walker, J. P., Ferrazzoli, P., Mironov, V., Bircher, S., Grant, J.P. and Kurum, M. (2017). Modelling the passive microwave signature from land surfaces: A review of recent results and application to the L-band SMOS & SMAP soil moisture retrieval algorithms. Remote Sensing of Environment, 192, 238-262.

Wigneron, J. P., Laguerre, L., and Kerr, Y. H. (2001). A simple parameterization of the L-band microwave emission from rough agricultural soils. IEEE Transactions on Geoscience and Remote Sensing, 39, 1697–1707.

Wigneron, J. P., Schwank, M., Baeza, E. L., Kerr, Y., Novello, N., Millan, C., Moisy, C., Richaume, P., Mialon, A., Al Bitar, A., et al. (2012). First evaluation of the simultaneous SMOS and ELBARA-II observations in the Mediterranean region. Remote Sensing of Environment, 124, 26–37.

Wigneron, J.P., Chanzy, A., Kerr, Y.H., Lawrence, H., Shi, J., Escorihuela, M.J., Mironov, V., Mialon, A., Demontoux, F., De Rosnay, P. and Saleh-Contell, K. (2011). Evaluating an improved parameterization of the soil emission in L-MEB. IEEE Transactions on Geoscience and Remote Sensing, 49(4), pp.1177-1189.

Wigneron, J.P., Jackson, T.J., O'neill, P., De Lannoy, G., De Rosnay, P., Walker, J.P., Ferrazzoli, P., Mironov, V., Bircher, S., Grant, J.P. and Kurum, M. (2017). Modelling the passive microwave signature from land surfaces: A review of recent results and application to the L-band SMOS & SMAP soil moisture retrieval algorithms. Remote Sensing of Environment, 192, pp.238-262.

Wilheit, T. T. (1978). Radiative transfer in a plane stratified dielectric. IEEE Transactions on Geoscience Electronics, 16(2), 138-143.

Wilson, K., Goldstein, A., Falge, E., Aubinet, M., Baldocchi, D., Berbigier, P., Bernhofer, C., Ceulemans, R., Dolman, H., Field, C. and Grelle, A. (2002). Energy balance closure at FLUXNET sites. Agricultural and Forest Meteorology, 113(1), pp.223-243.

Wilson, W., S. Yueh, S. Dinardo, S. Chazanoff, A. Kitiyakara, F. Li, and Y. Rahmat-Samii. (2001). Passive Active L- and S-Band (PALS) Microwave Sensor for Ocean Salinity and Soil Moisture Measurements. IEEE Trans. Geosci. Rem. Sens., Vol. 39, No. 5., pp. 1039-1048.

Wood, E. F. (1997). Effects of soil moisture aggregation on surface evaporative fluxes. Journal of Hydrology, 190(3-4), 397-412.

Wu, H., and Li, Z. L. (2009). Scale issues in remote sensing: A review on analysis, processing and modeling. Sensors, 9(3), 1768-1793.

Wu, X., Walker, J. P., Das, N. N., Panciera, R., and Rüdiger, C. (2014). Evaluation of the SMAP brightness temperature downscaling algorithm using active–passive microwave observations. Remote Sensing of Environment,155, 210-221.

Xie, J., Liu, T., Wei, P., Jia, Y., and Luo, C. (2007). Ecological application of wavelet analysis in the scaling of spatial distribution patterns of Ceratoides ewersmanniana. Acta Ecologica Sinica, 27(7), 2704-2714.

Ye, N. (2014). Mixed pixel retrieval of soil moisture from L-band passive microwave observations (Doctoral dissertation, Monash University. Faculty of Engineering. Department of Civil Engineering).

Yilmaz, M. T., Hunt, E. R., Goins, L. D., Ustin, S. L., Vanderbilt, V. C., and Jackson, T. J. (2008). Vegetation water content during SMEX04 from ground data and Landsat 5 Thematic Mapper imagery. Remote Sensing of Environment, 112(2), 350-362.

Zhan, X., Crow, W. T., Jackson, T. J., and O'Neill, P. E. (2008). Improving spaceborne radiometer soil moisture retrievals with alternative aggregation rules for ancillary parameters in highly heterogeneous vegetated areas. IEEE Geoscience and Remote Sensing Letters, 5(2), 261-265.

Zhixiong, L., Nan, C., Perdok, U. D., and Hoogmoed, W. B. (2005). Characterization of soil profile roughness, Biosystems Engineering, 91(3), 369-377.

Zobeck, T. M., and Onstad, C. A. (1987). Tillage and rainfall effects on random roughness: a review. Soil and Tillage Research, 9(1), 1-20.

APPENDIX

Consider a model defined as $Y = f(\mathbf{X})$, where Y is the output, $\mathbf{X} = (X_1, \ldots X_k)$ are k independent inputs, and f is the model function. If all the factors **X** are allowed to vary over their range of uncertainty, then the corresponding uncertainty of the model output $\boldsymbol{Y}$ is defined by its unconditional variance $\boldsymbol{V(Y)}$. The input factors are ranked based on the amount of variance removed from the output when we learn the true value of a given input factor X_i. That is $V_{X_{\sim i}}(Y|X_i = x_i^*)$, be the resulting conditional variance as it is fixed to its true value x_i^* taken over all $X_{\sim i}$(all factors but X_i). However, the true value x_i^* is unknown for each X_i. Hence, an average of $V_{X_{\sim i}}(Y|X_i = x_i^*)$ measured over all possible values x_i^*, will remove the dependence of x_i^* thereby resulting in $E_{X_i}\left[V_{X_{\sim i}}(Y|X_i)\right]$. Using the following property [Mood et al., 1974];

$$E_{X_i}\left[V_{X_{\sim i}}(Y|X_i)\right] + V_{X_i}\left[E_{X_{\sim i}}(Y|X_i)\right] = V(Y)$$

Thus, a small $E_{X_i}\left[V_{X_{\sim i}}(Y|X_i)\right]$ or a large $V_{X_i}\left[E_{X_{\sim i}}(Y|X_i)\right]$, will imply that X_i is an important factor. The conditional variance $V_{X_i}\left[E_{X_{\sim i}}(Y|X_i)\right]$ is the first-order (e.g., additive) effect of X_i on Y and the associated first-order sensitivity index of X_i on Y measure is written as : $\boldsymbol{S_i} = \frac{\boldsymbol{V_{X_i}\left[E_{X_{\sim i}}(Y|X_i)\right]}}{\boldsymbol{V(Y)}}$; while $E_{X_i}\left[V_{X_{\sim i}}(Y|X_i)\right]$ is customarily called the residual. As such S_i is a number always between 0 and 1.

Sobol [Sobol, 1993] introduced the decomposition of model function f into summands of increasing dimensionality:

$$f = f_0 + \sum_i f_i + \sum_i \sum_{j>i} f_{ij} + \cdots + f_{12\ldots k}$$

in which each individual term is square integrable over the domain of existence and are mutually orthogonal [Satelli et al., 2008]. These functions $f_{i_{1,},\ldots i_{k,}}$ are associated with partial variances through:

$$V_i = V\big(f_i(X_i)\big) = V_{X_i}\big[E_{X_{\sim i}}(Y|X_i)\big],$$

$$V_{ij} = V\left(f_{ij}\big(X_i, X_j\big)\right) = V_{X_iX_j}\left[E_{X_{\sim ij}}\big(Y\big|X_i, X_j\big)\right] - V_{X_i}\big[E_{X_{\sim i}}(Y|X_i)\big] - V_{X_j}\left[E_{X_{\sim j}}\big(Y\big|X_j\big)\right]$$

and so on for higher order terms. Assuming all inputs to be independent, these terms are linked as:

$V(Y) = \sum_i V_i + \sum_i \sum_{j>i} V_{ij} + \cdots + V_{12\ldots k}$. Dividing both sides of the equation by unconditional variance *V(Y)*, we obtain;

$$\sum_i S_i + \sum_i \sum_{j>i} S_{ij} + \cdots + S_{12\ldots k} = 1$$

where**, First Order Sensitivity Index** $\boldsymbol{S_i = \frac{V_i(Y)}{V(Y)}}$; **Second Order Sensitivity Index** $\boldsymbol{S_{ij}} = \frac{V_{ij}(Y)}{V(Y)}$; the amount of variance of $\boldsymbol{Y}$ explained by the interaction of the factors X_i and X_j (i.e. sensitivity to X_i and X_j not expressed in individual X_i and X_j); **Total Sensitivity Index** $\boldsymbol{S_{Ti}} = S_i + \sum_{i<j} S_{ij} + \sum_{i<j<l} S_{ijl} + \ldots S_{1,2,\ldots k}$; it accounts for all the contributions to the output variation due to factor X_i (i.e. first-order index plus all its interactions). S_{Ti} can also be defined by decomposing the output variance V(Y), in terms of main effect and residual, conditioning with respect to all factors but one i.e., $\boldsymbol{X_{\sim i}}$**.** The unconditional variance can be rewritten as; $V(Y) - V_{X_{\sim i}}\big[E_{X_i}(Y|X_{\sim i})\big] = E_{X_{\sim i}}\big[V_{X_i}(Y|X_{\sim i})\big]$, dividing both sides by unconditional variance results in:

$$\boldsymbol{S_{Ti} = 1 - \frac{V_{X_{\sim i}}\big[E_{X_i}(Y|X_{\sim i})\big]}{V(Y)} = \frac{E_{X_{\sim i}}\big[V_{X_i}(Y|X_{\sim i})\big]}{V(Y)}}$$

In other words, S_{Ti} index is defined as a summation of main, second, and higher order effects which involves the evaluation over a full range of parameter space. For further details on computation of sensitivity indices please refer to Saltelli (2002).